



## 저작자표시-비영리-변경금지 2.0 대한민국

이용자는 아래의 조건을 따르는 경우에 한하여 자유롭게

- 이 저작물을 복제, 배포, 전송, 전시, 공연 및 방송할 수 있습니다.

다음과 같은 조건을 따라야 합니다:



저작자표시. 귀하는 원저작자를 표시하여야 합니다.



비영리. 귀하는 이 저작물을 영리 목적으로 이용할 수 없습니다.



변경금지. 귀하는 이 저작물을 개작, 변형 또는 가공할 수 없습니다.

- 귀하는, 이 저작물의 재이용이나 배포의 경우, 이 저작물에 적용된 이용허락조건을 명확하게 나타내어야 합니다.
- 저작권자로부터 별도의 허가를 받으면 이러한 조건들은 적용되지 않습니다.

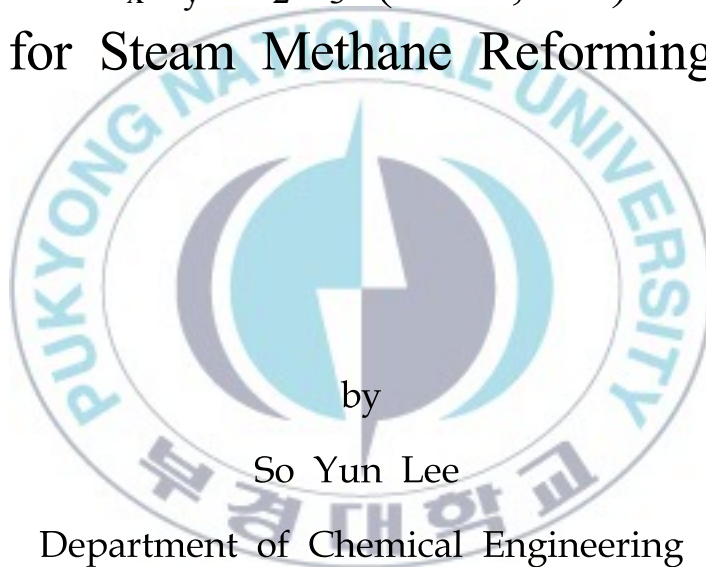
저작권법에 따른 이용자의 권리는 위의 내용에 의하여 영향을 받지 않습니다.

이것은 [이용허락규약\(Legal Code\)](#)을 이해하기 쉽게 요약한 것입니다.

[Disclaimer](#)

Thesis for the Degree of Doctor of Philosophy

Catalytic Activity and Characterizations  
of Ni/MTi<sub>x</sub>O<sub>y</sub>-Al<sub>2</sub>O<sub>3</sub> (M=K, Ca) Catalyst  
for Steam Methane Reforming



by

So Yun Lee

Department of Chemical Engineering

The Graduate School

Pukyong National University

February 2014

# Catalytic Activity and Characterizations of Ni/MTi<sub>x</sub>O<sub>y</sub>-Al<sub>2</sub>O<sub>3</sub> (M=K, Ca) Catalyst for Steam Methane Reforming

Ni/MTi<sub>x</sub>O<sub>y</sub>-Al<sub>2</sub>O<sub>3</sub> (M=K, Ca) 촉매의  
메탄 수증기 개질 반응활성 및 특성분석

Advisor: Prof. Hee Chul Woo

by  
So Yun Lee

A thesis submitted in partial fulfillment of the requirements  
for the degree of  
Doctor of Philosophy

in Department of Chemical Engineering, The Graduate School,  
Pukyong National University

February 2014

Catalytic Activity and Characterizations of Ni/MTi<sub>x</sub>O<sub>y</sub>-Al<sub>2</sub>O<sub>3</sub>  
(M=K, Ca) Catalyst for Steam Methane Reforming

A dissertation

by

So Yun Lee

Approved by:



Seok Hee Lee



Hee Chul Woo



Jun Heok Lim



Jay Liu



Jung Kyoo Lee

February 21, 2014

# CONTENTS

<b>CONTENTS</b>	<b>i</b>
<b>ABSTRACT</b>	<b>v</b>
<b>LIST OF TABLES</b>	<b>viii</b>
<b>LIST OF FIGURES</b>	<b>x</b>

## CHAPTER

<b>1. Introduction</b>	<b>1</b>
<b>2. Literature survey</b>	<b>6</b>
2.1. Thermodynamics	6
2.2. Steam methane reforming catalysts	9
2.2.1. Active metal	9
2.2.2. Catalyst support	13
2.2.2.1. Effect of support property	13
2.2.2.2. Roles of support in catalytic reactions	16
2.3. Reaction mechanism of steam methane reforming	20
2.4. Challenges for steam methane reforming catalyst	24
2.4.1. Sintering	24
2.4.2. Oxidation	26
2.4.3. Sulfur poisoning	27

2.4.4. Carbon formation·····	28
2.5. Catalyst promotion·····	32
2.6. Property of potassium titanate·····	34
<b>3. Experimental</b> ·····	<b>36</b>
3.1. Materials·····	36
3.2. Catalyst preparation·····	36
3.3. Characterizations·····	39
3.3.1. X-ray diffraction·····	39
3.3.2. Nitrogen physisorption·····	39
3.3.3. Temperature-programmed reduction·····	40
3.3.4. Scanning electron microscopy·····	40
3.3.5. X-ray photoelectron spectroscopy·····	40
3.3.6. Hydrogen chemisorption ·····	41
3.3.7. Elemental analysis ·····	41
3.4. Catalytic activity test ·····	42
<b>4. Catalytic Activity and Characterization of Ni/K<sub>2</sub>Ti<sub>x</sub>O<sub>y</sub>-Al<sub>2</sub>O<sub>3</sub> Catalyst for Steam Methane Reforming</b> ·····	<b>45</b>
4.1. Catalytic activity of Ni/K <sub>2</sub> Ti <sub>x</sub> O <sub>y</sub> -Al <sub>2</sub> O <sub>3</sub> catalyst for steam methane reforming·····	45
4.1.1. Characteristics of Ni/K <sub>2</sub> Ti <sub>x</sub> O <sub>y</sub> -Al <sub>2</sub> O <sub>3</sub> catalyst ·····	45

4.1.2. Activity of $\text{Ni/K}_2\text{Ti}_x\text{O}_y\text{-Al}_2\text{O}_3$ catalyst .....	62
4.1.3. Catalytic stability of $\text{Ni/K}_2\text{Ti}_x\text{O}_y\text{-Al}_2\text{O}_3$ catalyst .....	67
4.2. Role of $\text{K}_2\text{Ti}_x\text{O}_y$ additive on $\text{Ni/Al}_2\text{O}_3$ catalyst for steam methane reforming .....	71
 <b>5. Catalytic Activity and Characterization of <math>\text{Ni/K}_{2-x}\text{Ca}_{x/2}\text{Ti}_y\text{O}_z\text{-Al}_2\text{O}_3</math> Catalyst for Steam Methane Reforming .....</b>	<b>78</b>
5.1. Characteristics of $\text{Ni/K}_{2-x}\text{Ca}_{x/2}\text{Ti}_y\text{O}_z\text{-Al}_2\text{O}_3$ catalyst .....	79
5.2. Activity of $\text{Ni/K}_{2-x}\text{Ca}_{x/2}\text{Ti}_y\text{O}_z\text{-Al}_2\text{O}_3$ catalyst .....	85
5.3. Role of $\text{CaTiO}_3$ on $\text{Ni/Al}_2\text{O}_3$ catalyst for steam methane reforming .....	90
 <b>6. Catalytic Activity and Characterization of <math>\text{Ni/CaTi}_x\text{O}_y\text{-Al}_2\text{O}_3</math> Catalyst for Steam Methane Reforming .....</b>	<b>92</b>
6.1. Characteristics of $\text{Ni/CaTi}_x\text{O}_y\text{-Al}_2\text{O}_3$ catalyst .....	92
6.2. Activity of $\text{Ni/CaTi}_x\text{O}_y\text{-Al}_2\text{O}_3$ catalyst .....	101
6.3. Sulfur-tolerance ability of $\text{Ni/CaTi}_x\text{O}_y\text{-Al}_2\text{O}_3$ catalyst .....	105
6.4. Role of $\text{CaTi}_x\text{O}_y$ additive on $\text{Ni/Al}_2\text{O}_3$ catalyst for steam methane reforming .....	107



<b>7. Conclusions</b> .....	<b>111</b>
 요 약 .....	 114
<b>REFERENCES</b> .....	<b>117</b>
<b>CURRICULUM VITAE</b> .....	<b>129</b>
감사의 글 .....	136





**Catalytic Activity and Characterizations of Ni/MTi<sub>x</sub>O<sub>y</sub>-Al<sub>2</sub>O<sub>3</sub>  
(M=K, Ca) Catalyst for Steam Methane Reforming**

So Yun Lee

Department of Chemical Engineering, The Graduate School,  
Pukyong National University

**ABSTRACT**

Steam reforming of hydrocarbons has mainly considered as recent topic for fuel processing due to high productivity of hydrogen gas. Although the development of various catalysts for the process has studied, the catalyst deactivation is still a major drawback of technical advancement. Therefore, the objective of this study was to investigate the catalytic stability of modified nickel catalysts containing titanate and the effects of additives such as potassium and calcium. The activities and stabilities of Ni/MTi<sub>x</sub>O<sub>y</sub>-Al<sub>2</sub>O<sub>3</sub> (M=K and Ca) catalysts were compared with those of a commercial catalyst for methane steam reforming.

Nickel catalysts supported on the MTi<sub>x</sub>O<sub>y</sub>-Al<sub>2</sub>O<sub>3</sub> (M= K and/or Ca) were prepared by the wet impregnation method for steam methane reforming to produce hydrogen. X-ray diffraction, N<sub>2</sub> physisorption, scanning electron

microscopy with energy dispersive spectroscopy, the  $H_2$  temperature-programmed reduction technique, and X-ray photoelectron spectroscopy were employed for the characterization of catalyst samples.

The catalytic performance of the  $Ni/K_2Ti_xO_y-Al_2O_3$  catalysts was comparable to that of FCR-4 under the mild reaction condition. In particular, a stability test at  $800^\circ C$  and the reactant flow with the steam-to-carbon (S/C) feed ratio of 1.0 indicated that the  $Ni/K_2Ti_xO_y-Al_2O_3$  catalysts were more active, thermally stable and resistant to deactivation than the non-promoted  $Ni/Al_2O_3$ . It is considered that the appropriate interaction strength between nickel and the modified support and proper  $K_2Ti_xO_y$  phases with a surface monolayer coverage achieved at ca. 15 wt.% loading in the support play important roles in promoting the steam methane reforming activity as well as suppressing the sintering of the catalyst.

The  $Ni/K_{2-x}Ca_{x/2}Ti_yO_z(20)-Al_2O_3(80)$  catalysts have complex phases of K-Ca-Ti-O system and their nickel species were strongly interacted with the  $K_{2-x}Ca_{x/2}Ti_yO_z(20)-Al_2O_3(80)$  support, indicating their low reducibilities. The  $Ni/K_{2-x}Ca_{x/2}Ti_yO_z(20)-Al_2O_3(80)$  catalysts showed acceptable activities for steam methane reforming under the mild reaction condition. For the catalytic stability test, the  $Ni/CaTi_yO_z(20)-Al_2O_3(80)$  represented the superior stability than FCR-4,  $Ni/Al_2O_3$ , and any other catalysts in this work. For the  $Ni/K_{2-x}Ca_{x/2}Ti_yO_z-Al_2O_3$  catalyst (having higher than x of 0.6), the presence of perovskite oxide ( $CaTiO_3$ ) on the catalyst may derive acceptable catalytic activity with high resistance to coking due to its oxygen mobility.

The  $Ni/CaTi_xO_y-Al_2O_3$  catalysts have the medium interaction strength between nickel and support, weaker than that of  $NiO/Al_2O_3$ , and their nickel

species were well-dispersed in the support. They showed relatively lower activities for steam methane reforming under the mild reaction condition. However, the  $\text{Ni}/\text{CaTi}_x\text{O}_y\text{-Al}_2\text{O}_3$  catalysts presented good performance at a higher reaction temperature than  $800^\circ\text{C}$ , closed to thermodynamic limit. A sulfur-tolerance test result for the  $\text{Ni}/\text{CaTi}_x\text{O}_y\text{-Al}_2\text{O}_3$  catalysts under a severe reaction condition: at  $750^\circ\text{C}$ , in a reactant flow with S/C feed ratio of 2.5 containing sulfur compounds of 7 ppmv, and at a GHSV of  $15,000\text{ h}^{-1}$  demonstrated that they maintained their good stability for the reaction time of 300 min. On the other side, significant loss in activity was observed over the  $\text{Ni}/\text{Al}_2\text{O}_3$  catalyst. In particular, over the  $\text{Ni}/\text{CaTi}_x\text{O}_y(20)\text{-Al}_2\text{O}_3(80)$  catalyst, particle size of Ni metal was maintained to be same during the sulfur-tolerance test, indicating its superior resistance to sulfur.

Consequently, both potassium titanate ( $\text{K}_2\text{Ti}_x\text{O}_y$ ) and calcium titanate ( $\text{CaTi}_x\text{O}_y$ ) would be a promising additive material of alumina supported nickel catalyst for steam methane reforming reaction, effectively inhibiting deactivation from sintering of catalyst as well as sulfur poisoning.

## LIST OF TABLES

Table 1.1	Primary technologies used to produce hydrogen	4
Table 2.1	Relative activities for steam methane reforming	10
Table 2.2	Routes to carbon formation	29
Table 4.1	Physical properties of NiO/Al <sub>2</sub> O <sub>3</sub> and NiO/K <sub>2</sub> Ti <sub>x</sub> O <sub>y</sub> -Al <sub>2</sub> O <sub>3</sub> catalysts	49
Table 4.2	Quantitative data from H <sub>2</sub> temperature-programmed reduction profiles of NiO/Al <sub>2</sub> O <sub>3</sub> and NiO/K <sub>2</sub> Ti <sub>x</sub> O <sub>y</sub> -Al <sub>2</sub> O <sub>3</sub> catalysts	53
Table 4.3	Activities of steam methane reforming over Ni/K <sub>2</sub> Ti <sub>x</sub> O <sub>y</sub> -Al <sub>2</sub> O <sub>3</sub> catalysts	65
Table 4.4	Catalytic stability results of Ni/K <sub>2</sub> Ti <sub>x</sub> O <sub>y</sub> -Al <sub>2</sub> O <sub>3</sub> catalysts for steam methane reforming	70
Table 4.5	Amount of carbon and hydrogen deposition of the spent Ni catalysts for 100 h	72
Table 4.6	Crystalline phases change and Ni metal sizes of the catalysts before and after the stability test	75
Table 5.1	Surface area of NiO/K <sub>2-x</sub> Ca <sub>x/2</sub> Ti <sub>y</sub> O <sub>z</sub> -Al <sub>2</sub> O <sub>3</sub> samples	79
Table 5.2	Crystalline phases from XRD for the calcined Ni catalysts	82
Table 5.3	Activities of steam methane reforming over NiO/K <sub>2-x</sub> Ca <sub>x/2</sub> Ti <sub>y</sub> O <sub>z</sub> -Al <sub>2</sub> O <sub>3</sub> catalysts	86
Table 5.4	Catalytic stability results of Ni/K <sub>2-x</sub> Ca <sub>x/2</sub> Ti <sub>y</sub> O <sub>z</sub> -Al <sub>2</sub> O <sub>3</sub> and Ni/Al <sub>2</sub> O <sub>3</sub> catalysts	88

Table 6.1	Physical properties of $\text{NiO}/\text{CaTi}_x\text{O}_y\text{-Al}_2\text{O}_3$ catalysts	95
Table 6.2	Activities of steam methane reforming over $\text{Ni}/\text{CaTi}_x\text{O}_y\text{-Al}_2\text{O}_3$ catalysts	104
Table 6.3	Crystalline phases change and Ni metal sizes of the catalysts before and after the sulfur-tolerance test	110



## LIST OF FIGURES

Fig. 1.1	Fuel processing flow sheet for hydrogen and synthesis gas production.	2
Fig. 2.1	Equilibrium conversion of steam reforming of methane against temperature, pressure, and steam-to-carbon ratio.	8
Fig. 2.2	Mechanism of the water gas shift reaction (2.2) on Pt/CeO <sub>2</sub> .	18
Fig. 2.3	Crystalline structure of potassium titanate materials.	35
Fig. 3.1	Procedure for synthesis of Ni/K <sub>2</sub> Ti <sub>x</sub> O <sub>y</sub> -Al <sub>2</sub> O <sub>3</sub> catalyst.	38
Fig. 3.2	Schematic drawing of the experimental setup.	43
Fig. 4.1	X-ray diffraction patterns of (a) $\gamma$ -Al <sub>2</sub> O <sub>3</sub> , (b) NiO/Al <sub>2</sub> O <sub>3</sub> and NiO/K <sub>2</sub> Ti <sub>x</sub> O <sub>y</sub> -Al <sub>2</sub> O <sub>3</sub> catalysts with K <sub>2</sub> Ti <sub>x</sub> O <sub>y</sub> loading: (c) NiO/K <sub>2</sub> Ti <sub>x</sub> O <sub>y</sub> (5)-Al <sub>2</sub> O <sub>3</sub> (95), (d) NiO/K <sub>2</sub> Ti <sub>x</sub> O <sub>y</sub> (11)-Al <sub>2</sub> O <sub>3</sub> (89), (e) NiO/K <sub>2</sub> Ti <sub>x</sub> O <sub>y</sub> (20)-Al <sub>2</sub> O <sub>3</sub> (80), (f) NiO/K <sub>2</sub> Ti <sub>x</sub> O <sub>y</sub> (30)-Al <sub>2</sub> O <sub>3</sub> (70), and (g) NiO/K <sub>2</sub> Ti <sub>x</sub> O <sub>y</sub> (50)-Al <sub>2</sub> O <sub>3</sub> (50).	48
Fig. 4.2	H <sub>2</sub> temperature-programmed reduction (TPR) profiles for (a) NiO/Al <sub>2</sub> O <sub>3</sub> and NiO/K <sub>2</sub> Ti <sub>x</sub> O <sub>y</sub> -Al <sub>2</sub> O <sub>3</sub> catalysts with K <sub>2</sub> Ti <sub>x</sub> O <sub>y</sub> loading: (b) NiO/K <sub>2</sub> Ti <sub>x</sub> O <sub>y</sub> (5)-Al <sub>2</sub> O <sub>3</sub> (95), (c) NiO/K <sub>2</sub> Ti <sub>x</sub> O <sub>y</sub> (11)-Al <sub>2</sub> O <sub>3</sub> (89), (d) NiO/K <sub>2</sub> Ti <sub>x</sub> O <sub>y</sub> (20)-Al <sub>2</sub> O <sub>3</sub> (80), (e) NiO/K <sub>2</sub> Ti <sub>x</sub> O <sub>y</sub> (30)-Al <sub>2</sub> O <sub>3</sub> (70), and (f) NiO/K <sub>2</sub> Ti <sub>x</sub> O <sub>y</sub> (50)-Al <sub>2</sub> O <sub>3</sub> (50).	52
Fig. 4.3	Scanning electron microscopy (SEM) images of the Ni catalysts: (a) NiO/Al <sub>2</sub> O <sub>3</sub> , (b) NiO/K <sub>2</sub> Ti <sub>x</sub> O <sub>y</sub> (5)-Al <sub>2</sub> O <sub>3</sub> (95), (c) NiO/K <sub>2</sub> Ti <sub>x</sub> O <sub>y</sub> (11)-Al <sub>2</sub> O <sub>3</sub> (89), (d) NiO/K <sub>2</sub> Ti <sub>x</sub> O <sub>y</sub> (20)-Al <sub>2</sub> O <sub>3</sub> (80), (e) NiO/K <sub>2</sub> Ti <sub>x</sub> O <sub>y</sub> (30)-Al <sub>2</sub> O <sub>3</sub> (70), and (f) NiO/K <sub>2</sub> Ti <sub>x</sub> O <sub>y</sub> (50)-Al <sub>2</sub> O <sub>3</sub> (50).	55



Fig. 4.4	Scanning electron spectroscopy (SEM) and electron dispersive spectroscopy (EDS) mapping images for Al, K, and Ti element on the Ni catalysts: (a)-(f) are same as in Fig. 4.3.	56
Fig. 4.5	Scanning electron spectroscopy (SEM) and electron dispersive spectroscopy (EDS) mapping images for Ni element on the Ni catalysts: (a)-(f) are same as in Fig. 4.3.	57
Fig. 4.6	X-ray photoelectron spectroscopy analysis of NiO/K <sub>2</sub> Ti <sub>x</sub> O <sub>y</sub> -Al <sub>2</sub> O <sub>3</sub> catalyst as a function of K <sub>2</sub> Ti <sub>x</sub> O <sub>y</sub> loading.	59
Fig. 4.7	X-ray photoelectron spectra of O 1s for the Ni catalysts: (a) NOAl <sub>2</sub> O <sub>3</sub> , (b) NiO/K <sub>2</sub> Ti <sub>x</sub> O <sub>y</sub> (5)-Al <sub>2</sub> O <sub>3</sub> (95), (c) NiO/K <sub>2</sub> Ti <sub>x</sub> O <sub>y</sub> (11)-Al <sub>2</sub> O <sub>3</sub> (89), (d) NiO/K <sub>2</sub> Ti <sub>x</sub> O <sub>y</sub> (20)-Al <sub>2</sub> O <sub>3</sub> (80), (e) NiO/K <sub>2</sub> Ti <sub>x</sub> O <sub>y</sub> (30)-Al <sub>2</sub> O <sub>3</sub> (70), and (f) NiO/K <sub>2</sub> Ti <sub>x</sub> O <sub>y</sub> (50)-Al <sub>2</sub> O <sub>3</sub> (50).	61
Fig. 4.8	Comparison of thermodynamic equilibrium value and catalytic activity of Ni/K <sub>2</sub> Ti <sub>x</sub> O <sub>y</sub> (11)-Al <sub>2</sub> O <sub>3</sub> (89) catalyst for steam reforming under the reaction condition: GHSV=15,000 h <sup>-1</sup> , T=750 °C, and time on stream=20 h.	63
Fig. 4.9	Reaction temperature (a) and gas hourly space velocity (b) effects for steam methane reforming over Ni/K <sub>2</sub> Ti <sub>x</sub> O <sub>y</sub> (11)-Al <sub>2</sub> O <sub>3</sub> (89) catalyst for time-on-stream=20 h (the reaction conditions: (a) S/C=2.5 and GHSV=15,000 h <sup>-1</sup> ; (b) S/C=2.5 and T=750 °C).	64



Fig. 4.10	Change in activity of Ni/K <sub>2</sub> Ti <sub>x</sub> O <sub>y</sub> -Al <sub>2</sub> O <sub>3</sub> catalysts and reference catalysts with time-on-stream. (Reaction condition: S/C=1.0, GHSV=200,000 h <sup>-1</sup> , T=800 °C, and time-on-stream=100 h)	69
Fig. 4.11	X-ray diffraction patterns of fresh and spent samples of Ni/K <sub>2</sub> Ti <sub>x</sub> O <sub>y</sub> -Al <sub>2</sub> O <sub>3</sub> catalysts: (a) fresh and (b) spent Ni/Al <sub>2</sub> O <sub>3</sub> , (c) fresh and (d) spent Ni/K <sub>2</sub> Ti <sub>x</sub> O <sub>y</sub> (5)-Al <sub>2</sub> O <sub>3</sub> (95), (e) fresh and (f) spent Ni/K <sub>2</sub> Ti <sub>x</sub> O <sub>y</sub> (11)-Al <sub>2</sub> O <sub>3</sub> (89), (g) fresh and (h) spent Ni/K <sub>2</sub> Ti <sub>x</sub> O <sub>y</sub> (20)-Al <sub>2</sub> O <sub>3</sub> (80), (i) fresh and (j) spent Ni/K <sub>2</sub> Ti <sub>x</sub> O <sub>y</sub> (30)-Al <sub>2</sub> O <sub>3</sub> (70). (Fresh samples were after the reduction pretreatment and spent samples were after the stability test with reaction conditions as in Fig. 4.10).	74
Fig. 5.1	X-ray diffraction patterns of NiO/Al <sub>2</sub> O <sub>3</sub> and NiO/K <sub>2-x</sub> Ca <sub>x/2</sub> Ti <sub>y</sub> O <sub>z</sub> -Al <sub>2</sub> O <sub>3</sub> catalysts.	81
Fig. 5.2	H <sub>2</sub> temperature-programmed reduction (TPR) profiles for NiO/K <sub>2-x</sub> Ca <sub>x/2</sub> Ti <sub>y</sub> O <sub>z</sub> -Al <sub>2</sub> O <sub>3</sub> catalysts with Ca contents.	84
Fig. 5.3	Activity change of steam methane reforming over Ni/K <sub>2-x</sub> Ca <sub>x/2</sub> Ti <sub>y</sub> O <sub>z</sub> -Al <sub>2</sub> O <sub>3</sub> catalysts with Ca content. (Reaction conditions: S/C=2.5, GHSV=15,000 h <sup>-1</sup> , T=750 °C, and time-on-stream=20 h)	87
Fig. 5.4	Change in activity of Ni/Al <sub>2</sub> O <sub>3</sub> and Ni/K <sub>2-x</sub> Ca <sub>x/2</sub> Ti <sub>y</sub> O <sub>z</sub> -Al <sub>2</sub> O <sub>3</sub> catalysts with different Ca content for steam methane reforming. (Reaction conditions as Fig. 4.10)	89
Fig. 6.1	X-ray diffraction patterns of NiO/CaTi <sub>x</sub> O <sub>y</sub> -Al <sub>2</sub> O <sub>3</sub> catalysts with CaTi <sub>x</sub> O <sub>y</sub> loading: (a) NiO/CaTi <sub>x</sub> O <sub>y</sub> (5)-Al <sub>2</sub> O <sub>3</sub> (95), (b) NiO/CaTi <sub>x</sub> O <sub>y</sub> (11)-Al <sub>2</sub> O <sub>3</sub> (89), (c) NiO/CaTi <sub>x</sub> O <sub>y</sub> (20)-Al <sub>2</sub> O <sub>3</sub> (80), and (d) NiO/CaTi <sub>x</sub> O <sub>y</sub> (30)-Al <sub>2</sub> O <sub>3</sub> (70).	94

- Fig. 6.2  $H_2$  temperature-programmed reduction (TPR) profiles for 97  
NiO/CaTi<sub>x</sub>O<sub>y</sub>-Al<sub>2</sub>O<sub>3</sub> catalysts with CaTi<sub>x</sub>O<sub>y</sub> loading: (a)  
NiO/CaTi<sub>x</sub>O<sub>y</sub>(5)-Al<sub>2</sub>O<sub>3</sub>(95), (b) NiO/CaTi<sub>x</sub>O<sub>y</sub>(11)-Al<sub>2</sub>O<sub>3</sub>(89),  
(c) NiO/CaTi<sub>x</sub>O<sub>y</sub>(20)-Al<sub>2</sub>O<sub>3</sub>(80), and (d) NiO/CaTi<sub>x</sub>O<sub>y</sub>(30)-Al<sub>2</sub>O<sub>3</sub>(70).
- Fig. 6.3 Scanning electron microscopy (SEM) images of 99  
NiO/CaTi<sub>x</sub>O<sub>y</sub>-Al<sub>2</sub>O<sub>3</sub> catalysts with CaTi<sub>x</sub>O<sub>y</sub> loading: (a)  
NiO/CaTi<sub>x</sub>O<sub>y</sub>(5)-Al<sub>2</sub>O<sub>3</sub>(95), (b) NiO/CaTi<sub>x</sub>O<sub>y</sub>(11)-Al<sub>2</sub>O<sub>3</sub>(89), (c)  
NiO/CaTi<sub>x</sub>O<sub>y</sub>(20)-Al<sub>2</sub>O<sub>3</sub>(80), and (d) NiO/CaTi<sub>x</sub>O<sub>y</sub>(30)-Al<sub>2</sub>O<sub>3</sub>(70).
- Fig. 6.4 Scanning electron spectroscopy (SEM) and electron 100  
dispersive spectroscopy (EDS) mapping images for Ni,  
O, Al, Ca, and Ti element on the NiO/CaTi<sub>x</sub>O<sub>y</sub>-Al<sub>2</sub>O<sub>3</sub>  
catalysts: (a)-(d) are same as in Fig. 6.3.
- Fig. 6.5 Reaction temperature effect for steam methane 102  
reforming over Ni/CaTi<sub>x</sub>O<sub>y</sub>(20)-Al<sub>2</sub>O<sub>3</sub>(80) catalyst  
under the reaction condition: GHSV=15,000 h<sup>-1</sup>, and  
time on stream=20 h.
- Fig. 6.6 Sulfur-tolerance performances over Ni/CaTi<sub>x</sub>O<sub>y</sub>-Al<sub>2</sub>O<sub>3</sub> 106  
catalysts and reference catalysts for steam methane  
reforming. (Reaction condition: S/C=2.5, GHSV=15,000  
h<sup>-1</sup>, T=750 °C, time-on-stream=300 min, and sulfur  
concentration of 7 ppmv)
- Fig. 6.7 X-ray diffraction patterns of fresh and spent samples of 109  
Ni/CaTi<sub>x</sub>O<sub>y</sub>-Al<sub>2</sub>O<sub>3</sub> catalysts: (a) fresh and (b) spent Ni/Al<sub>2</sub>O<sub>3</sub>, (c) fresh and  
(d) spent Ni/CaTi<sub>x</sub>O<sub>y</sub>(5)-Al<sub>2</sub>O<sub>3</sub>(95), (e) fresh and (f) spent  
Ni/CaTi<sub>x</sub>O<sub>y</sub>(11)-Al<sub>2</sub>O<sub>3</sub>(89), (g) fresh and (h) spent Ni/CaTi<sub>x</sub>O<sub>y</sub>(20)-Al<sub>2</sub>O<sub>3</sub>(80),  
(i) fresh and (j) spent Ni/CaTi<sub>x</sub>O<sub>y</sub>(30)-Al<sub>2</sub>O<sub>3</sub>(70). (Fresh samples were  
after the reduction pretreatment and spent samples were after the  
sulfur-tolerance test with reaction conditions as in Fig. 6.6)

## 1. Introduction

Since the first oil embargo in the 1970s, there has been interest in developing alternative fuels to power global society [1,2]. The decline and stabilization of oil prices following the embargo decreased the interest in alternative fuels. However, with substantial uncertainty in the world today, particularly in the Middle East, increased demand from developing countries has caused the cost of oil to increase substantially in the past few years [3]. In addition to cost there are significant environmental concerns with petroleum usage. Recent analysis estimated that pollutants may be high enough to affect public health and/or the environment in areas where 50% of Americans live [4]. Light vehicles are responsible for a significant amount of carbon dioxide and volatile organic compound (VOC) emissions, and a majority of carbon monoxide and nitrogen oxide (NO<sub>x</sub>) emissions produced in the United States [5]. To deal with these issues, there has been an effort to diversify our energy supply particularly for the transportation sector and to find cleaner fuels. Most of alternative fuels are not available everywhere and require a different engine technology for efficient operation. However, hydrogen can be produced from all of these feedstocks as well as many others making it a universal fuel. Recently there has been international attention on the

development of new hydrogen technologies as a potential solution to the current fears and to increase energy and economic security [6]. In addition to using the hydrogen as energy directly in fuel cells, the hydrogen rich streams can be used for the production of gasoline, methanol, ethanol and other high value chemicals. Fig. 1.1 shows the conceptual flow sheet of hydrogen production technologies. Synthesis gas from a reforming process consists of a mixture of hydrogen and carbon monoxide and is an important intermediate in the industrial syntheses of a wide range of bulk fuels and chemicals [7,8].

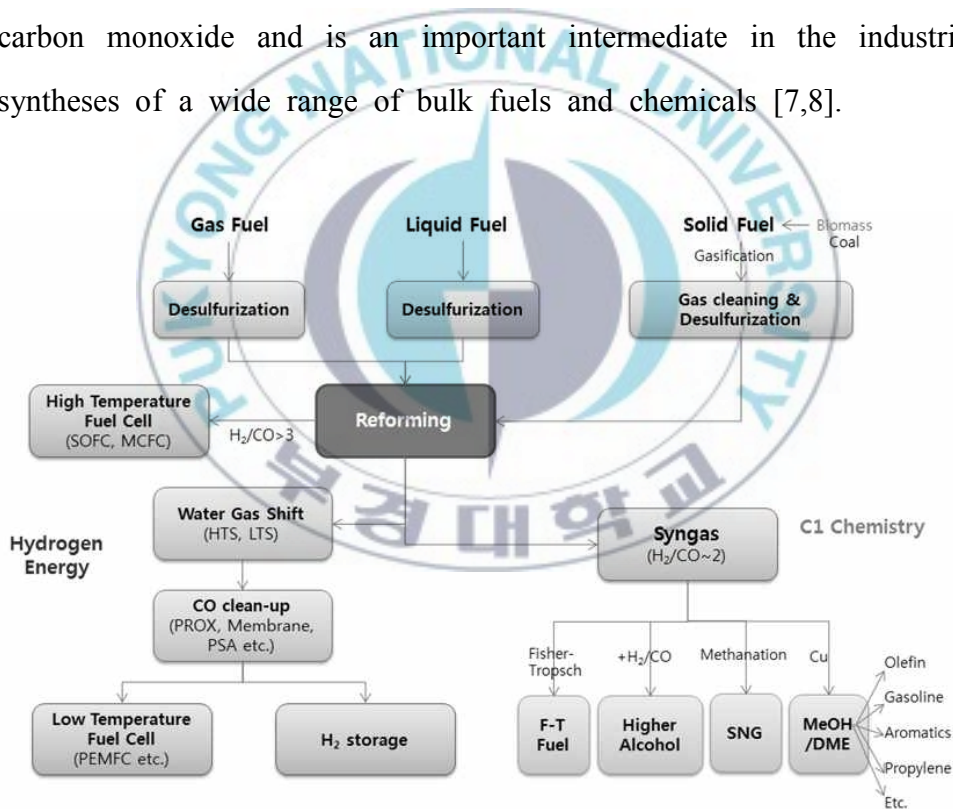


Fig. 1.1 Fuel processing flow sheet for hydrogen and synthesis gas production.

There are three primary techniques used to produce hydrogen from hydrocarbon fuels: steam reforming, partial oxidation (POX), and autothermal reforming (ATR). Table 1.1 summarizes the advantages and challenges of each of these processes. The reforming process produces a gas stream composed primarily of hydrogen, carbon monoxide and carbon dioxide. Endothermic steam reforming of hydrocarbons requires an external heat source. Steam reforming does not require oxygen, has a lower operating temperature than POX and ATR, and produces the reformat with a high  $H_2/CO$  ratio (3/1). Partial oxidation converts hydrocarbons to hydrogen by partially combusting the hydrocarbon with oxygen. It does not require a catalyst for operation and is more sulfur tolerant than the other processes. The process occurs at high temperatures with some soot formation and the  $H_2/CO$  ratio ( $\sim 2/1$ ) is favored for the feeds to hydrocarbon synthesis reactors such as Fischer-Tropsch. Autothermal reforming uses the partial oxidation to provide the heat and steam reforming to increase the hydrogen production resulting in a thermally neutral process. Since POX is exothermic and ATR incorporates POX, these processes do not need an external heat source for the reactor. However, they require an expensive and complex oxygen separation unit in order to feed pure oxygen to the reactor. Steam reforming is typically the preferred process for hydrogen production in industry [9,10].

Table 1.1 Primary technologies used to produce hydrogen (adapted from [6])

Technology	Traits	Pros	Cons
Steam reforming	<ul style="list-style-type: none"> <li>•H<sub>2</sub>, CO, CO<sub>2</sub> product</li> <li>•Typically preferred process for hydrogen production in industry</li> <li>•Strong endothermic</li> </ul>	<ul style="list-style-type: none"> <li>•Most extensive industrial experience</li> <li>•Oxygen not required</li> <li>•Lowest process temperature</li> <li>•Best H<sub>2</sub>/CO ratio for H<sub>2</sub> production (~4.0)</li> </ul>	<ul style="list-style-type: none"> <li>•Highest air emissions</li> <li>•Requires an external heat source</li> </ul>
Partial oxidation	<ul style="list-style-type: none"> <li>•Combustion</li> <li>•Exothermic</li> <li>•Catalytic POX</li> </ul>	<ul style="list-style-type: none"> <li>•Decreased desulfurization requirement</li> <li>•No catalyst required</li> <li>•Low methane slip</li> </ul>	<ul style="list-style-type: none"> <li>• Low H<sub>2</sub>/CO ratio (1.0-2.0)</li> <li>• Very high processing temperatures</li> <li>• Soot formation/handling adds process complexity</li> </ul>
Autothermal reforming	<ul style="list-style-type: none"> <li>•SR+POX</li> <li>•Thermally neutral</li> </ul>	<ul style="list-style-type: none"> <li>• Lower process temperature than POX</li> <li>• Low methane slip</li> </ul>	<ul style="list-style-type: none"> <li>• Limited commercial experience</li> <li>• Requires air or oxygen</li> <li>• Requires Expensive, complex separation unit</li> </ul>



The work presented in this dissertation examined the activity of steam methane reforming to hydrogen-rich stream using  $\text{MTi}_x\text{O}_y$  ( $\text{M}=\text{K}$  and/or  $\text{Ca}$ )–added nickel-based catalysts. There were two motivations on this research of the nickel-based catalyst modified by using  $\text{MTi}_x\text{O}_y$  as an additive. First, it is widely accepted that alkali (earth) metals such as potassium and calcium can inhibit carbon deposition on the active metal and titanium oxide has resistance to sulfur poisoning on catalysts surface for various reactions [11,12]. Next, potassium titanate-promoted nickel catalyst showed a stable activity for internal reforming in anode side of solid oxide fuel cell [13]. In particular, it is a solution to the drawback of potassium which is easy to loss for long operation at high reaction temperature.

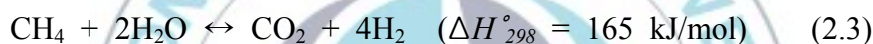
The objective of this study is to evaluate the promoting effect of potassium (and/or calcium) titanate in a nickel catalyst for steam methane reforming. In addition to activity and stability of the nickel catalyst for the reaction, it contains the investigating the relationship between physicochemical properties of the titanate-promoted nickel catalysts and their stable activity through characterizing the catalysts.



## 2. Literature survey

### 2.1. Thermodynamics

Steam reforming of methane consists of three reversible reactions: the strongly endothermic reforming reactions, (2.1) and (2.3), and the moderately exothermic water-gas shift (WGS) reaction (2.2) [14].



CO<sub>2</sub> is not only produced through the shift reaction (2.2), but also directly through the steam reforming reaction (2.3). In fact, reaction (2.3) results from the combination of reaction (2.1) and (2.2). Because of the endothermic behavior of steam reforming, high temperature is favored. In addition, because volume expansion occurs, low pressure is favored. In contrast, reaction (2.2) the exothermic reaction is favored by low temperature, while changes in pressure have no effect. Reforming reactions (2.1) and the associated water gas shift reaction (2.2) are carried out normally over a supported nickel catalyst at elevated temperatures, typically above 500°C.

Reactions (2.1) and (2.3) are reversible and normally reach

equilibrium over an active catalyst, at high temperatures. The overall product gas is a mixture of carbon monoxide, carbon dioxide, hydrogen, and unconverted methane and steam. The temperature of the reactor, the operating pressure, the composition of the feed gas, and the proportion of steam fed to the reactor governs the product from the reformer. The amount of carbon monoxide produced through steam reforming of methane is quite high; because the water gas shift reaction, shown in equation (2.2), is thermodynamically favorable at higher temperatures. The amount of carbon monoxide in the final product from the steam reforming of methane is determined by the thermodynamics and kinetics of the reaction within the reformer. This also determines the downstream processes necessary to reduce CO concentration, which is desired by proton-exchange membrane. This is accomplished by a combination of WGS reactions at lower temperatures and the preferential oxidation reaction.

Joensen and Rostrup-Nielsen showed a typical equilibrium conversion graph of steam reforming of methane against temperature, pressure and steam/carbon ratio [15]. As shown in Fig. 2.1, thermodynamic equilibrium calculations carried out by HSC Chemistry 5 software were matched to the reference [15]. It can be observed from those data that in order to maintain a high methane conversion, it is necessary to operate the system at high temperature, low

pressure, and relatively high steam-to-carbon ratio.

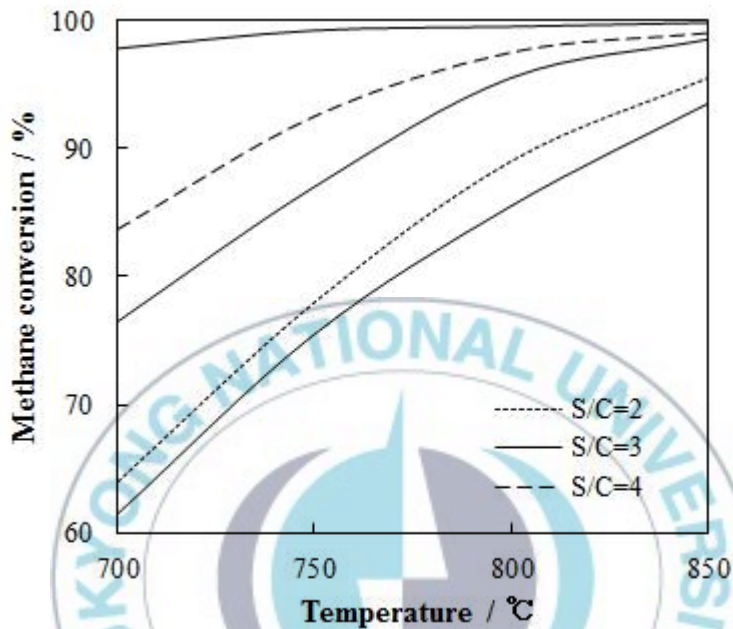


Fig. 2.1 Equilibrium conversion of steam reforming of methane against temperature, pressure, and steam-to-carbon ratio.

In practice, the steam reforming process is divided in two sections: a section at high temperature and pressure (typically 800–1000°C and 30–40 bar) in which the reforming and shift reactions occur, followed by an additional (two step) shift-section at lower temperature (typically 200–400°C) in order to maximize the CO conversion via reaction (2.2). In such a process CO concentrations as low as 0.1% can be achieved.

## **2.2. Steam methane reforming catalysts**

The higher the active surface area of the catalyst, the greater the number of product molecules produced per unit time. Therefore, much of the art and science of catalyst preparation deals with high-surface-area materials (typically 100–400 m<sup>2</sup>/g). These are prepared in such a way that they are often crystalline with well-defined microstructures and behave as active components of the catalyst system in spite of their accepted name 'supports'. The (transition) metal atoms are then deposited in the micropores, and the sample is subsequently heated and reduced to produce small metal particles, ideally 10–10<sup>2</sup> Å in size with virtually all the atoms located on the surface.

### **2.2.1. Active metal**

For steam-reforming, usually Ni or the noble metals Ru, Rh, Pd, Ir, Pt are used as the active metal in catalysts. Because of its low costs, Ni is the most widely used metal among these set. However, Ni is less active (Table 2.1) and usually more prone to deactivation by carbon formation or oxidation.

Table 2.1 Relative activities for steam methane reforming [16]

Catalyst metal content (wt.%)	Relative rate
Ni (16)	1.0
Ru (1.4)	2.1
Rh (1.1)	1.9
Pd (1.2)	0.4
Ir (0.9)	1.1
Pt (0.9)	0.5

Reaction condition: S/C=4, T=550°C, and P=1 bar.

The activity of a catalyst is related to the metal surface area (i.e. the number of active sites). This implies that, generally, the catalytic activity benefits from a high dispersion of the metal particles. Common dispersions for Ni catalysts are of 2–5%, with metal particles of 20–50 nm [7]. There is an optimum beyond which an increase in Ni-content does not produce any increase in activity, usually around 15–20 wt.%, depending on support structure and surface. Although the nickel surface area is generally increased with higher loadings, the dispersion or utilization of the nickel tends to decrease with increasing nickel content. Hence, the activity will not increase any further.

Apart from the amount of available metal surface area, also the structure of the available surface area strongly influences the catalyst activity. For example, the close-packed (111) surface of nickel is less active than the more open (110) surface. In fact, metal atoms in surface steps and near defects are much more reactive than metal atoms in the higher coordinated surface terrace sites. For instance, it is known that Ni particles are composed of a number of single crystals (i.e. the metal particles are polycrystalline) [17], which, however, are not completely 'space filling'. Therefore, some lattice distortion is required and these dislocations are expected to play a role in the catalytic reaction [18]. This agrees with the conclusions of Wei and Iglesia [19], who investigated the catalytic activity of catalysts with different loadings of Rh on  $\text{Al}_2\text{O}_3$  and  $\text{ZrO}_2$  supports. They found that  $\text{CH}_4$  reforming turnover rates increased as the size of Rh clusters decreased, suggesting that coordinatively unsaturated Rh surface atoms prevalent in smaller clusters activate C-H bonds more effectively than atoms on lower-index surfaces. This is confirmed by the results of the theoretical studies performed by Nørskov and co-workers [20,21], which indicate that steps are much more reactive than the close-packed surface. They also investigated the negative effect of K on the activity of Ni-catalysts. They found that K blocks sites at step edges, thereby inhibiting the role of steps in the reaction



process.

In contrast with the discussion above, however, it was concluded by Rostrup-Nielsen et al. [7 and references therein] that the activity per unit metal surface area (the specific activity) decreases with increasing dispersion (i.e. with smaller metal crystal size). This effect may be explained by a decrease of large ensemble landing sites [22] on the smaller particles (i.e. an entropy-effect). Alternatively, it may be explained in terms of a change in electronic state of the metal particles: Yokota and co-workers [23] showed for Rh-based catalysts that a higher dispersion may result in a less metallic character of the Rh particles. Still, the reasons for these discrepancies remain unclear.

The synergism between different metals has also been investigated. For instance, Rh-promoted Ni/ $\alpha$ -Al<sub>2</sub>O<sub>3</sub> was found to possess higher activity than either Ni/ $\alpha$ -Al<sub>2</sub>O<sub>3</sub> or Rh/ $\alpha$ -Al<sub>2</sub>O<sub>3</sub> catalysts in the methane reforming with CO<sub>2</sub> [24]. In this case, Rh improved the dispersion of Ni, retarded the sintering of Ni, and increased the activation of CO<sub>2</sub> and CH<sub>4</sub>. Several works were dedicated to study the properties of Au [25-27], Ag [28], Pt [29], Pd, Rh [30], or Ru [31] as a promoter in Ni catalysts suppressing deactivation of the catalysts.



### 2.2.2. Catalyst support

The influence of the support on the steam-reforming reaction can be underestimated. It determines the dispersion of the catalytically active metal particles or the catalyst's resistance to sintering. It also affects the reactivity and coke resistance of the metal particles, and may even participate in the catalytic reaction itself. In other words, the support is a fundamental part of the catalyst.

#### 2.2.2.1. Effect of support property

Literally, the role of the support is to provide a support for the catalytically active metal, in order to obtain a stable and high active surface area. Among the most common supports for methane reforming are  $\alpha$ - and  $\gamma$ - $\text{Al}_2\text{O}_3$ ,  $\text{MgO}$ ,  $\text{MgAl}_2\text{O}_4$ ,  $\text{SiO}_2$ ,  $\text{ZrO}_2$ , and  $\text{TiO}_2$ . These supports have good porosity, which results in a long contact-time between reactants and catalyst. Maintaining a high active surface area is also important: the support can affect the migration and coalescence of metal particles in various ways. Pore structure, morphology, and phase transitions of the support determine the final particle size of the metal.

Obviously, due to the nature of the chemical bonding between the support and the metal atoms, the electronic properties of the metal is affected. For example, acidity in the support is known to facilitate the

decomposition of methane, but it will also promote cracking and polymerization, producing carbon. In general, a strong interaction between metal and support makes a catalyst more resistant to sintering and coking, thus resulting in a longer time of catalyst stability [32].

Apart from the common supports, various support materials were investigated:  $\text{CeO}_2$  [33-35], hydrotalcite-like compounds [36], perovskites (i.e.  $\text{LaAlO}_3$ ,  $\text{LaFeO}_3$ ,  $\text{SrTiO}_3$ , and  $\text{La}_{0.4}\text{Ba}_{0.6}\text{Co}_{0.2}\text{Fe}_{0.8}\text{O}_{3-\delta}$ ) [37], and so on.

Bradford *et al.* [38] found for Ni/MgO catalysts that formation of a partially reducible NiO-MgO solid solution appeared to stabilize surface Ni-Ni bonds and prevent carbon diffusion into nickel particles. They suggest that indeed the support influences the catalyst activity by altering the electron donating ability of the reduced nickel surfaces. In addition they found that a strong metal-support interaction emerges for Ni/TiO<sub>2</sub> catalysts which leads to blockage of the active nickel sites due to migration of TiO<sub>x</sub>-species from the TiO<sub>2</sub>-carrier [38-40]. As a result of this site blocking, carbon formation is drastically reduced on Ni/TiO<sub>2</sub>. In contrast, it was concluded that a lack of metal-support interaction in Ni/SiO<sub>2</sub> permitted substantial formation of filamentous whisker carbon.

The effect of the support on the electronic properties of the catalytically active metal is also illustrated by Yokota and co-workers

[23]. They found that 0.5 wt% Rh on SiO<sub>2</sub> is more active than 0.5 wt% Rh on  $\gamma$ -Al<sub>2</sub>O<sub>3</sub> for the CH<sub>4</sub> reforming reaction with CO<sub>2</sub> at 700°C, despite the higher dispersion of Rh on  $\gamma$ -Al<sub>2</sub>O<sub>3</sub>. This seemingly contradictory result is probably caused by the fact that a stronger metal-support interaction exists for Rh on  $\gamma$ -Al<sub>2</sub>O<sub>3</sub>. Accordingly, the Rh/ $\gamma$ -Al<sub>2</sub>O<sub>3</sub> system tends to maximize its number of metal-support bonds, resulting in a higher dispersion. Then, as a consequence of this stronger metal-support interaction, Rh loses its metallic character (i.e. electrons are withdrawn from Rh) and because of that, Rh possesses a rather cationic character on  $\gamma$ -Al<sub>2</sub>O<sub>3</sub>, resulting in the formation of less reactive Rh<sub>2</sub>O<sub>3</sub>-like structures.

In contrary, Wei and Iglesia claim that the support does not influence the turnover frequency of methane activation for Rh/Al<sub>2</sub>O<sub>3</sub> and Rh/ZrO<sub>2</sub> catalysts in the CO<sub>2</sub> and H<sub>2</sub>O reforming of methane [19].

For *amorphous* CeO<sub>2</sub> as a support for Pd catalysts, a strong metal-support interaction leads to partial encapsulation of Pd particles, resulting in significantly reduced catalytic activity for steam reforming [33].

For more complex supports, synergetic effects can appear. For instance, Ni supported on MgO–CaO showed high basicity and lower coke forming ability, attributed to the addition of CaO [41]. Roh et

al.[34] combined a gamma-alumina support with 30% MgO obtained from Sasol. They found that nickel dispersion was 12% and constant activity was maintained for one day, and the methane conversion for SMR over Ni/MgO-Al<sub>2</sub>O<sub>3</sub> improved by more than 25% as compared to the non-promoted Ni/Al<sub>2</sub>O<sub>3</sub>. Temperature-programmed reduction (TPR) results of the catalyst indicated a strong metal-support interaction in the Ni-MgO-Al<sub>2</sub>O<sub>3</sub> system, as shown by the high temperatures required to reduce nickel species. For another example, Al<sub>2</sub>O<sub>3</sub>-CeO<sub>2</sub> is known for its catalytic stability and coking resistance, whereas CeO<sub>2</sub> itself may lead to significantly reduced catalytic activity [42]. In the case of the combined Al<sub>2</sub>O<sub>3</sub>-CeO<sub>2</sub> support, the beneficial effects (i.e. high porosity and increased stability) of both supports are utilized [33,43] – at least, when crystalline (i.e. oxidized) instead of amorphous (i.e. reduced) CeO<sub>2</sub> is used, as mentioned above. In fact, CeO<sub>2</sub> is actually contributing the reaction mechanism itself.

#### 2.2.2.2. Roles of support in catalytic reactions

In addition to the effects of the support on catalytic activity, the support may also actively participate in the catalytic reaction itself. For instance, supports with a basic nature, such as MgO, are known to enhance the activation of steam (i.e. dissociation into reactive OH and H species). Also, stabilization of different CH<sub>x</sub>-intermediates

contributes to the overall reaction mechanism.

An important factor for catalyst reactivity and stability lies in the catalyst's resistance to carbon deposits, which could lead to active site blocking. There is a route to use a support which suppresses carbon deposition. This can be achieved with so-called oxy-transporters, such as  $\text{ZrO}_2$  or  $\text{CeO}_2$ , which are capable of oxidizing deposited carbon. Additionally, because of their oxygen conducting properties, these supports can actively participate in the catalytic reaction by oxidizing or reducing reaction intermediates. As an example, the role of  $\text{CeO}_2$  in the water gas shift reaction (2.2) is shown in Fig. 2.2. The oxygen transport properties of  $\text{CeO}_2$  and their involvement in the WGS reaction are clearly illustrated. Also, the synergism between Pt and  $\text{CeO}_2$  is apparent: while Pt activates CO,  $\text{CeO}_2$  activates  $\text{H}_2\text{O}$  and provides the required oxygen for the oxidation of CO.

The role of ceria-containing supports has attracted a lot of attention in recent catalyst research. Especially  $\text{CeO}_2\text{-Al}_2\text{O}_3$ ,  $\text{Ce}_x\text{Zr}_{1-x}\text{O}_2$ , and  $\text{CeZrO}_x\text{-Al}_2\text{O}_3$  supports are extensively investigated. For instance, Dong et al. [45] investigated methane reforming over  $\text{Ni/Ce}_{0.15}\text{Zr}_{0.85}\text{O}_2$  catalysts. They concluded that two kinds of active sites exist, one for methane activation (on Ni) and one for steam or oxygen activation (on the  $\text{Ce}_x\text{Zr}_{1-x}\text{O}_2$ -support). This is in line with the mechanism for WGS shown in Fig. 2.2: Due to the addition of ceria, the ability to

store, release, and transfer oxygen species is acquired, resulting in an enhanced ability to prevent carbon formation that would normally accumulate on the metal or metal-support interface.

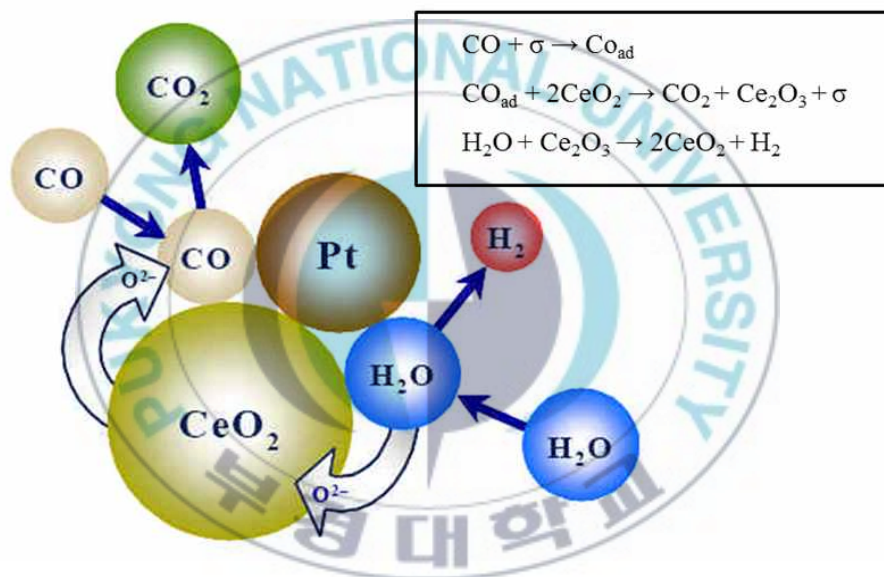


Fig. 2.2 Mechanism of the water gas shift reaction (2.2) on Pt/CeO<sub>2</sub> [44].



Another intriguing example of active involvement of the support during the reforming of  $\text{CH}_4$  is observed by Zhang and Verykios [39,46]. They reported that the  $\text{Ni/La}_2\text{O}_3$  catalyst showed high stability during the reaction of  $\text{CH}_4$  with  $\text{CO}_2$ , because an alternate reaction pathway occurred at the  $\text{Ni/La}_2\text{O}_3$  interface. They proposed a mechanism in which  $\text{CH}_4$  mainly cracks on the Ni crystallites to form  $\text{H}_2$  and surface carbon species ( $\text{CH}_x$ ), while  $\text{CO}_2$  preferably adsorbs on the  $\text{La}_2\text{O}_3$  support to form  $\text{La}_2\text{O}_2\text{CO}_3$  species. The nickel particles are partially covered by these  $\text{La}_2\text{O}_2\text{CO}_3$  species, which participate directly in reactions with surface carbon species on the neighbouring Ni sites to form CO. Due to the existence of such synergetic sites which consist of Ni and La elements, the deposited carbon on the Ni sites is favorably removed by the oxycarbonate species originating from  $\text{La}_2\text{O}_2\text{CO}_3$ , thus resulting in an active and stable performance.



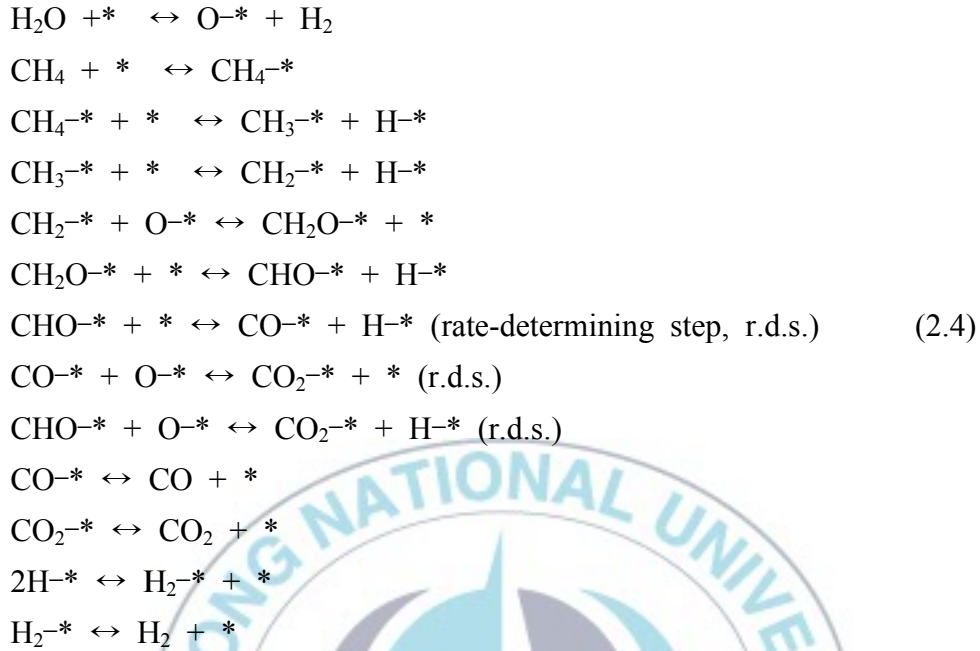
### 2.3. Reaction mechanism of steam methane reforming

The reaction mechanism of the steam-reforming process strongly depends on the catalyst, i.e. on the catalytically active metal and the nature of the support. In this section, ‘conventional’ reaction mechanisms are discussed on ‘standard’ catalyst, providing insight into typical reaction steps and rate limiting steps.

Xu and Froment [47] extensively studied the kinetic and mechanistic details of steam-methane reforming on a  $\text{Ni/MgAl}_2\text{O}_4$  catalyst. They arrived at the following reaction mechanism:

1.  $\text{H}_2\text{O}$  reacts with surface nickel atoms, yielding adsorbed oxygen and gaseous hydrogen.
2. The  $\text{H}_2$  formed is directly released into the gas phase and/or the gaseous  $\text{H}_2$  is in equilibrium with adsorbed H and  $\text{H}_2$ .
3. Methane is adsorbed on surface nickel atoms. The adsorbed methane either reacts with the adsorbed oxygen or dissociates to form chemisorbed radicals,  $\text{CH}_x$  with  $x = 0.3$ .
4. The adsorbed oxygen and the carbon-containing radicals react to form chemisorbed  $\text{CH}_2\text{O}$ ,  $\text{CHO}$ ,  $\text{CO}$ , or  $\text{CO}_2$ .
5.  $\text{CO}$  and  $\text{CO}_2$  are formed out of  $\text{CHO}$  and  $\text{CH}_2\text{O}$  species.

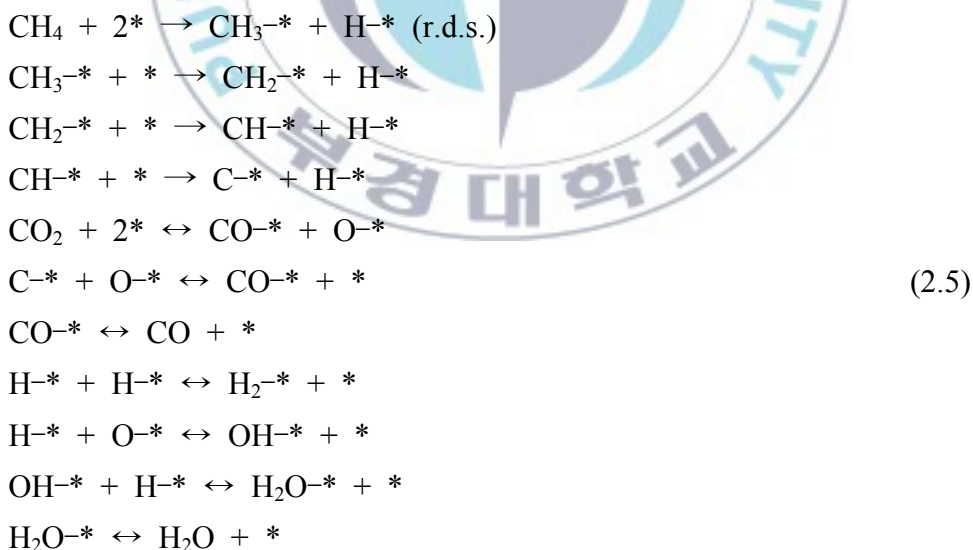
This results in the following reaction scheme (‘\*’ denotes a surface site):



This model nicely illustrates the many possible steps involved in the steam reforming of methane. It should be noted, however, that Rostrup-Nielsen *et al.* [21] argue that the model by Xu and Froment is not consistent with the current understanding of methane dissociation, which has been shown not to proceed via an adsorbed precursor state [48].

Wei and Iglesia [19] investigated the mechanisms for the reactions of  $\text{CH}_4$  with  $\text{CO}_2$  and  $\text{H}_2\text{O}$  on Rh clusters. Interestingly, they found that reaction rates were proportional to  $\text{CH}_4$  partial pressure, but independent of  $\text{CO}_2$  and  $\text{H}_2\text{O}$  pressures, which leads to the conclusion of sole kinetic relevance of C-H bond activation steps. Their data

indicate that co-reactant (CO<sub>2</sub> or H<sub>2</sub>O) activation and its kinetic coupling with CH<sub>4</sub> activation via scavenging of chemisorbed carbon intermediates are fast steps and lead to Rh surfaces essentially uncovered by reactive intermediates. It was also shown that C-H bond activation elementary steps are irreversible and that recombinative desorption steps of H atoms with OH groups to form H<sub>2</sub> or H<sub>2</sub>O are quasi-equilibrated. The quasi-equilibrated nature of these and other steps confirms that water-gas shift reaction (2.2) is also at equilibrium. And remarkably, any involvement of the support in the activation of co-reactants was found not to be kinetically relevant. They then arrive at the following mechanism for CH<sub>4</sub> activation:



When ‘\*’ is the most abundant surface intermediate, it is found

that only the rate constant for the  $\text{CH}_4 + 2^* \rightarrow \text{CH}_3^* + \text{H}^*$  reaction appears in the rate expression and the overall  $\text{CH}_4$  conversion rates become proportional to  $\text{CH}_4$  concentration and independent of the identity or concentration of co-reactants.

Note the fundamental difference in rate determining steps between Eqs. (2.4) and (2.5). The first mechanism indicates that reactions of carbon-intermediates with adsorbed oxygen are rate determining, suggesting that the properties of the oxygen present may determine to a large extent the reaction kinetics. This again emphasizes the possible importance of a oxygenconducting support, such as ceria. On the other hand, the second mechanism indicates that the reactivity of the metal towards C-H bond breaking governs the overall reaction kinetics. This emphasizes the importance of the catalytic activity of the metal. In general, a well-balanced interplay between the metal and support will undoubtedly lead to the best catalytic performance.

## 2.4. Challenges for steam methane reforming catalyst

There can be many reasons for catalyst deactivation. Understanding the causes of deactivation and developing new catalysts that are more resistant to poisoning are constant concerns of the catalytic chemist. It should be mentioned here that a distinction between poisoning and thermal deactivation can be made: If, on continued use, the activity decreases more rapidly than surface area, then poisoning may be suspected, whereas, if a decrease in surface area is concomitant with a decrease in activity, then thermal deactivation is indicated.

### 2.4.1. Sintering

Sintering is the process of agglomeration of the crystallites of the active phase, which leads to loss of active surface and, consequently, a decrease in activity. Apart from reduced dispersion, also ideally shaped crystallites are formed, which are generally less reactive. According to the Rule of Tammann, sintering is generally to be expected at temperatures above  $0.5T_m$ , where  $T_m$  is the melting temperature of the metal in Kelvin. Surface diffusion is already expected to occur above  $0.33T_m$  (Huttig Temperature).

The actual rate and extent of sintering depends on many factors,

including the metal concerned, the metal content, initial crystallite size and size distribution, the dispersion of the metal across the support, the nature of the support material and the operating conditions. The most important factors are the temperature and the atmosphere in contact with the catalyst: elevated temperatures and the presence of water significantly enhance sintering. Also, sintering tends to be faster for narrow particle size distributions on the support. It has been proposed that the pore structure, morphology, and phase transitions of the support determine the final particle size of the metal [7].

In most catalytic processes the temperatures and the size of the metal crystallites are such that, without the presence of a support, extensive agglomeration would occur in seconds. The effectiveness of the support in hindering metal movement and the movement of the support itself, factors controlled primarily by catalyst formulation, are thus of great importance.

The aggregation of metal particles necessarily involves the transport of metal within the catalyst, although it is often difficult to determine whether this occurs by the migration of metal atoms (Ostwald ripening) or by crystallite migration and coalescence. Alternatively, sintering may occur by atoms through the gas phase (usually promoted by poisons or reactants which form compounds with the metal) [7].

For both of these surface migration processes, the driving force for sintering is the difference in particle surface energy, which varies inversely with particle size. In both processes, sintering slows down with time and results in a semi-stable state, with characteristic particle size distributions.

Most studies of sintering indicate that the particle migration and coalescence is the preferred process over atom migration, although experiments suggest that at higher temperatures atom migration becomes more dominant [21 and references therein].

#### **2.4.2. Oxidation**

Oxidation of the metal particles may occur at a high steam-to-carbon ratio and a low catalyst activity. Especially nickel catalysts are prone to oxidation. Since the catalytically active phase is the metallic phase, oxidation leads to deactivation of the catalyst. Usually, nickel catalysts are activated by reducing with a hydrogen-rich gas, prior to steam-reforming operation. Noble metal catalysts are generally not sensitive to oxidation [10].

Preferential oxidation of (poor) Ni catalysts readily occurs at low temperatures (below 500°C) and has under these conditions an even stronger deactivating effect than carbon formation [49,50]. This can be understood if one realizes that, at low temperatures, CH<sub>4</sub> conversion is



low and hence, the oxidizing  $\text{H}_2\text{O}$  concentration is high and the reducing  $\text{H}_2$  concentration is low. Under 'regular' steam-reforming conditions though, sufficient hydrogen will be present to keep most of the active nickel surface reduced.

#### 2.4.3. Sulfur poisoning

Many of the catalyst poisons act by blocking active surface sites. In addition, poisons may change the atomic surface structure in a way that reduces the catalytic activity. Sulfur is the most severe poison for steam reforming catalysts. The sensitivity of the reforming catalyst to poisoning increases at lower operating temperatures. So, while poisoning of the (nickel) catalyst occurs with about 5 ppm of sulfur in the feed gas at a temperature of  $800^\circ\text{C}$ , concentrations of the order of 0.01 ppm poison the catalyst already at  $500^\circ\text{C}$ . This can be understood if one realizes that the poisoning process can be represented by a simple exothermic adsorption process. It is known that sulfur actually changes the surface structure of nickel (adsorbate induced surface reconstruction) [51].

Sulfur is, under reforming conditions, present in the form of  $\text{H}_2\text{S}$ , which is chemisorbed on transition-metal surfaces [10]:



In principle, it is possible to regenerate the poisoned catalyst by treatment with hydrogen [the reverse of reaction (2.6)], but the driving force is extremely small. Alternatively, sulfur may be removed by oxidation and controlled re-reduction of the catalyst.

#### **2.4.4. Carbon formation**

At the operating temperatures some of the reactant  $\text{CH}_x$ -species may completely decompose and deposit a thick layer of inactive carbon on the catalyst surface (coke). Especially with nickel based catalysts, steam reforming involves the risk of carbon formation, which may cause serious operational problems and catalyst deactivation. Generally, higher hydrocarbons are more prone to carbon formation than methane. This is related to the fact that for higher hydrocarbons the initial surface carbon intermediates are more readily formed. The concentration of these intermediates is an important factor, and is critical in influencing the delicate balance between carbon-forming and carbon-removing reactions.

On nickel surfaces, carbon formation may take place mainly by three routes, as summarized in Table 2.2.

Table 2.2 Routes to carbon formation [52]

Carbon type	Reactions involved	Phenomena	Critical parameters
Gum	$C_nH_m \rightarrow (CH_2)_n \rightarrow \text{gum}$	Blocking of surface by polymerization of adsorbed $C_nH_m$ radicals: progressive deactivation	Low S/C ratio, absence of $H_2$ , low temperature (below $\sim 500^\circ\text{C}$ ), presence of aromatics
Whisker carbon, amorphous carbon	$CH_4 \rightarrow C + 2H_2$ $2CO \rightarrow C + CO_2$ $CO + H_2 \rightarrow C + H_2O$ $C_nH_m \rightarrow nC + m/2H_2$	Break-up of catalyst pellet (whisker carbon: <i>no</i> deactivation of the surface)	Low S/C ratio, high temperature (above $\sim 450^\circ\text{C}$ ), presence of olefins, aromatics
Pyrolytic coke	$C_nH_m \rightarrow \text{olefins} \rightarrow \text{coke}$	Encapsulation of catalyst pellet (deactivation), deposits on tube wall	High temperature (above $\sim 600^\circ\text{C}$ ), high residence time, presence of olefins, sulfur poisoning

At lower temperatures (500°C and below), adsorbed hydrocarbons may accumulate on the surface and slowly be transformed into a non-reactive polymer film ('gum') blocking and deactivating the surface. This phenomenon can be retarded by hydrogen. Note that because of the endothermic nature of the steam-reforming reaction, high catalyst activity leads to a low temperature at the reaction site, resulting in a higher risk for carbon formation.

At higher temperatures, whisker carbon is the principal product of carbon formation on nickel catalysts. The underlying mechanism is quite comprehensive, it involves diffusion of carbon atoms through the metal particles [7].

The rate of carbon formation was found to be far less on noble metals than on nickel [16]. This result may be explained by the fact that the noble metals do not dissolve carbon. The carbon formed on the noble metals was observed to be of a structure that was difficult to distinguish from the catalyst structure.

The carbon formation depends on the kinetic balance between the surface reaction of the adsorbed hydrocarbons with oxygen species and the further dissociation of the hydrocarbon into adsorbed carbon atoms.

For a given hydrocarbon feed, temperature and pressure, carbon will be formed below a critical steam-to-carbon ratio (S/C) [21,53].

This critical S/C ratio increases with temperature and is dictated by thermodynamics. In practice however, carbon formation generally occurs before the thermodynamic limit is reached (e.g., by poisons, temperature and concentration gradients, etc.). By promotion of the catalyst, it is possible to push the carbon formation limit to the thermodynamic limit. For instance, Haldor Topsoe A/S developed a process (SPARG) in which by 'controlled passivation' of the catalyst surface by sulfur, carbon deposition is inhibited [54]. By using noble metal catalysts, it is possible to push the carbon limit even beyond the thermodynamic limit.

As already indicated in Table 2.2, not all carbon formation necessarily leads to catalyst deactivation. It is the nature of the deposited carbon that determines to what extent the catalytic activity will be affected. For instance, for dry reforming of methane it is shown that the relative ease with which carbon is removed (oxidized) from the surface affects the catalytic activity more than the actual amount of carbon that is present on the catalyst surface [42]. It was concluded that graphitic carbon is more reactive than amorphous carbon, which in turn causes the varying catalytic activity and stability of the catalyst. This is consistent with Table 2.2: 'Whisker carbon', which does not necessarily lead to deactivation, is known to be graphitic [7].

## 2.5. Catalyst promotion

A promoter may increase the surface area available for adsorption and reaction, it may inhibit unwanted side reactions to occur, or it may increase the catalyst activity per unit surface area. In the latter case, promoters are usually electron donors (alkali metals) or electron acceptors (halogens), which act as bonding modifiers for adsorbed reactants. (In principle, modifications to the support as discussed in Section 2.2.2, should also be considered as promoters. In literature, modifying the support is also termed 'doping'.)

In the case of methane reforming, the purpose of a promoter is usually to inhibit carbon deposition on the active metal. In practice, suppression of carbon formation on (Ni-based) catalysts is usually achieved by adding small amounts of an alkali metal to the catalyst. As discussed in Section 2.2.2.1, acidic supports will promote cracking of methane, and thus producing carbon. Introducing basicity into the catalyst by addition of alkali metals will therefore suppress carbon formation. A different point of view to the promoting effect of alkali metals is given by Bengaard et al. [20]. Their theoretical studies using density functional theory (DFT) indicated that on Ni surfaces, potassium forms rows with oxygen along steps. Based on these results, it was suggested that the major carbon-preventing effect of these promoters is to block the steps and hence remove the nucleation



sites for graphite formation. In this case, addition of promoters decrease the activity of the catalyst [21].

The decrease should be determined by the promoter coverage at steps. The promoters need not cover all step sites to prevent carbon (graphene) nucleation, because a graphene island of a certain finite size is needed for it to be stable. Promotion can therefore hamper graphite formation without destroying the activity completely. As an alternative to K, it was suggested to promote the catalyst with Au. The decoration of steps with gold would be more effective, because Au will spread out along the step, whereas the interaction of potassium with oxygen leads to attractive interactions between the potassium atoms. The addition of less than almost complete step coverage will lead to a fraction of the steps being completely covered while the rest are free and open for reaction. This implies that promotion will decrease activity, but the activation energy should be unaltered because the nature of the active site does not change.

Additives other than alkali metals which suppress carbon formation on nickel catalysts are also reported, e.g.,  $\text{MoO}_3$  [55] and Mn [56].



## 2.6. Property of potassium titanate

Crystalline structure of potassium titanate is composed to type of  $K_2O \cdot nTiO_2$ , with  $n = 1, 2, 4, 6$ , and  $8$ . Among those potassium titanate with different  $n$  value, both  $K_2O \cdot TiO_2$  and  $K_2O \cdot 2TiO_2$  ( $n=1$  and  $2$ ) materials have titanate structure with layered ordering, in which potassium ions are sandwiched between titanate layers (Fig 2.3). Those potassium ions have portable property, unlike potassium ions of  $K_2O \cdot nTiO_2$  with higher  $n$  than  $2$ . Therefore, potassium titanate with  $K_2O \cdot nTiO_2$  ( $n=1$  or  $2$ ) are used in ion-exchanger, photo-catalyst, and host materials for intercalation of organic compounds. This property, portable potassium ions sandwiched with titanate layers, can make potassium more stable in catalysis by a promoter without loss [13].

On the other hand,  $K_2O \cdot nTiO_2$  ( $n>4$ ) has been applied to advanced reinforcing materials for brakes (by DuPont).

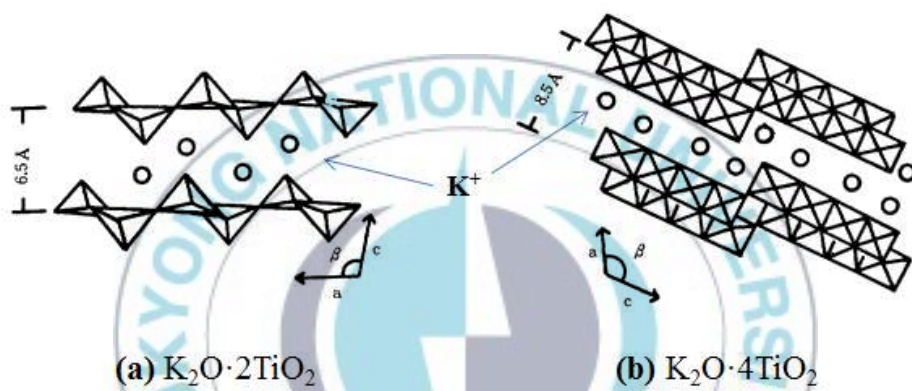


Fig. 2.3 Crystalline structure of potassium titanate materials [57].

### 3. Experimental

#### 3.1. Materials

A support used in this study was  $\text{Al}_2\text{O}_3$  (Aldrich, activated, acidic, Brockmann I, standard grade,  $S_{\text{BET}} = 173.7 \text{ m}^2/\text{g}$ , gamma phase). The chemicals used in the synthesis of the catalysts were  $\text{TiO}_2$  (Degussa, P-25),  $\text{K}_2\text{CO}_3$  (Katayama, 99.5%), and  $\text{Ni}(\text{NO}_3)_2 \cdot 6\text{H}_2\text{O}$  (Junsei, 97%). The gases were utilized in the activity study were  $\text{CH}_4$  (Deokyang Energen Co., >99.5%),  $\text{H}_2$  (Daesung Industrial Gases Co. Ltd., >99.999%), and He (Daesung Industrial Gases Co. Ltd., >99.999%). For a characterization of a reduced catalyst, 1%  $\text{O}_2/\text{He}$  (Daesung Industrial Gases Co. Ltd., HUP Grade, 99.99%) mixture gas was employed.

#### 3.2. Catalyst preparation

$\text{Ni}/\text{K}_2\text{Ti}_x\text{O}_y\text{-Al}_2\text{O}_3$  catalysts were synthesized by the procedure shown in Fig. 3.1, using the wet impregnation method. The catalysts were prepared with a fixed 10 wt.% nickel loading, and varying amounts of potassium titanate,  $\text{K}_2\text{Ti}_x\text{O}_y$ , 5 to 50 wt.% of the support. In order to investigate potassium titanate effect in  $\text{Ni}/\text{Al}_2\text{O}_3$  catalyst, different amounts of  $\text{K}_2\text{Ti}_x\text{O}_y$  were applied and they were denoted as  $\text{Ni}/\text{K}_2\text{Ti}_x\text{O}_y(\text{wt.}\%)\text{-Al}_2\text{O}_3(\text{wt.}\%)$ :  $\text{Ni}/\text{K}_2\text{Ti}_x\text{O}_y(5)\text{-Al}_2\text{O}_3(95)$ ,  $\text{Ni}/\text{K}_2\text{Ti}_x\text{O}_y(11)\text{-Al}_2\text{O}_3(89)$ ,  $\text{Ni}/\text{K}_2\text{Ti}_x\text{O}_y(20)\text{-Al}_2\text{O}_3(80)$ ,  $\text{Ni}/\text{K}_2\text{Ti}_x\text{O}_y(30)\text{-Al}_2\text{O}_3(70)$ , and  $\text{Ni}/\text{K}_2\text{Ti}_x\text{O}_y(50)\text{-Al}_2\text{O}_3(50)$ ;

their samples before reduction were denoted as  $\text{NiO/K}_2\text{Ti}_x\text{O}_y(\text{wt.}\%)\text{-Al}_2\text{O}_3(\text{wt.}\%)$ . The catalysts were synthesized in two steps: modification of alumina support with potassium titanate and loading of nickel. In the first step,  $\text{K}_2\text{CO}_3$  was dissolved in distilled water and  $\text{TiO}_2$  was added to form a sol. Then alumina was added in the sol and kept for 10 minutes under stirring. In order to remove water, the sol mixture was heated and evacuated for 3 hours by a rotary evaporator (Eyela, N-1110S-W). After evaporation, the collected wet powder was dried at  $110^\circ\text{C}$  for overnight and calcined at  $850^\circ\text{C}$  for 6 hours. In the second step,  $\text{Ni}(\text{NO}_3)_2 \cdot 6\text{H}_2\text{O}$  of 5.11 g was dissolved in distilled water of  $100\text{ cm}^3$  and the calcined powder of 9 g in the former step was added in this solution and stirred for 10 minutes. Then the water in the mixture was removed using the rotary evaporator with the same manner. The collected powder was at  $110^\circ\text{C}$  for overnight and calcined at  $850^\circ\text{C}$  for 6 hours.

The obtained materials were denoted as  $\text{NiO/K}_2\text{Ti}_x\text{O}_y\text{-Al}_2\text{O}_3$ , and after reduction denoted as  $\text{Ni/K}_2\text{Ti}_x\text{O}_y\text{-Al}_2\text{O}_3$ . Reduction procedure was utilized to convert  $\text{NiO/K}_2\text{Ti}_x\text{O}_y\text{-Al}_2\text{O}_3$  into  $\text{Ni/K}_2\text{Ti}_x\text{O}_y\text{-Al}_2\text{O}_3$  catalysts, carried out at  $800^\circ\text{C}$  for 2 hours under  $\text{H}_2$  flow of  $100\text{ cm}^3/\text{min}$  as a pretreatment condition of catalytic activity test. At the end of the pretreatment procedure, a sample was cooled in He flow to room

temperature and passivated under 1% O<sub>2</sub>/He flow of 30 cm<sup>3</sup>/min for 2 hours in order to prevent oxidation of the sample.

For a comparison, NiO/Al<sub>2</sub>O<sub>3</sub> was prepared by the same method of the former second step, using Al<sub>2</sub>O<sub>3</sub> of 9 g instead of K<sub>2</sub>Ti<sub>x</sub>O<sub>y</sub>-Al<sub>2</sub>O<sub>3</sub>, and commercial catalyst FCR-4 (Süd-Chemie Co., 12 wt.% Ni/ $\alpha$ -Al<sub>2</sub>O<sub>3</sub>) was used. Ni/CaTi<sub>x</sub>O<sub>y</sub>-Al<sub>2</sub>O<sub>3</sub> catalysts were prepared by the same method with only calcium precursor changed to calcium carbonate or nitrate.

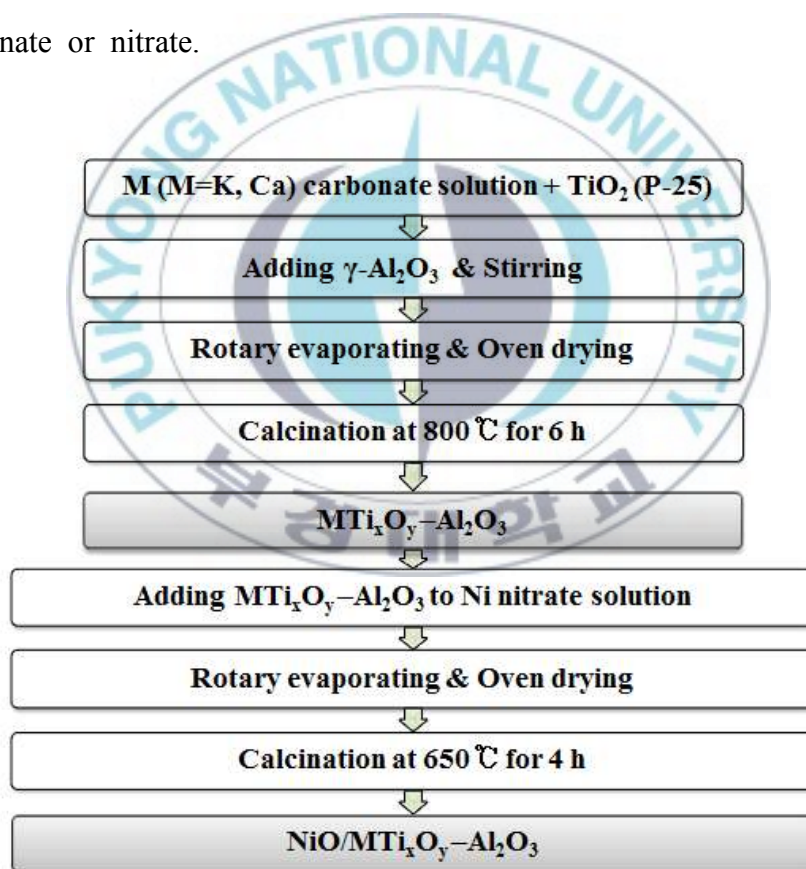


Fig. 3.1. Procedure for synthesis of Ni/K<sub>2</sub>Ti<sub>x</sub>O<sub>y</sub>-Al<sub>2</sub>O<sub>3</sub> catalyst.

### 3.3. Characterizations

#### 3.3.1. X-ray diffraction

X-ray diffraction (XRD) patterns of both the calcined and spent samples were measured with a X-ray diffractometer (Rigaku, D/MAX2500) operated at 45 kV and 40 mA, using Cu- $K\alpha$  monochromatized radiation ( $\lambda=0.154178$  nm). A particle size of Ni or NiO on the catalyst was calculated from Scherrer equation

$$d = \frac{K\lambda}{\beta \cos \theta} \quad (3.1)$$

where  $\lambda$  is the X-ray wavelength (1.542 Å), K is the Scherrer constant (0.94), and  $\beta$  is the angular full width at half maximum expressed in terms of radians. The diffraction pattern was identified through comparison with those included in the JCPDS (Joint Committee of Powder Diffraction Standards) database.

#### 3.3.2. Nitrogen physisorption

The surface area of the catalysts was measured on a surface area analyzer (Micromeritics, TriStar II), after degassing at 300°C for 3 hours under vacuum, by using nitrogen physisorption. The specific surface area was determined according to the Brunauer-Emmett-Teller (BET) equation in the relative pressure range of 0.05-0.25.



### 3.3.3. Temperature-programmed reduction

Temperature-programmed reduction (TPR) technique was used to investigate reduction characters of the calcined samples with hydrogen flow. For H<sub>2</sub>-TPR test, a sample of 0.1 g was loaded in a quartz U-tube and heated from 30 to 900°C with 10°C/min in 10% H<sub>2</sub>/He of 60 cm<sup>3</sup>/min. During the TPR procedure, a portion of the exist gas flow was sampled through a leak valve into a mass spectrometer (HIDEN, HPR-20), and the masses 2(H<sub>2</sub>), 4(He), and 18(H<sub>2</sub>O) were monitored.

### 3.3.4. Scanning electron microscopy

The microscopic feature and element distribution of the samples was observed by means of scanning electron microscopy (SEM) (Hitachi, S-2700) coupled with energy dispersive spectroscopy (EDS) (Horiba, EDXS).

### 3.3.5. X-ray photoelectron spectroscopy

X-ray photoelectron spectra were taken with a Thermo VG Scientific MultiLab2000 spectrometer equipped with an electrostatic analyser. The analysis had been done under a vacuum of at least  $1 \times 10^{-10}$  torr. X-ray source was the Al-K $\alpha$  radiation. Survey scans were conducted between 0 and 1,300 eV binding energy with rate of 1.0

eV/sec. Binding energies were recorded for the Ni 2p, K 2p, Ti 2p, Al 2p, O 1s, and C 1s regions.

#### 3.3.6. Hydrogen chemisorption

Nickel dispersion was determined by static equilibrium adsorption of H<sub>2</sub> at 40°C by the pulse method using a chemisorption analyser (Micromeritics, AutoChem II 2920). Before measurement, a 0.2 g catalyst sample was reduced *in situ* in a H<sub>2</sub> flow at 800°C for 1 hour. Uptake of H<sub>2</sub> at monolayer coverage of the Ni species was used to estimate Ni metal dispersion, assuming the stoichiometry of H/Ni atom was equal to 1. The equation used to calculate dispersion was

$$\%D = \frac{1.17 X}{W} \quad (3.2)$$

where X is H<sub>2</sub> uptake in  $\mu\text{mol}\cdot\text{g}^{-1}$  of catalyst, W is the weight percent of Ni.

#### 3.3.7. Elemental analysis

The amount of carbon and hydrogen deposited on the used catalysts was determined by CHNS elemental analysis (Elementar, VarioMICRO). In this instrument, a thermal conductivity detector (TCD) was equipped and its detection limitation was below 20 ppm

for carbon and hydrogen. Test methods were based in ASTM D5373-93 and D5291-93.

### **3.4. Catalytic activity test**

The activity test of the catalysts for methane steam reforming was operated using the system illustrated in Fig. 3.2, including a continuous flow fixed-bed reactor made with quartz or Inconel material. Reaction tests were carried out at 750 to 850°C under atmospheric pressure. The steam to carbon ratio (S/C) of feed stream and gas hourly space velocity (GHSV) were 1.0 to 3.0 and 15,000 to 200,000 h<sup>-1</sup>, respectively. The inlet and outlet gas after cooled using cold trap were analyzed on line by the gas chromatograph (Donam Instrument, DS6200). After one hour of steady-state operation at each temperature, the concentrations of H<sub>2</sub>, CH<sub>4</sub>, CO, CO<sub>2</sub> contents in gas products were analyzed by a thermal conductivity detector (TCD) with a HayeSep DB column and a flame ionized detector (FID) with OV-101-10% column.

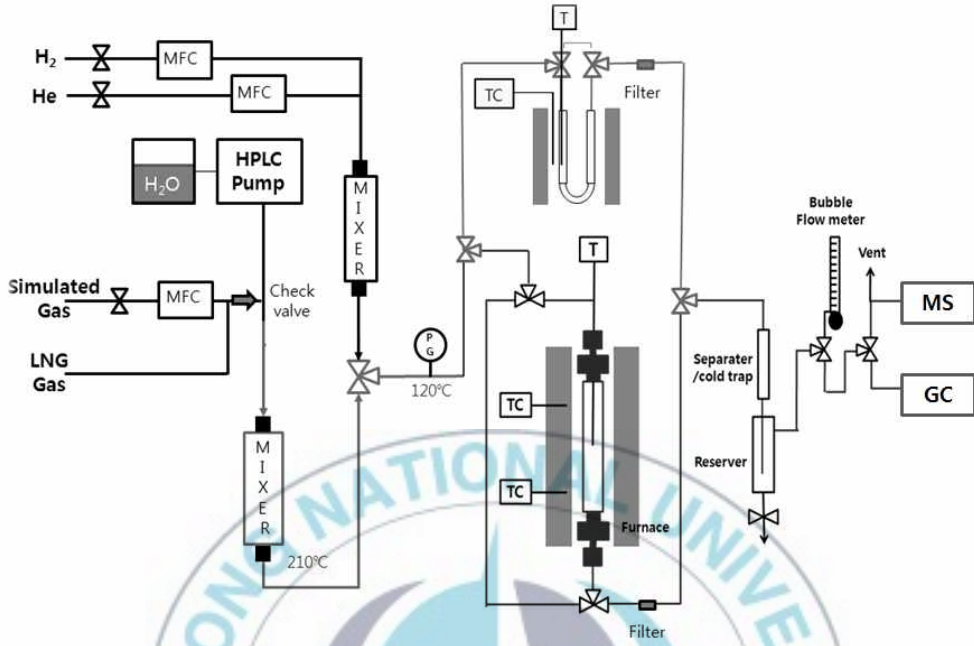


Fig. 3.2. Schematic drawing of the experimental setup.

Conversion of  $\text{CH}_4$  (eq. 3.3) and selectivity of  $\text{CO}$  (eq. 3.4),  $\text{H}_2$  (eq. 3.5), and  $\text{CO}_2$  (eq. 3.6) were calculated by the following equations [28].

$$X = \frac{(F_{\text{CH}_4,0} - F_{\text{CH}_4})}{F_{\text{CH}_4,0}} \quad (3.3)$$

$$S_{\text{CO}/\text{CH}_4} = \frac{(F_{\text{CH}_4}X - F_{\text{CO}_2})}{F_{\text{CH}_4}X} \quad (3.4)$$

$$S_{\text{H}_2/\text{CH}_4} = \frac{(3F_{\text{CH}_4}X + F_{\text{CO}_2})}{F_{\text{CH}_4}X} \quad (3.5)$$

$$S_{CO_2/CH_4} = \frac{F_{CO_2}}{F_{CH_4}X} \quad (3.6)$$

$F_{CH_4,0}$  : molar flow rate at which  $CH_4$  is fed to the system

$F_{CH_4}$  : molar flow rate at which  $CH_4$  leaves the system

$F_{CH_4}X$  : molar flow rate at which  $CH_4$  is consumed with in the system

$F_{CO_2}$  : molar flow rate at which  $CO_2$  leaves the system



## **4. Catalytic Activity and Characterization of Ni/K<sub>2</sub>Ti<sub>x</sub>O<sub>y</sub>-Al<sub>2</sub>O<sub>3</sub> Catalyst for Steam Methane Reforming**

The work described in this chapter are the effect of K<sub>2</sub>Ti<sub>x</sub>O<sub>y</sub> content, reaction conditions (temperature, steam-to-carbon ratio, and gas hourly space velocity), and K<sub>2</sub>Ti<sub>x</sub>O<sub>y</sub> additives on the activity and stability of Ni/K<sub>2</sub>Ti<sub>x</sub>O<sub>y</sub>-Al<sub>2</sub>O<sub>3</sub> for steam methane reforming. The catalyst preparation methods, experimental apparatus, and analytical equipment are presented in the Chapter 3. The correlation between characteristics of the catalyst surface and its catalytic activity is also discussed.

### **4.1. Catalytic activity of Ni/K<sub>2</sub>Ti<sub>x</sub>O<sub>y</sub>-Al<sub>2</sub>O<sub>3</sub> catalyst for steam methane reforming**

#### **4.1.1. Characteristics of Ni/K<sub>2</sub>Ti<sub>x</sub>O<sub>y</sub>-Al<sub>2</sub>O<sub>3</sub> catalyst**

X-ray diffraction patterns of  $\gamma$ -Al<sub>2</sub>O<sub>3</sub>, NiO/Al<sub>2</sub>O<sub>3</sub>, and NiO/K<sub>2</sub>Ti<sub>x</sub>O<sub>y</sub>-Al<sub>2</sub>O<sub>3</sub> catalysts are presented in Fig 4.1. The patterns displayed several distinctive features. First, the NiO/Al<sub>2</sub>O<sub>3</sub> sample shows the appearance of a single phase, which is assigned to spinel NiAl<sub>2</sub>O<sub>4</sub> (JCPDS 10-0339). The XRD peaks' angles of the sample are



slightly shifted from those of  $\gamma$ - $\text{Al}_2\text{O}_3$  (JCPDS 10-0425). Secondly, for the samples including lower contents of  $\text{K}_2\text{Ti}_x\text{O}_y$  (Fig. 4.1, c and d), nickel oxide phase is well-dispersed and titanium component is isolated on the catalysts. Thirdly, for the catalysts having higher contents of  $\text{K}_2\text{Ti}_x\text{O}_y$  (Fig. 4.1, e to g), these samples have mixed phases derived from K-Ti-O system such as  $\text{K}_2\text{Ti}_2\text{O}_5$ ,  $\text{K}_2\text{Ti}_6\text{O}_{13}$ , and  $\text{K}_3\text{Ti}_8\text{O}_{17}$ . With increase of the  $\text{K}_2\text{Ti}_x\text{O}_y$  amount, the peak intensities of nickel oxide phase are increased obviously, indicating the agglomeration of NiO particles and their isolation onto the supports.

The crystalline diameters of NiO on  $\text{K}_2\text{Ti}_x\text{O}_y$ - $\text{Al}_2\text{O}_3$  catalysts are calculated to be 9.6 to 19.5 nm (Table 4.1) and the size of NiO increases with increasing  $\text{K}_2\text{Ti}_x\text{O}_y$  content in the samples. Table 4.1 compares the surface areas of the reference catalyst, NiO/ $\text{Al}_2\text{O}_3$ , to modified NiO/ $\text{K}_2\text{Ti}_x\text{O}_y$ - $\text{Al}_2\text{O}_3$  catalysts. After the  $\text{K}_2\text{Ti}_x\text{O}_y$  loading, the surface areas (11-73  $\text{m}^2/\text{g}$ ) of the nickel catalysts were smaller than that (106  $\text{m}^2/\text{g}$ ) of NiO/ $\text{Al}_2\text{O}_3$  mainly because the density of the  $\text{K}_2\text{Ti}_x\text{O}_y$  particles is larger than that of the porous  $\text{Al}_2\text{O}_3$  and some of the pores may be blocked by  $\text{K}_2\text{Ti}_x\text{O}_y$  nanoparticles. Therefore it can be concluded that NiO particles became isolated from the support for the catalysts with higher contents of  $\text{K}_2\text{Ti}_x\text{O}_y$ . Like case of any promoter [28-31,34], it is likely that appropriate amount, not high, of  $\text{K}_2\text{Ti}_x\text{O}_y$  can induce dispersing nickel component onto a support.

Therefore, we confirmed that NiO particles do not be isolated and can be well-dispersed onto only the  $\text{K}_2\text{Ti}_x\text{O}_y\text{-Al}_2\text{O}_3$  supports having below 20 wt.%  $\text{K}_2\text{Ti}_x\text{O}_y$ .



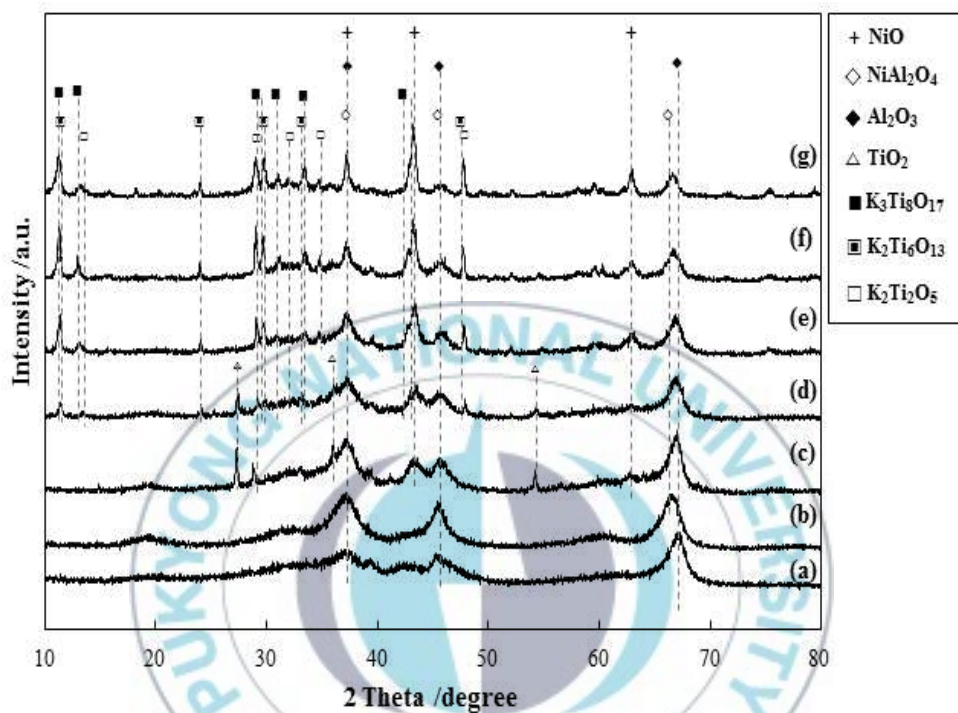


Fig. 4.1 X-ray diffraction patterns of (a)  $\gamma$ - $\text{Al}_2\text{O}_3$ , (b)  $\text{NiO}/\text{Al}_2\text{O}_3$  and  $\text{NiO}/\text{K}_2\text{Ti}_x\text{O}_y\text{-Al}_2\text{O}_3$  catalysts with  $\text{K}_2\text{Ti}_x\text{O}_y$  loading: (c)  $\text{NiO}/\text{K}_2\text{Ti}_x\text{O}_y(5)\text{-Al}_2\text{O}_3(95)$ , (d)  $\text{NiO}/\text{K}_2\text{Ti}_x\text{O}_y(11)\text{-Al}_2\text{O}_3(89)$ , (e)  $\text{NiO}/\text{K}_2\text{Ti}_x\text{O}_y(20)\text{-Al}_2\text{O}_3(80)$ , (f)  $\text{NiO}/\text{K}_2\text{Ti}_x\text{O}_y(30)\text{-Al}_2\text{O}_3(70)$ , and (g)  $\text{NiO}/\text{K}_2\text{Ti}_x\text{O}_y(50)\text{-Al}_2\text{O}_3(50)$ .

Table 4.1 Physical properties of NiO/Al<sub>2</sub>O<sub>3</sub> and NiO/K<sub>2</sub>Ti<sub>x</sub>O<sub>y</sub>-Al<sub>2</sub>O<sub>3</sub> catalysts

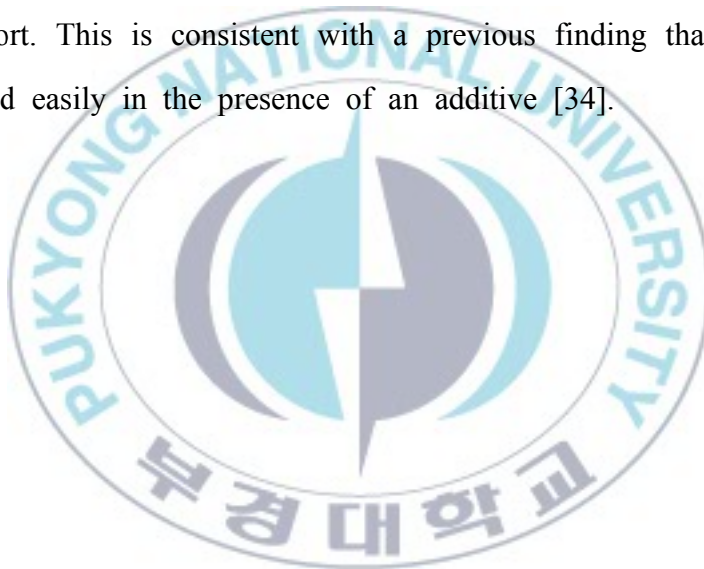
Catalyst	BET surface area (m <sup>2</sup> ·g <sub>ca</sub> <sup>-1</sup> )	Crystallite size <sup>a</sup> (nm)
NiO/Al <sub>2</sub> O <sub>3</sub>	106.1	-
NiO/K <sub>2</sub> Ti <sub>x</sub> O <sub>y</sub> (5)-Al <sub>2</sub> O <sub>3</sub> (95)	68.6	9.6
NiO/K <sub>2</sub> Ti <sub>x</sub> O <sub>y</sub> (11)-Al <sub>2</sub> O <sub>3</sub> (89)	73.1	11.1
NiO/K <sub>2</sub> Ti <sub>x</sub> O <sub>y</sub> (20)-Al <sub>2</sub> O <sub>3</sub> (80)	67.9	14.0
NiO/K <sub>2</sub> Ti <sub>x</sub> O <sub>y</sub> (30)-Al <sub>2</sub> O <sub>3</sub> (70)	48.8	18.5
NiO/K <sub>2</sub> Ti <sub>x</sub> O <sub>y</sub> (50)-Al <sub>2</sub> O <sub>3</sub> (50)	11.5	19.5

<sup>a</sup> Calculated from NiO (220) plane using Scherrer equation from XRD for calcined samples.

Since TPR profiles of supported metal catalysts are strongly affected by the character of metal-support interaction [58], TPR measurements are carried out to examine the interaction between nickel species and  $K_2Ti_xO_y-Al_2O_3$  support. Fig. 4.2 shows  $H_2$ -TPR profiles of calcined catalyst samples with various  $K_2Ti_xO_y$  contents. The  $H_2O$  (amu=18) generating curves derived from  $H_2$  consumption are fitted by Gaussian-type functions and the quantitative results are listed in Table 4.2.  $NiO/Al_2O_3$  (Fig. 4.2a) exhibits single reduction band at around  $790^\circ C$ , indicating the existence of nickel aluminate phase. It is known that  $NiO$  can react with  $Al_2O_3$  to form a highly stable  $NiAl_2O_4$  phase which has a lower reducibility than that of  $NiO$  [59].

All results of Fig. 4.2 and Table 4.2 show that  $NiO/K_2Ti_xO_y-Al_2O_3$  catalysts have more than two reduction peaks and their dominant reduction peaks are located at lower temperature with higher  $K_2Ti_xO_y$  contents. As Zhang et al. [60,61] states, the reducible  $NiO$  peaks of the supported catalysts can be approximately classified into three types:  $\alpha$ -type (weak interaction between the  $NiO$  and support,  $300-475^\circ C$ ),  $\beta$ -type (medium interaction,  $475-755^\circ C$ ), and  $\gamma$ -type (strong interaction,  $755-900^\circ C$ ). As a result (Fig. 4.2, b to f), we can see the reducible  $NiO$  peaks of  $NiO/K_2Ti_xO_y-Al_2O_3$  are widely located in the range of  $400-850^\circ C$ , including three sub-peaks corresponding to

$\alpha$ -,  $\beta$ -, and  $\gamma$ -type. In particular,  $\beta$ -type NiO becomes dominant with the  $K_2Ti_xO_y$  presence (55.6-69.4%) and the fraction of  $\gamma$ -type NiO decreases with the  $K_2Ti_xO_y$  loading (34.2% for NiO/ $K_2Ti_xO_y$ (5)- $Al_2O_3$ (95) to 0% for NiO/ $K_2Ti_xO_y$ (50)- $Al_2O_3$ (50)). In short, the metal-support interaction in NiO/ $K_2Ti_xO_y$ - $Al_2O_3$  is weaker than that of NiO/ $Al_2O_3$ . On the other words,  $K_2Ti_xO_y$  in a  $Al_2O_3$ -supported Ni catalyst played a role in varying NiO species with weaker interaction between metal and support. This is consistent with a previous finding that NiO can be reduced easily in the presence of an additive [34].





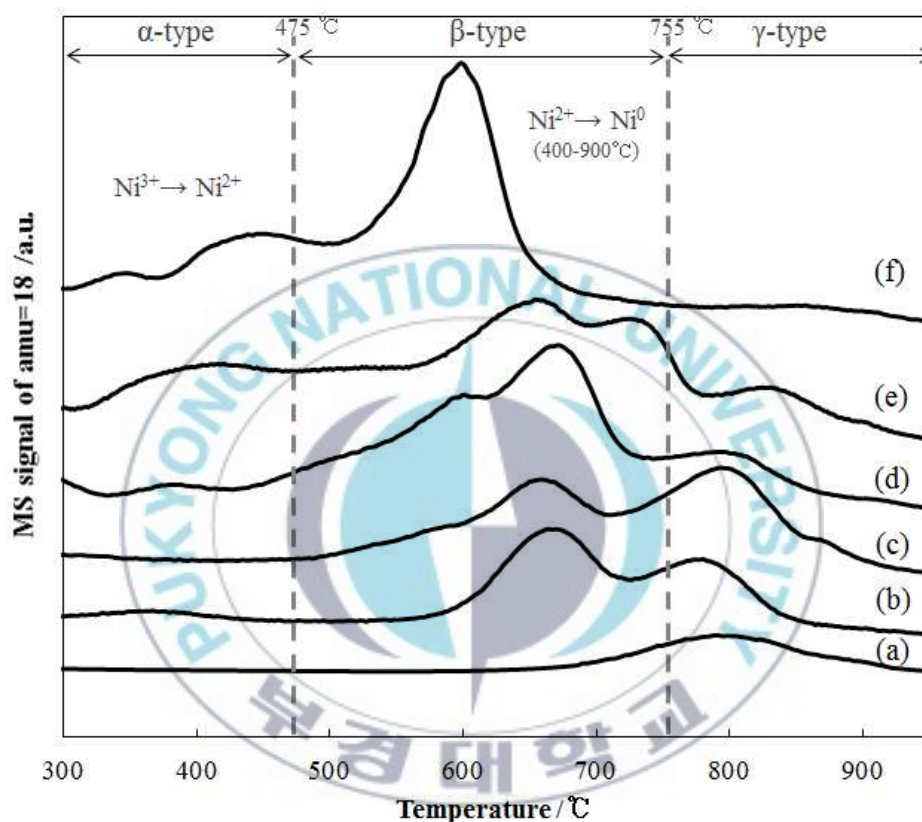


Fig. 4.2.  $\text{H}_2$  temperature-programmed reduction (TPR) profiles for (a)  $\text{NiO}/\text{Al}_2\text{O}_3$  and  $\text{NiO}/\text{K}_2\text{Ti}_x\text{O}_y\text{-Al}_2\text{O}_3$  catalysts with  $\text{K}_2\text{Ti}_x\text{O}_y$  loading: (b)  $\text{NiO}/\text{K}_2\text{Ti}_x\text{O}_y(5)\text{-Al}_2\text{O}_3(95)$ , (c)  $\text{NiO}/\text{K}_2\text{Ti}_x\text{O}_y(11)\text{-Al}_2\text{O}_3(89)$ , (d)  $\text{NiO}/\text{K}_2\text{Ti}_x\text{O}_y(20)\text{-Al}_2\text{O}_3(80)$ , (e)  $\text{NiO}/\text{K}_2\text{Ti}_x\text{O}_y(30)\text{-Al}_2\text{O}_3(70)$ , and (f)  $\text{NiO}/\text{K}_2\text{Ti}_x\text{O}_y(50)\text{-Al}_2\text{O}_3(50)$ .

Table 4.2 Quantitative data from H<sub>2</sub> temperature-programmed reduction profiles of NiO/Al<sub>2</sub>O<sub>3</sub> and NiO/K<sub>2</sub>Ti<sub>x</sub>O<sub>y</sub>-Al<sub>2</sub>O<sub>3</sub> catalysts

Catalysts	T <sub>m</sub> (°C)			Fraction of total area (%)		
	$\alpha$ -type NiO	$\beta$ -type NiO	$\gamma$ -type NiO	$\alpha$ -type NiO	$\beta$ -type NiO	$\gamma$ -type NiO
NiO/Al <sub>2</sub> O <sub>3</sub>	-	-	790	-	-	100.0
NiO/K <sub>2</sub> Ti <sub>x</sub> O <sub>y</sub> (5)-Al <sub>2</sub> O <sub>3</sub> (95)	367	665	776	9.9	55.9	34.2
NiO/K <sub>2</sub> Ti <sub>x</sub> O <sub>y</sub> (11)-Al <sub>2</sub> O <sub>3</sub> (89)	380	667	788	8.1	69.4	22.5
NiO/K <sub>2</sub> Ti <sub>x</sub> O <sub>y</sub> (20)-Al <sub>2</sub> O <sub>3</sub> (80)	381	603, 672	788	7.8	66.6	25.6
NiO/K <sub>2</sub> Ti <sub>x</sub> O <sub>y</sub> (30)-Al <sub>2</sub> O <sub>3</sub> (70)	414	665, 724	824	30.2	55.6	14.2
NiO/K <sub>2</sub> Ti <sub>x</sub> O <sub>y</sub> (50)-Al <sub>2</sub> O <sub>3</sub> (50)	434	598	857	34.4	65.6	-

SEM images and elemental mapping by EDS for NiO/Al<sub>2</sub>O<sub>3</sub> and NiO/K<sub>2</sub>Ti<sub>x</sub>O<sub>y</sub>-Al<sub>2</sub>O<sub>3</sub> are shown in Fig. 4.3-5. Accordingly, NiO/Al<sub>2</sub>O<sub>3</sub> (Fig. 4.3a) possesses larger particles with uniform size (about 100 μm in diameter). In contrast, NiO/K<sub>2</sub>Ti<sub>x</sub>O<sub>y</sub>-Al<sub>2</sub>O<sub>3</sub> (Fig. 4.3, b to f) are consisted of small particles distributed with various sizes (10 to 100 μm in diameter). Fig. 4.4 presents the distribution of each K and Ti element on Al<sub>2</sub>O<sub>3</sub> indicating well-dispersed K<sub>2</sub>Ti<sub>x</sub>O<sub>y</sub> on the substrate, Al<sub>2</sub>O<sub>3</sub>. However, Ti element were partially aggregated on the samples with K<sub>2</sub>Ti<sub>x</sub>O<sub>y</sub> of high loading (Fig. 4.4, d-f). For Fig. 4.5, (a) to (e) samples, the mapping results show that the NiO particles are uniformly dispersed on the support. NiO/K<sub>2</sub>Ti<sub>x</sub>O<sub>y</sub>(50)-Al<sub>2</sub>O<sub>3</sub>(50) sample (Fig. 4.5, f) presents some in homogeneity in the dispersion of Ni species, which is consistent with XRD result described.

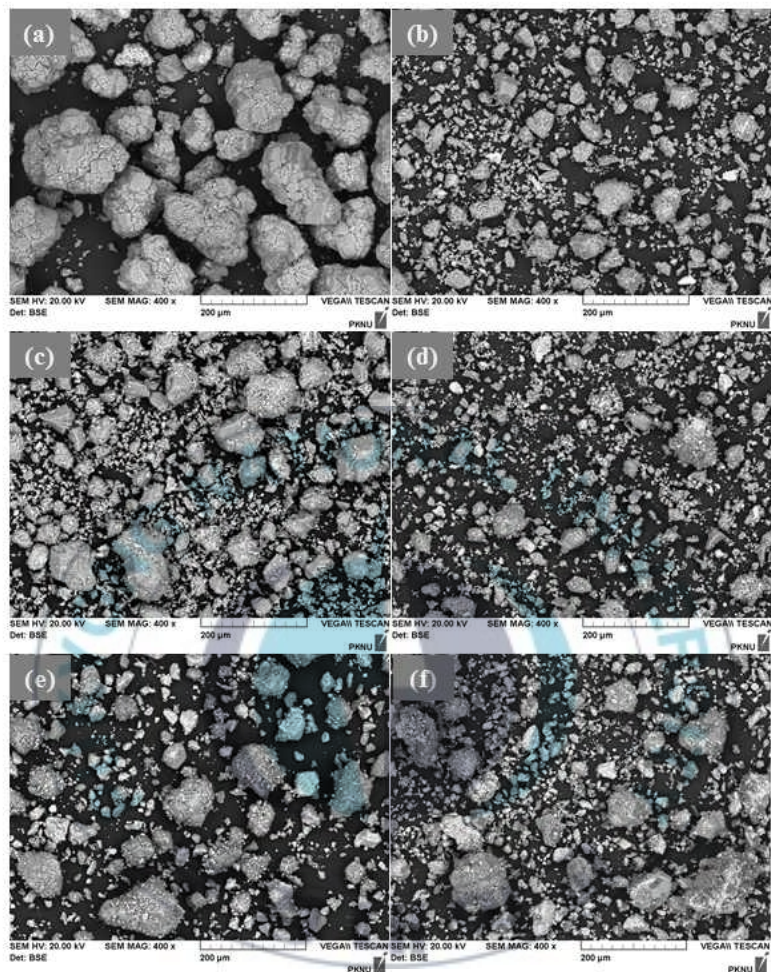


Fig. 4.3. Scanning electron microscopy (SEM) images of the Ni catalysts: (a) NiO/Al<sub>2</sub>O<sub>3</sub>, (b) NiO/K<sub>2</sub>Ti<sub>x</sub>O<sub>y</sub>(5)-Al<sub>2</sub>O<sub>3</sub>(95), (c) NiO/K<sub>2</sub>Ti<sub>x</sub>O<sub>y</sub>(11)-Al<sub>2</sub>O<sub>3</sub>(89), (d) NiO/K<sub>2</sub>Ti<sub>x</sub>O<sub>y</sub>(20)-Al<sub>2</sub>O<sub>3</sub>(80), (e) NiO/K<sub>2</sub>Ti<sub>x</sub>O<sub>y</sub>(30)-Al<sub>2</sub>O<sub>3</sub>(70), and (f) NiO/K<sub>2</sub>Ti<sub>x</sub>O<sub>y</sub>(50)-Al<sub>2</sub>O<sub>3</sub>(50).

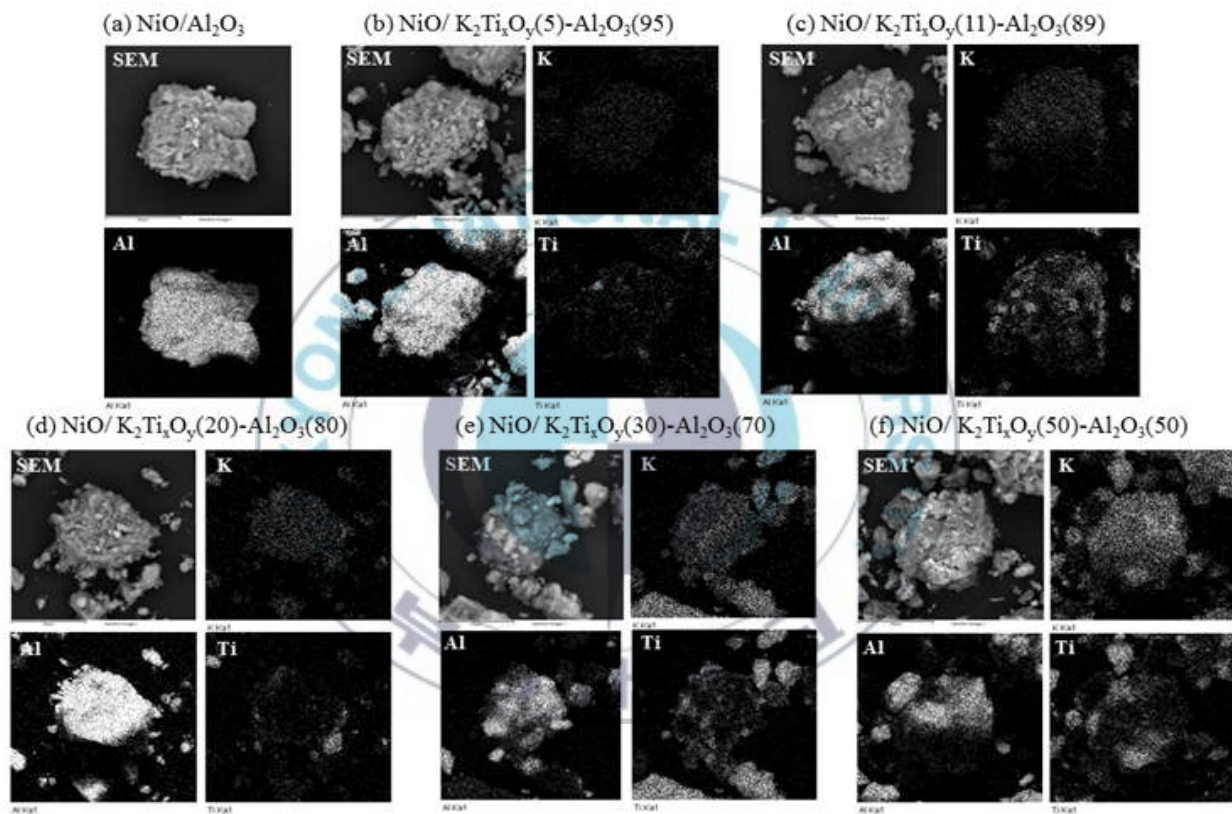


Fig. 4.4 Scanning electron spectroscopy (SEM) and electron dispersive spectroscopy (EDS) mapping images for Al, K, and Ti element on the Ni catalysts: (a)-(f) are same as in Fig. 4.3.



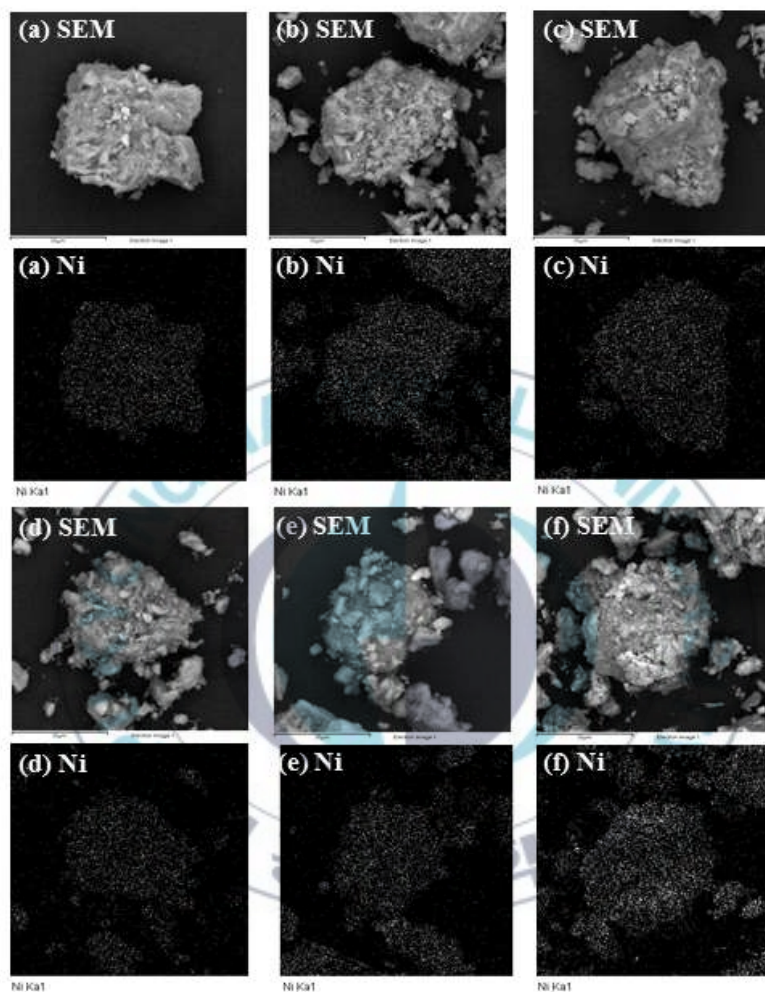


Fig. 4.5 Scanning electron spectroscopy (SEM) and electron dispersive spectroscopy (EDS) mapping images for Ni element on the Ni catalysts: (a)-(f) are same as in Fig. 4.3.



The different X-ray photoelectron spectroscopy (XPS) cross-sections of the two-dimensional metal oxide overlayer and metal oxide crystallites also may be used for the determination of monolayer coverage. In these studies, a dramatic change in slope occurs when the XPS surface signal is plotted as a function of bulk composition because of these very different cross-sections. The XPS cross-section for the two-dimensional phase is significantly greater than that for the agglomerated crystalline phase, since not all metal oxide can be detected by the XPS measurement in the crystalline phase due to the limited depth analysis of this technique [62]. Fig. 4.6 shows the XPS analysis of the  $K_2Ti_xO_y/Al_2O_3$  system as a function of  $K_2Ti_xO_y$  loading. At low  $K_2Ti_xO_y$  loading, the surface Ti signal, which is represented by the XPS Ti(2p)/Al(2p) ratio referenced against the  $Al_2O_3$  support signal, increases linearly with the bulk Ti content, which is represented by the  $K_2Ti_xO_y$  loading, because every Ti atom in this two-dimensional structure is detected by the XPS measurement. However, at loadings above 11%  $K_2Ti_xO_y$ , the surface Ti signal deviates from linearity with increasing bulk Ti content because of the formation of three-dimensional  $K_2Ti_xO_y$  crystals. Thus, in agreement with the above XRD and SEM-EDS characterization studies, the XPS measurements also reveal that the surface potassium titanate monolayer coverage is achieved at approximately 15%  $K_2Ti_xO_y$  loading on this

alumina support, which corresponds to the loading value at the tangent of two slopes shown in Fig. 4.6.

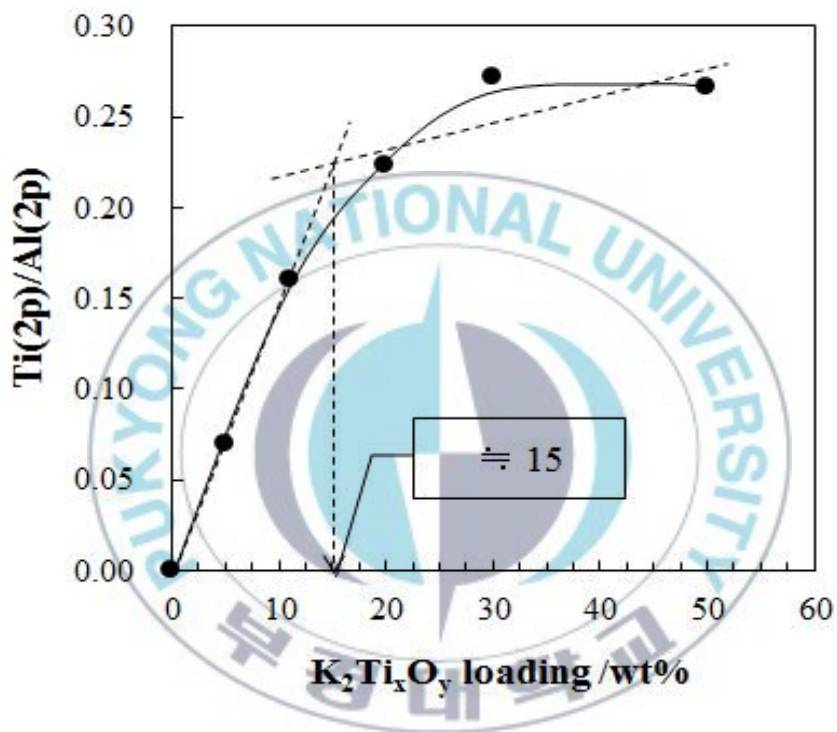
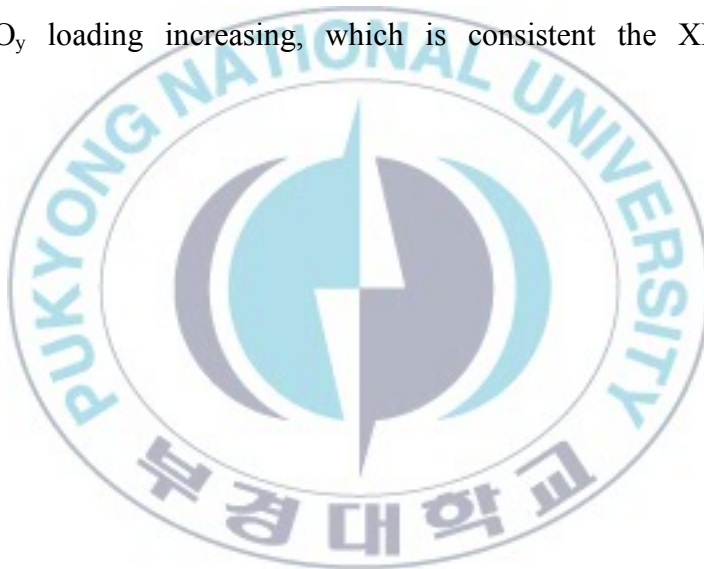


Fig. 4.6 X-ray photoelectron spectroscopy analysis of  $NiO/K_2Ti_xO_y-Al_2O_3$  catalyst as a function of  $K_2Ti_xO_y$  loading.

The O 1s signals in Fig. 4.7 for NiO/K<sub>2</sub>Ti<sub>x</sub>O<sub>y</sub>-Al<sub>2</sub>O<sub>3</sub> catalyst can be fitted to three peaks around 530, 531, and 532 eV, respectively. The three sub-peaks corresponding to three types O on NiO (530 eV), Al<sub>2</sub>O<sub>3</sub> (531 eV), and NiAl<sub>2</sub>O<sub>4</sub> (532 eV) because of the strong interaction between Ni and support Al<sub>2</sub>O<sub>3</sub>, respectively [63-65]. With the increase in the K<sub>2</sub>Ti<sub>x</sub>O<sub>y</sub> loading, the proportion of O in NiO (530 eV) increase. This suggests that NiO is isolated from the support with its K<sub>2</sub>Ti<sub>x</sub>O<sub>y</sub> loading increasing, which is consistent the XRD results above.



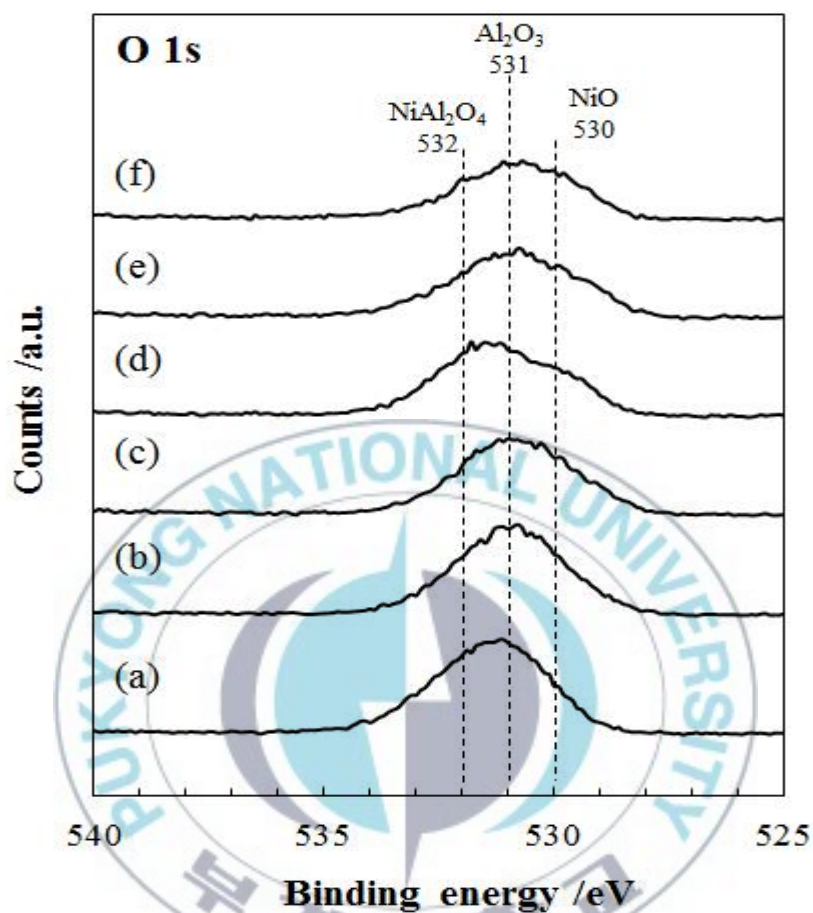


Fig. 4.7 X-ray photoelectron spectra of O 1s for the Ni catalysts: (a) NiO/Al<sub>2</sub>O<sub>3</sub>, (b) NiO/K<sub>2</sub>Ti<sub>x</sub>O<sub>y</sub>(5)-Al<sub>2</sub>O<sub>3</sub>(95), (c) NiO/K<sub>2</sub>Ti<sub>x</sub>O<sub>y</sub>(11)-Al<sub>2</sub>O<sub>3</sub>(89), (d) NiO/K<sub>2</sub>Ti<sub>x</sub>O<sub>y</sub>(20)-Al<sub>2</sub>O<sub>3</sub>(80), (e) NiO/K<sub>2</sub>Ti<sub>x</sub>O<sub>y</sub>(30)-Al<sub>2</sub>O<sub>3</sub>(70), and (f) NiO/K<sub>2</sub>Ti<sub>x</sub>O<sub>y</sub>(50)-Al<sub>2</sub>O<sub>3</sub>(50).

#### 4.1.2. Activity of Ni/K<sub>2</sub>Ti<sub>x</sub>O<sub>y</sub>-Al<sub>2</sub>O<sub>3</sub> catalyst

In order to investigate the effect of reaction condition over Ni/K<sub>2</sub>Ti<sub>x</sub>O<sub>y</sub>-Al<sub>2</sub>O<sub>3</sub> catalysts, Ni/K<sub>2</sub>Ti<sub>x</sub>O<sub>y</sub>(11)-Al<sub>2</sub>O<sub>3</sub>(89) catalyst was tested under different S/C ratio and GHSV. Thermodynamic equilibrium calculations were carried out by HSC Chemistry 5 software, compared to the experimental activity in Fig. 4.8. While thermodynamic methane conversion increases with S/C ratio at 750°C of temperature, experimental methane conversion over the catalyst increased until to be 2.5 of S/C ratio and decreased under 3.0 of S/C. Activity result of Ni/K<sub>2</sub>Ti<sub>x</sub>O<sub>y</sub>(11)-Al<sub>2</sub>O<sub>3</sub>(89) catalyst was close to equilibrium limit as well as superior to that of Ni/perovskite (77-80%) reported in the previous research [37]. In addition, the effect of reaction temperature and GHSV over the catalyst was indicated in Fig. 4.9. From the results, both of methane conversion and hydrogen selectivity was sharply decreasing in the highest space velocity (150,000 h<sup>-1</sup> of GHSV).

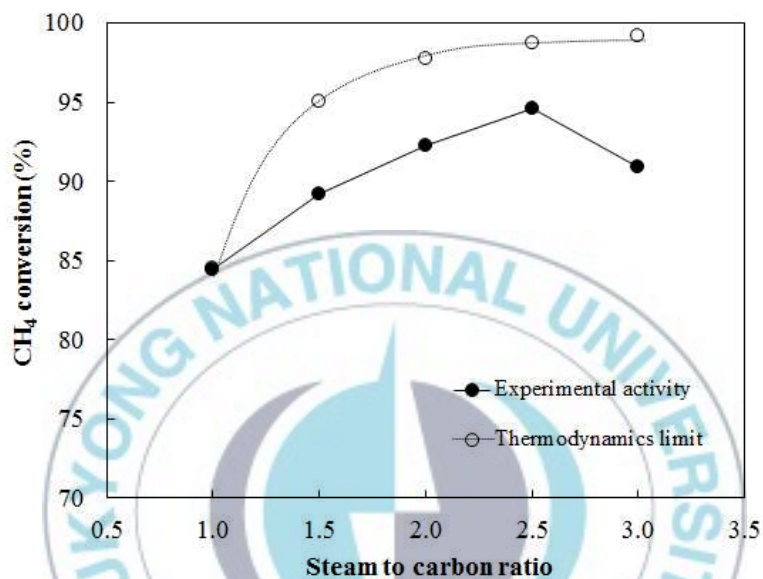


Fig. 4.8 Comparison of thermodynamic equilibrium value and catalytic activity of  $\text{Ni/K}_2\text{Ti}_x\text{O}_y(11)\text{-Al}_2\text{O}_3(89)$  catalyst for steam reforming under the reaction condition:  $\text{GHSV}=15,000 \text{ h}^{-1}$ ,  $T=750^\circ\text{C}$ , and time on stream=20 h.

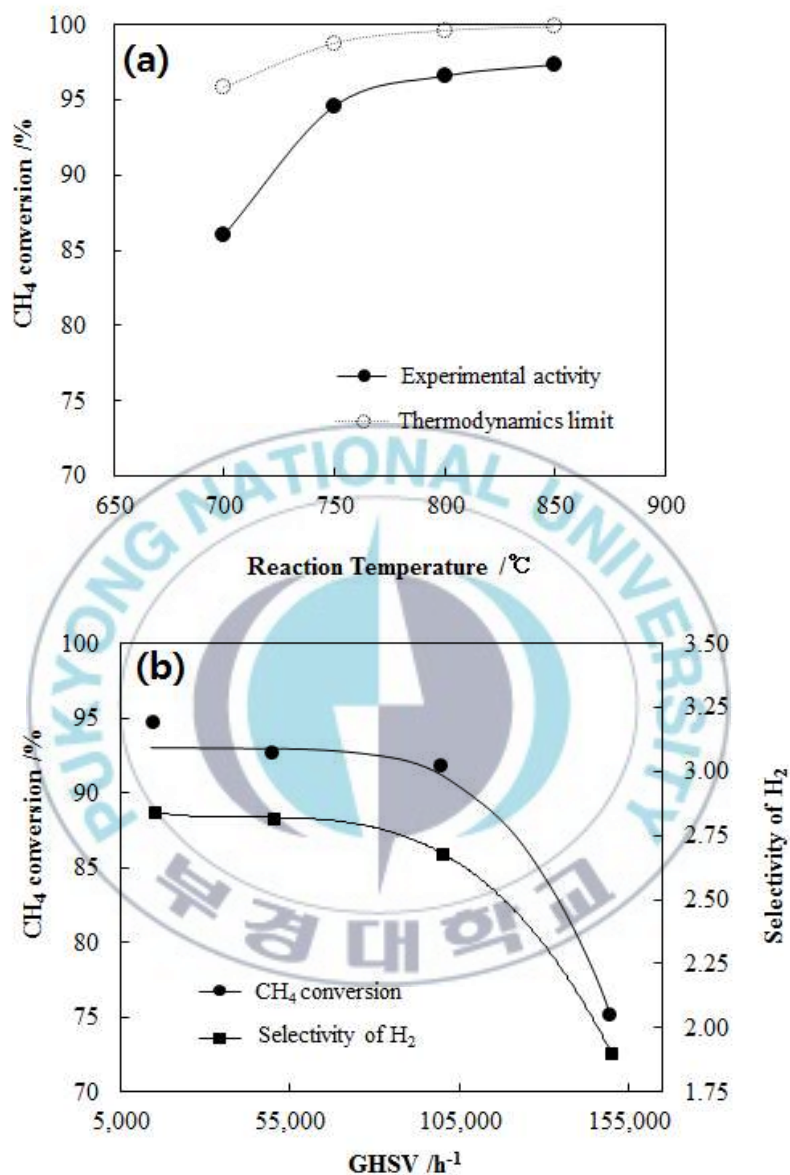


Fig. 4.9 Reaction temperature (a) and gas hourly space velocity (b) effects for steam methane reforming over Ni/K<sub>2</sub>Ti<sub>x</sub>O<sub>y</sub>(11)-Al<sub>2</sub>O<sub>3</sub>(89) catalyst for time-on-stream=20 h (the reaction conditions: (a) S/C=2.5 and GHSV=15,000 h<sup>-1</sup>; (b) S/C=2.5 and T=750 °C).



The activity for steam methane reforming over  $\text{Ni/K}_2\text{Ti}_x\text{O}_y\text{-Al}_2\text{O}_3$  catalysts was tested under the mild reaction condition and the average results in steady state after 1 hour reaction were listed in Table 4.3. With increasing the  $\text{K}_2\text{Ti}_x\text{O}_y$  content, the catalytic activities over  $\text{Ni/K}_2\text{Ti}_x\text{O}_y\text{-Al}_2\text{O}_3$  catalysts showed no tendency to increase. Among  $\text{Ni/K}_2\text{Ti}_x\text{O}_y\text{-Al}_2\text{O}_3$  catalysts having different  $\text{K}_2\text{Ti}_x\text{O}_y$  loading,  $\text{Ni/K}_2\text{Ti}_x\text{O}_y(20)\text{-Al}_2\text{O}_3(80)$  catalyst showed both maximum conversion of methane (97.2%) and selectivity of hydrogen (3.01), which were closed to the thermodynamic equilibrium values (98.8% and 3.32, respectively). Compared to FCR-4 catalyst,  $\text{Ni/K}_2\text{Ti}_x\text{O}_y\text{-Al}_2\text{O}_3$  catalysts exhibited similar performances for the steam methane reforming under the reaction condition.

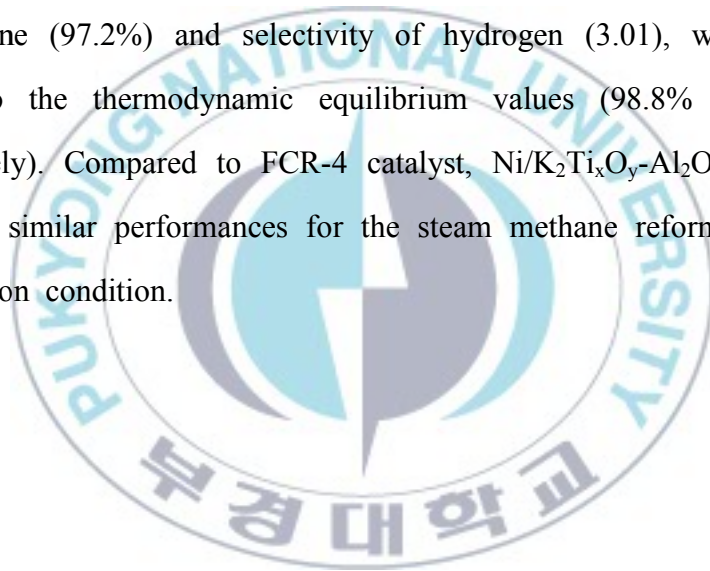


Table 4.3 Activities of steam methane reforming over Ni/K<sub>2</sub>Ti<sub>x</sub>O<sub>y</sub>-Al<sub>2</sub>O<sub>3</sub> catalysts

Catalyst	X <sub>CH<sub>4</sub></sub> (%)	S <sub>H<sub>2</sub>/CH<sub>4</sub></sub>	S <sub>CO/CH<sub>4</sub></sub>	S <sub>CO<sub>2</sub>/CH<sub>4</sub></sub>
FCR-4	97.5	3.06	0.73	0.22
Ni/Al <sub>2</sub> O <sub>3</sub>	96.9	2.97	0.79	0.15
Ni/K <sub>2</sub> Ti <sub>x</sub> O <sub>y</sub> (5)-Al <sub>2</sub> O <sub>3</sub> (95)	95.6	2.90	0.76	0.15
Ni/K <sub>2</sub> Ti <sub>x</sub> O <sub>y</sub> (11)-Al <sub>2</sub> O <sub>3</sub> (89)	94.6	2.84	0.74	0.16
Ni/K <sub>2</sub> Ti <sub>x</sub> O <sub>y</sub> (20)-Al <sub>2</sub> O <sub>3</sub> (80)	97.2	3.01	0.77	0.18
Ni/K <sub>2</sub> Ti <sub>x</sub> O <sub>y</sub> (30)-Al <sub>2</sub> O <sub>3</sub> (70)	91.9	2.69	0.69	0.16
Ni/K <sub>2</sub> Ti <sub>x</sub> O <sub>y</sub> (50)-Al <sub>2</sub> O <sub>3</sub> (50)	94.7	2.86	0.73	0.17

The reaction conditions: S/C=2.5, GHSV=15,000 h<sup>-1</sup>, T=750°C, and time-on-stream=10 h.

#### 4.1.3. Catalytic stability of Ni/K<sub>2</sub>Ti<sub>x</sub>O<sub>y</sub>-Al<sub>2</sub>O<sub>3</sub> catalyst

Catalytic stability test for steam methane reforming over the Ni/K<sub>2</sub>Ti<sub>x</sub>O<sub>y</sub>-Al<sub>2</sub>O<sub>3</sub> catalysts was performed under a severe condition of reaction (Fig. 4.10). The severe condition used is with low steam-to-carbon ratio of 1.0 and through time-on-stream of 100 hours at reaction temperature of 800°C, deriving deactivation in steam methane reforming reaction. We applied FCR-4 and Ni/Al<sub>2</sub>O<sub>3</sub> as reference catalysts to this stability test and compared their activities with those of Ni/K<sub>2</sub>Ti<sub>x</sub>O<sub>y</sub>-Al<sub>2</sub>O<sub>3</sub> catalysts. In this long-term stability test, we focused the decreasing degree of activity, called to deactivation degree, to evaluate all catalysts applied. The deactivation degrees of the catalysts were estimated from the difference between initial average activity (during the initial time period, 20 to 23 hours in steady state after 20 hour reaction) and terminal average activity (during the terminal time period, 97 to 100 hours), shown in Table 4.4. According to the results, for FCR-4 and Ni/Al<sub>2</sub>O<sub>3</sub> catalyst, deactivation degrees were 4.0 and 7.1%, respectively. Although FCR-4 showed a relatively stable activity after 20 hour, its terminal activity was lower than those of the Ni/K<sub>2</sub>Ti<sub>x</sub>O<sub>y</sub>-Al<sub>2</sub>O<sub>3</sub> catalysts. On the other hand, deactivation degrees for Ni/K<sub>2</sub>Ti<sub>x</sub>O<sub>y</sub>(5)-Al<sub>2</sub>O<sub>3</sub>(95), Ni/K<sub>2</sub>Ti<sub>x</sub>O<sub>y</sub>(11)-Al<sub>2</sub>O<sub>3</sub>(89), Ni/K<sub>2</sub>Ti<sub>x</sub>O<sub>y</sub>(20)-Al<sub>2</sub>O<sub>3</sub>(80), and Ni/K<sub>2</sub>Ti<sub>x</sub>O<sub>y</sub>(30)-Al<sub>2</sub>O<sub>3</sub>(70) were 1.7, 1.5, 8.1, and 4.7%, respectively. It can be seen from the results that deactivation of

$\text{Ni/K}_2\text{Ti}_x\text{O}_y\text{-Al}_2\text{O}_3$  became increased with increasing  $\text{K}_2\text{Ti}_x\text{O}_y$  loading. Particularly,  $\text{Ni/K}_2\text{Ti}_x\text{O}_y\text{-Al}_2\text{O}_3$  catalysts including appropriate amount of  $\text{K}_2\text{Ti}_x\text{O}_y$  (11 wt.% or less) represented resistance to deactivation, which may be derived from carbon coking or sintering of a catalyst.



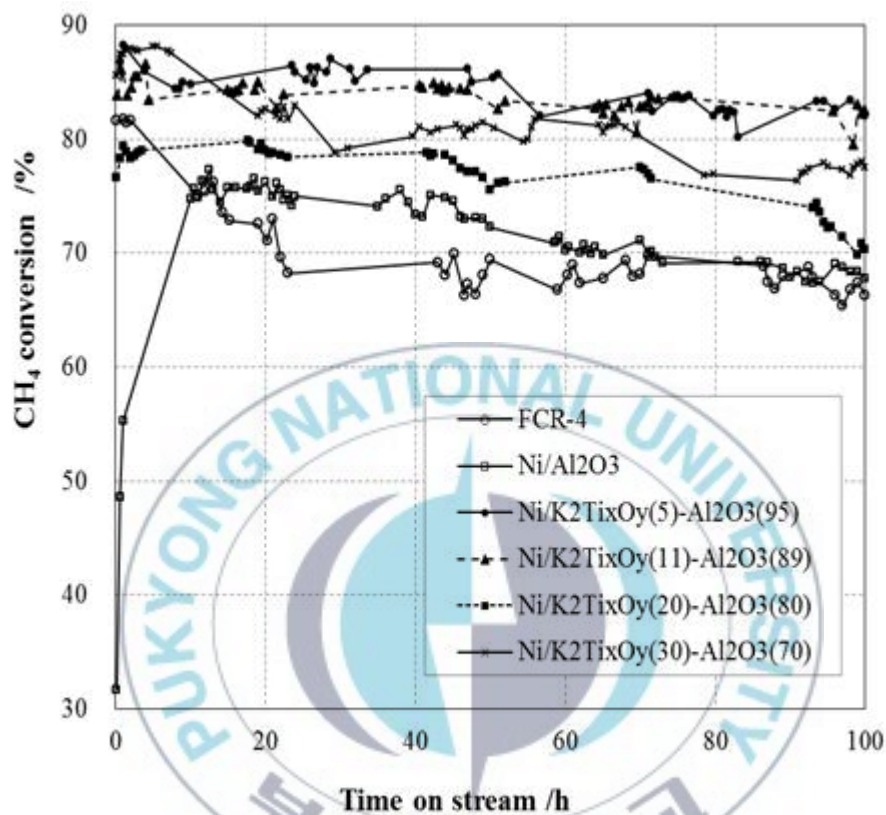


Fig. 4.10 Change in activity of Ni/K<sub>2</sub>Ti<sub>x</sub>O<sub>y</sub>-Al<sub>2</sub>O<sub>3</sub> catalysts and reference catalysts with time-on-stream. (Reaction condition: S/C=1.0, GHSV=200,000 h<sup>-1</sup>, T=800°C, and time-on-stream=100 h)

Table 4.4 Catalytic stability results of Ni/K<sub>2</sub>Ti<sub>x</sub>O<sub>y</sub>-Al<sub>2</sub>O<sub>3</sub> catalysts for steam methane reforming

Catalyst	Terminal X <sub>CH<sub>4</sub></sub> (%) <sup>a</sup>	Deactivation degree (%) <sup>b</sup>
FCR-4	66.5	4.0
Ni/Al <sub>2</sub> O <sub>3</sub>	68.3	7.1
Ni/K <sub>2</sub> Ti <sub>x</sub> O <sub>y</sub> (5)-Al <sub>2</sub> O <sub>3</sub> (95)	82.7	1.7
Ni/K <sub>2</sub> Ti <sub>x</sub> O <sub>y</sub> (11)-Al <sub>2</sub> O <sub>3</sub> (89)	81.8	1.5
Ni/K <sub>2</sub> Ti <sub>x</sub> O <sub>y</sub> (20)-Al <sub>2</sub> O <sub>3</sub> (80)	70.6	8.1
Ni/K <sub>2</sub> Ti <sub>x</sub> O <sub>y</sub> (30)-Al <sub>2</sub> O <sub>3</sub> (70)	77.5	4.7

The reaction conditions were same as in Fig. 4.10.

<sup>a</sup> Average X<sub>CH<sub>4</sub></sub> during the terminal time period from 97 to 100 hours

<sup>b</sup> Calculated from the equation: [Average X<sub>CH<sub>4</sub></sub> during the time period from 20 to 23 hours]-[Average X<sub>CH<sub>4</sub></sub> during the terminal time period from 97 to 100 hours]

#### **4.2. Role of $K_2Ti_xO_y$ additive on $Ni/Al_2O_3$ catalyst for steam methane reforming**

In order to determine the cause of the deactivation from the stability test for steam methane reforming, amount of carbon and hydrogen deposited of the spent catalysts were measured by CHNS elemental analysis, shown in Table 4.5. All spent samples had not much amount of carbon, even unstable nickel catalysts such as  $Ni/Al_2O_3$  and  $Ni/K_2Ti_xO_y(30)-Al_2O_3(70)$  were not much contaminated by carbon deposition. According to another research [66], a good-resistant catalyst was contained with carbon of only around 3-4% after longevity test. K. Urasaki et al. [67] suggests that these carbons are intermediate carbon and it can be the acceleration of gasification reaction between adsorbed intermediate carbon species and adsorbed steam ( $-OH_2$ ) or hydroxyl molecules ( $-OH$ ). Therefore, carbon deposition did not affect deactivation of the nickel catalysts for the steam methane reforming.



Table 4.5 Amount of carbon and hydrogen deposition of the spent Ni catalysts for 100 h

Sample	Deposition amount (wt%) <sup>a</sup>		H/C molar Ratio
	C	H	
FCR-4	0.32	0.00	0.00
Ni/Al <sub>2</sub> O <sub>3</sub>	2.96	0.43	1.74
Ni/K <sub>2</sub> Ti <sub>x</sub> O <sub>y</sub> (5)-Al <sub>2</sub> O <sub>3</sub> (95)	1.90	0.35	2.21
Ni/K <sub>2</sub> Ti <sub>x</sub> O <sub>y</sub> (11)-Al <sub>2</sub> O <sub>3</sub> (89)	3.87	0.38	1.17
Ni/K <sub>2</sub> Ti <sub>x</sub> O <sub>y</sub> (20)-Al <sub>2</sub> O <sub>3</sub> (80)	1.61	0.43	3.21
Ni/K <sub>2</sub> Ti <sub>x</sub> O <sub>y</sub> (30)-Al <sub>2</sub> O <sub>3</sub> (70)	0.49	0.24	5.88

<sup>a</sup> Determined by CHNS elemental analysis  
For the samples after the stability test as in Fig. 4.10.

Fig. 4.11 shows the XRD patterns of reduced  $\text{Ni/K}_2\text{Ti}_x\text{O}_y\text{-Al}_2\text{O}_3$  catalysts before and after the stability test. Crystalline phase change and nickel crystal size of the catalyst and reference catalysts are listed in Table 4.6. For  $\text{Ni/K}_2\text{Ti}_x\text{O}_y(5)\text{-Al}_2\text{O}_3(95)$ ,  $\text{Ni/K}_2\text{Ti}_x\text{O}_y(30)\text{-Al}_2\text{O}_3(70)$ , and FCR-4, the diffraction peaks of nickel metal ( $2\theta=44.5, 51.7$ , and  $76.7^\circ$ ) were almost disappeared, oxidizing onto NiO. For  $\text{Ni/Al}_2\text{O}_3$  and  $\text{Ni/K}_2\text{Ti}_x\text{O}_y(11)\text{-Al}_2\text{O}_3(89)$  catalysts, nickel metal phases were retained and their amount decreased, indicating larger Ni particles than those of before the reaction. Over only  $\text{Ni/K}_2\text{Ti}_x\text{O}_y(20)\text{-Al}_2\text{O}_3(80)$  catalyst, amount of nickel metal increased. According to these XRD results, those stability test results agree with the suggestion of previous researcher [36] that the rate of deactivation increases with increasing Ni particle size. In particular, the reduced and spent  $\text{Ni/K}_2\text{Ti}_x\text{O}_y(11)\text{-Al}_2\text{O}_3(89)$  catalysts have a dominant phase, which is assigned to  $\text{KTi}_8\text{O}_{13}$  (JCPDS 41-1097). In addition, nickel particles of spent  $\text{Ni/K}_2\text{Ti}_x\text{O}_y(11)\text{-Al}_2\text{O}_3(89)$  were well-dispersed on the support without strong sintering and oxidizing. Therefore, 11wt.%  $\text{K}_2\text{Ti}_x\text{O}_y$  loading in alumina-supported nickel catalyst can be considered to play important roles in suppressing sintering and oxidizing of active metal.

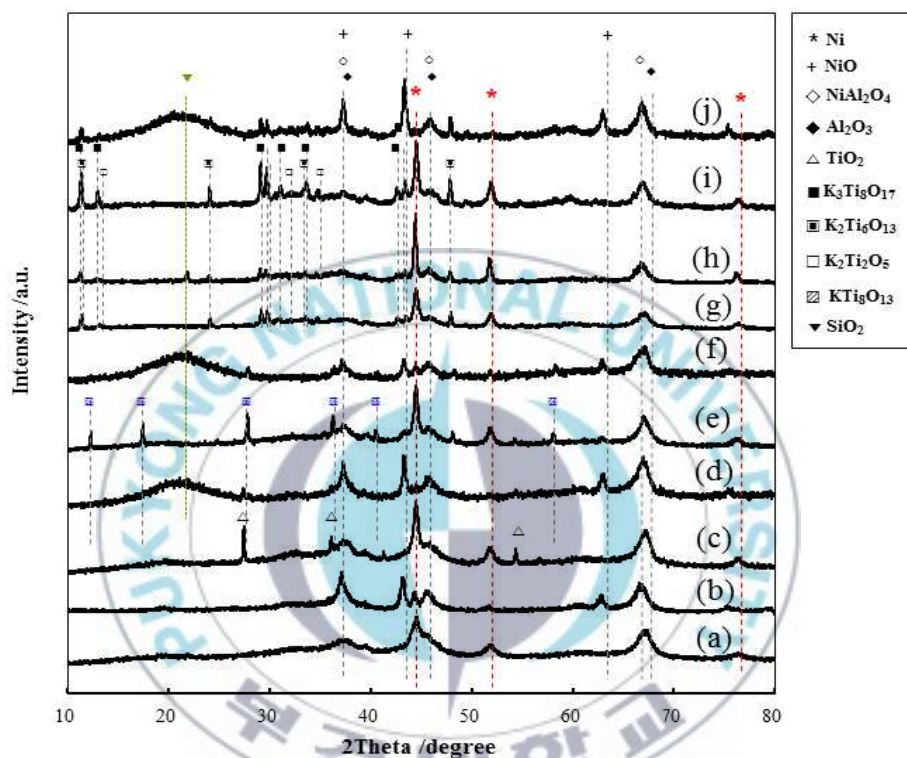


Fig. 4.11 X-ray diffraction patterns of fresh and spent samples of Ni/K<sub>2</sub>Ti<sub>x</sub>O<sub>y</sub>-Al<sub>2</sub>O<sub>3</sub> catalysts: (a) fresh and (b) spent Ni/Al<sub>2</sub>O<sub>3</sub>, (c) fresh and (d) spent Ni/K<sub>2</sub>Ti<sub>5</sub>O<sub>17</sub>(5)-Al<sub>2</sub>O<sub>3</sub>(95), (e) fresh and (f) spent Ni/K<sub>2</sub>Ti<sub>6</sub>O<sub>13</sub>(11)-Al<sub>2</sub>O<sub>3</sub>(89), (g) fresh and (h) spent Ni/K<sub>2</sub>Ti<sub>2</sub>O<sub>5</sub>(20)-Al<sub>2</sub>O<sub>3</sub>(80), (i) fresh and (j) spent Ni/KTi<sub>8</sub>O<sub>13</sub>(30)-Al<sub>2</sub>O<sub>3</sub>(70). (Fresh samples were after the reduction pretreatment and spent samples were after the stability test with reaction conditions as in Fig. 4.10)

Table 4.6 Crystalline phases change and Ni metal sizes of the catalysts before and after the stability test

Sample	Crystalline phases		Crystalline size of Ni (nm) <sup>c</sup>	
	Retained <sup>a</sup>	Changed <sup>b</sup>	Before test	After test
FCR-4	Ni	↑NiO, ↓Ni	31.0	36.4
Ni/Al <sub>2</sub> O <sub>3</sub>	Ni, NiAl <sub>2</sub> O <sub>4</sub> , γ-Al <sub>2</sub> O <sub>3</sub>	↑NiO, ↓Ni	12.6	23.9
Ni/K <sub>2</sub> Ti <sub>x</sub> O <sub>y</sub> (5)-Al <sub>2</sub> O <sub>3</sub> (95)	Ni, TiO <sub>2</sub> , NiAl <sub>2</sub> O <sub>4</sub> , γ-Al <sub>2</sub> O <sub>3</sub>	↑NiO, ↓Ni, ↓TiO <sub>2</sub>	17.4	-
Ni/K <sub>2</sub> Ti <sub>x</sub> O <sub>y</sub> (11)-Al <sub>2</sub> O <sub>3</sub> (89)	Ni, KTi <sub>8</sub> O <sub>13</sub> , TiO <sub>2</sub> , NiO, NiAl <sub>2</sub> O <sub>4</sub> , γ-Al <sub>2</sub> O <sub>3</sub>	↑NiO, ↓Ni, ↓KTi <sub>8</sub> O <sub>13</sub>	18.8	26.0
Ni/K <sub>2</sub> Ti <sub>x</sub> O <sub>y</sub> (20)-Al <sub>2</sub> O <sub>3</sub> (80)	Ni, K <sub>3</sub> Ti <sub>8</sub> O <sub>17</sub> , K <sub>2</sub> Ti <sub>6</sub> O <sub>13</sub> , K <sub>2</sub> Ti <sub>2</sub> O <sub>5</sub> , NiAl <sub>2</sub> O <sub>4</sub> , γ-Al <sub>2</sub> O <sub>3</sub>	↑Ni	16.1	30.5
Ni/K <sub>2</sub> Ti <sub>x</sub> O <sub>y</sub> (30)-Al <sub>2</sub> O <sub>3</sub> (70)	Ni, K <sub>3</sub> Ti <sub>8</sub> O <sub>17</sub> , K <sub>2</sub> Ti <sub>6</sub> O <sub>13</sub> , K <sub>2</sub> Ti <sub>2</sub> O <sub>5</sub> , NiAl <sub>2</sub> O <sub>4</sub> , γ-Al <sub>2</sub> O <sub>3</sub>	↑NiO, ↓Ni	21.1	-

<sup>a</sup> For reduced samples.

<sup>b</sup> After the stability test with reaction conditions as in Fig. 4.10.

<sup>c</sup> Calculated from Ni metal (111) plane using Scherrer equation by XRD.

Comparing the stability results of the catalysts with their  $H_2$ -TPR features (Table 4.2), catalysts having both  $\beta$  and  $\gamma$  type reducible NiO higher than 90% showed better catalytic stability. It means that catalysts having mainly weaker interaction between Ni and support such as  $NiO/K_2Ti_xO_y(50)-Al_2O_3(50)$  and  $NiO/K_2Ti_xO_y(30)-Al_2O_3(70)$  cannot lead longevity performance. Previously, much efforts have been made to understand the interaction between the metal component and the support, and the strong metal support interaction (SMSI) was often used to explain experimental phenomena [68-70]. However, TPR characterization results demonstrate that  $NiO/K_2Ti_xO_y-Al_2O_3$  catalysts have weaker metal-support interactions compared with the  $NiO/Al_2O_3$ , but they show better catalytic stability. Therefore, the SMSI model is not perfectly proper to understand above phenomena. We thus can consider that utilization of Ni species leading proper strength to the interaction between Ni and the support can contribute to good catalytic stability of the catalyst.

As we known, there are several factors for deactivation of reforming catalysts such as carbon deposition as well as sulfur poisoning [37]. Thus, it is necessary to investigate the resistance of  $Ni/K_2Ti_xO_y-Al_2O_3$  catalysts to sulfur compounds in gaseous fuel, i.e. city gas. In our future work, these performance and further

characteristics of the  $\text{Ni/K}_2\text{Ti}_x\text{O}_y\text{-Al}_2\text{O}_3$  catalysts will be revealed by using more pragmatic methods.

In this investigation, we report the characterization and catalytic performance of  $\text{K}_2\text{Ti}_x\text{O}_y\text{-Al}_2\text{O}_3$  supported Ni catalyst for the steam methane reforming. It reveals that the  $\text{Ni/K}_2\text{Ti}_x\text{O}_y\text{-Al}_2\text{O}_3$  catalysts show comparable catalytic activity to FCR-4 under the mild experimental condition: at  $750^\circ\text{C}$ , in reactant flow with S/C feed ratio of 2.5, and at a GHSV of  $15,000\text{ h}^{-1}$ , and under atmospheric pressure. Stability test under the severe reaction condition, at  $800^\circ\text{C}$ , in flow with S/C feed ratio of 1.0, and at a GHSV of  $200,000\text{ h}^{-1}$ , over the  $\text{Ni/K}_2\text{Ti}_x\text{O}_y\text{-Al}_2\text{O}_3$  catalysts, demonstrates that the  $\text{Ni/K}_2\text{Ti}_x\text{O}_y\text{-Al}_2\text{O}_3$  catalysts having less than 11%  $\text{K}_2\text{Ti}_x\text{O}_y$  of the support maintain their good stability for the reaction time of 100 hours. It is found that the main factors accounting for the better catalytic performance over the  $\text{Ni/K}_2\text{Ti}_x\text{O}_y\text{-Al}_2\text{O}_3$  catalysts than  $\text{Ni/Al}_2\text{O}_3$  are the medium strength of interaction between Ni and support, proper amount of  $\text{K}_2\text{Ti}_x\text{O}_y$  additive, and their superior stability. This work figures out that the proper amount of  $\text{K}_2\text{Ti}_x\text{O}_y$  would be an promising additive material of alumina supported nickel catalyst for steam methane reforming process.



## 5. Catalytic Activity and Characterization of

### **Ni/K<sub>2-x</sub>Ca<sub>x/2</sub>Ti<sub>y</sub>O<sub>z</sub>-Al<sub>2</sub>O<sub>3</sub> Catalyst for Steam Methane**

### **Reforming**

The work described in this chapter are about the Ca content effect of K<sub>2-x</sub>Ca<sub>x/2</sub>Ti<sub>y</sub>O<sub>z</sub> used as additive for Ni/Al<sub>2</sub>O<sub>3</sub> catalyst. The catalyst preparation methods, experimental apparatus and analytical equipment are presented in the Chapter 3. The correlation between characteristics of the catalyst surface and its catalytic activity is also discussed.

The catalysts were prepared with a fixed 10 wt.% nickel loading in the catalyst, 20 wt.% loading an mixed oxide additive, K<sub>2-x</sub>Ca<sub>x/2</sub>Ti<sub>y</sub>O<sub>z</sub>, in the support, and varying amounts of Ca of the additive: x=0.0, 0.1, 0.6, 1.0, 1.4, 2.0. In those samples, the x=0.0 sample is the same with Ni/K<sub>2</sub>Ti<sub>y</sub>O<sub>z</sub>(20)-Al<sub>2</sub>O<sub>3</sub>(80) in Chapter 3. In order to examine composition effect of an additive in the nickel catalyst-Ni/K<sub>2-x</sub>Ca<sub>x/2</sub>Ti<sub>y</sub>O<sub>z</sub>(20)-Al<sub>2</sub>O<sub>3</sub>(80), different contents of K<sub>2-x</sub>Ca<sub>x/2</sub>Ti<sub>y</sub>O<sub>z</sub> were applied and they were denoted as x=0.0, x=0.1, x=0.6, x=1.0, x=1.4, and x=2.0, indicating Ni/K<sub>2</sub>Ti<sub>y</sub>O<sub>z</sub>(20)-Al<sub>2</sub>O<sub>3</sub>(80), Ni/K<sub>1.9</sub>Ca<sub>0.05</sub>Ti<sub>y</sub>O<sub>z</sub>(20)-Al<sub>2</sub>O<sub>3</sub>(80), Ni/K<sub>1.9</sub>Ca<sub>0.05</sub>Ti<sub>y</sub>O<sub>z</sub>(20)-Al<sub>2</sub>O<sub>3</sub>(80), Ni/K<sub>1.4</sub>Ca<sub>0.3</sub>Ti<sub>y</sub>O<sub>z</sub>(20)-Al<sub>2</sub>O<sub>3</sub>(80), Ni/K<sub>1.0</sub>Ca<sub>0.5</sub>Ti<sub>y</sub>O<sub>z</sub>(20)-Al<sub>2</sub>O<sub>3</sub>(80), Ni/K<sub>0.6</sub>Ca<sub>0.7</sub>Ti<sub>y</sub>O<sub>z</sub>(20)-Al<sub>2</sub>O<sub>3</sub>(80), and

Ni/CaTi<sub>y</sub>O<sub>z</sub>(20)-Al<sub>2</sub>O<sub>3</sub>(80); their samples before reduction were denoted as NiO/K<sub>2-x</sub>Ca<sub>x/2</sub>Ti<sub>y</sub>O<sub>z</sub>(20)-Al<sub>2</sub>O<sub>3</sub>(80).

### 5.1. Characteristics of Ni/K<sub>2-x</sub>Ca<sub>x/2</sub>Ti<sub>y</sub>O<sub>z</sub>-Al<sub>2</sub>O<sub>3</sub> catalyst

Table 5.1 compiles the surface areas of the K<sub>2-x</sub>Ca<sub>x/2</sub>Ti<sub>y</sub>O<sub>z</sub>-Al<sub>2</sub>O<sub>3</sub> and NiO/K<sub>2-x</sub>Ca<sub>x/2</sub>Ti<sub>y</sub>O<sub>z</sub>-Al<sub>2</sub>O<sub>3</sub> samples, which is before and after loading nickel component, respectively. After K<sub>2-x</sub>Ca<sub>x/2</sub>Ti<sub>y</sub>O<sub>z</sub> loading on Al<sub>2</sub>O<sub>3</sub> (S<sub>BET</sub>=173.1 m<sup>2</sup>/g), the surface areas of all K<sub>2-x</sub>Ca<sub>x/2</sub>Ti<sub>y</sub>O<sub>z</sub>-Al<sub>2</sub>O<sub>3</sub> severely diminish, compared to NiO/Al<sub>2</sub>O<sub>3</sub> (106.1 m<sup>2</sup>/g). In the next step, after NiO loading, the surface areas of most NiO/K<sub>2-x</sub>Ca<sub>x/2</sub>Ti<sub>y</sub>O<sub>z</sub>-Al<sub>2</sub>O<sub>3</sub> samples slightly decrease, indicating smaller than those of NiO/K<sub>2</sub>Ti<sub>x</sub>O<sub>y</sub>-Al<sub>2</sub>O<sub>3</sub> (Table 4.1). However, the surface area of the x=0.0 sample slightly increase. In particular, the x=0.6 sample has the smallest surface area, because its additive may make blocking most of pores of Al<sub>2</sub>O<sub>3</sub>.

Table 5.1 Surface area of NiO/K<sub>2-x</sub>Ca<sub>x/2</sub>Ti<sub>y</sub>O<sub>z</sub>-Al<sub>2</sub>O<sub>3</sub> samples

S <sub>BET</sub> (m <sup>2</sup> /g)	x of K <sub>2-x</sub> Ca <sub>x/2</sub> Ti <sub>y</sub> O <sub>z</sub> -Al <sub>2</sub> O <sub>3</sub>					
	0.0	0.1	0.6	1.0	1.4	2.0
K <sub>2-x</sub> Ca <sub>x/2</sub> Ti <sub>y</sub> O <sub>z</sub> -Al <sub>2</sub> O <sub>3</sub>	61.0	47.2	19.7	69.3	59.6	55.6

Fig 5.1 presents the X-ray diffraction patterns of the calcined samples,  $\text{NiO/K}_{2-x}\text{Ca}_{x/2}\text{Ti}_y\text{O}_z\text{-Al}_2\text{O}_3$ , and a reference sample,  $\text{NiO/Al}_2\text{O}_3$ . Their crystalline phases are also listed in Table 5.2. Those patterns of  $\text{NiO/K}_{2-x}\text{Ca}_{x/2}\text{Ti}_y\text{O}_z\text{-Al}_2\text{O}_3$  catalysts represents several distinctive features. First of all, for all samples, spinel  $\text{NiAl}_2\text{O}_4$  phase is possessed. As mentioned in Chapter 3, the XRD peaks' angles of the sample are slightly shifted from those of  $\gamma\text{-Al}_2\text{O}_3$ . Next, for the samples including the lowest Ca contents (Fig. 5.1c), various potassium titanates derived from K-Ti-O system such as  $\text{K}_3\text{Ti}_8\text{O}_{16}$ ,  $\text{K}_2\text{Ti}_6\text{O}_{13}$ , and  $\text{K}_2\text{Ti}_2\text{O}_5$  are appeared on the catalysts.

In addition, for the catalysts having Ca contents of higher than  $x=0.6$ , the diffraction peaks at  $33.3^\circ$ ,  $50.2^\circ$ , and  $59.5^\circ$  are the typical feature of calcium titanate (pervoskite,  $\text{CaTiO}_3$ , JCPDS no. 65-3287) phase, and the other phases from Ca-Ti-O are not exist. Apart from these features for the samples ( $>x=0.6$ ), another potassium titanates are not produced except for  $\text{KTi}_8\text{O}_{16}$ . That  $\text{KTi}_8\text{O}_{16}$  is also not appeared in the  $\text{NiO/K}_2\text{Ti}_x\text{O}_y\text{-Al}_2\text{O}_3$  containing various loading of  $\text{K}_2\text{Ti}_x\text{O}_y$ , as shown in Chapter 3. In fact, since Ca/Ti molar ratio = 1 is enough for formation of  $\text{CaTiO}_3$ , remained titanium is isolated by type of  $\text{TiO}_2$  for all samples containing Ca.

On the other hand, most of the samples containing Ca have not NiO phase except for the  $x=0.6$  sample. It means that their NiO

particles are well-dispersed and/or become solid states such as  $\text{NiTiO}_3$  and  $\text{NiAl}_2\text{O}_4$  with  $\text{TiO}_2$  and  $\text{Al}_2\text{O}_3$ , respectively. As expected, for the  $x=2.0$  sample,  $\text{Ni}/\text{CaTi}_y\text{O}_z(20)\text{-Al}_2\text{O}_3(80)$ , the peaks attributed to  $\text{NiTiO}_3$  (JCPDS no. 85-0451) are detected. Therefore,  $\text{NiO}/\text{K}_{2-x}\text{Ca}_{x/2}\text{Ti}_y\text{O}_z\text{-Al}_2\text{O}_3$  catalysts have mainly phases of  $\text{KTi}_8\text{O}_{16}$ ,  $\text{CaTiO}_3$ ,  $\text{TiO}_2$ , and  $\text{NiAl}_2\text{O}_4$ .

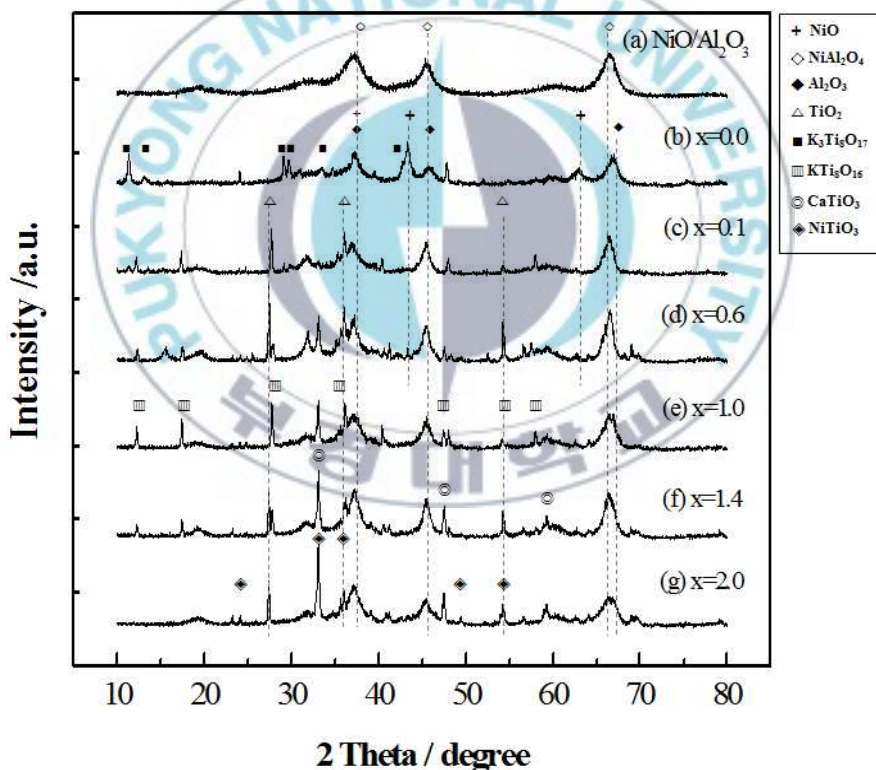


Fig. 5.1 X-ray diffraction patterns of  $\text{NiO}/\text{Al}_2\text{O}_3$  and  $\text{NiO}/\text{K}_{2-x}\text{Ca}_{x/2}\text{Ti}_y\text{O}_z\text{-Al}_2\text{O}_3$  catalysts.

Table 5.2 Crystalline phases from XRD for the calcined Ni catalysts

Catalyst	Crystallite size
NiO/Al <sub>2</sub> O <sub>3</sub>	NiAl <sub>2</sub> O <sub>4</sub> , $\gamma$ -Al <sub>2</sub> O <sub>3</sub>
x=0.0, NiO/K <sub>2</sub> Ti <sub>x</sub> O <sub>y</sub> (20)-Al <sub>2</sub> O <sub>3</sub> (80)	NiO, K <sub>3</sub> Ti <sub>8</sub> O <sub>17</sub> , K <sub>2</sub> Ti <sub>6</sub> O <sub>13</sub> , K <sub>2</sub> Ti <sub>2</sub> O <sub>5</sub> , NiAl <sub>2</sub> O <sub>4</sub> , $\gamma$ -Al <sub>2</sub> O <sub>3</sub>
x=0.1, NiO/K <sub>1.9</sub> Ca <sub>0.05</sub> Ti <sub>y</sub> O <sub>z</sub> (20)-Al <sub>2</sub> O <sub>3</sub> (80)	TiO <sub>2</sub> , KTi <sub>8</sub> O <sub>16</sub> , K <sub>3</sub> Ti <sub>8</sub> O <sub>17</sub> , NiAl <sub>2</sub> O <sub>4</sub> , $\gamma$ -Al <sub>2</sub> O <sub>3</sub>
x=0.6, NiO/K <sub>1.4</sub> Ca <sub>0.3</sub> Ti <sub>y</sub> O <sub>z</sub> (20)-Al <sub>2</sub> O <sub>3</sub> (80)	TiO <sub>2</sub> , CaTiO <sub>3</sub> , KTi <sub>8</sub> O <sub>16</sub> , NiO, NiAl <sub>2</sub> O <sub>4</sub> , $\gamma$ -Al <sub>2</sub> O <sub>3</sub>
x=1.0, NiO/K <sub>1.0</sub> Ca <sub>0.5</sub> Ti <sub>y</sub> O <sub>z</sub> (20)-Al <sub>2</sub> O <sub>3</sub> (80)	CaTiO <sub>3</sub> , KTi <sub>8</sub> O <sub>16</sub> , TiO <sub>2</sub> , NiAl <sub>2</sub> O <sub>4</sub> , $\gamma$ -Al <sub>2</sub> O <sub>3</sub>
x=1.4, NiO/K <sub>0.6</sub> Ca <sub>0.7</sub> Ti <sub>y</sub> O <sub>z</sub> (20)-Al <sub>2</sub> O <sub>3</sub> (80)	CaTiO <sub>3</sub> , TiO <sub>2</sub> , KTi <sub>8</sub> O <sub>16</sub> , NiAl <sub>2</sub> O <sub>4</sub> , $\gamma$ -Al <sub>2</sub> O <sub>3</sub>
x=2.0, NiO/CaTi <sub>y</sub> O <sub>z</sub> (20)-Al <sub>2</sub> O <sub>3</sub> (80)	CaTiO <sub>3</sub> , TiO <sub>2</sub> , NiTiO <sub>3</sub> , NiAl <sub>2</sub> O <sub>4</sub> , $\gamma$ -Al <sub>2</sub> O <sub>3</sub>

Like the case of  $\text{NiO}/\text{K}_2\text{Ti}_x\text{O}_y\text{-Al}_2\text{O}_3$  in Chapter 3, TPR measurements are carried out to examine the interaction between nickel species and  $\text{K}_{2-x}\text{Ca}_{x/2}\text{Ti}_y\text{O}_z\text{-Al}_2\text{O}_3$  support. Fig. 5.2 shows  $\text{H}_2$ -TPR profiles of calcined catalyst samples with various Ca contents. All samples containing Ca exhibits a dominant reduction band at higher than  $800^\circ\text{C}$ , indicating the existence of  $\gamma$ -type NiO (higher than temperature,  $755^\circ\text{C}$  at dot line in Fig 5.2) and nickel aluminate phase. It is consistent with above XRD results. This suggests the reduction of NiO for  $\text{NiO}/\text{K}_{2-x}\text{Ca}_{x/2}\text{Ti}_y\text{O}_z\text{-Al}_2\text{O}_3$  is so difficult, unlike that of  $\text{NiO}/\text{K}_2\text{Ti}_x\text{O}_y\text{-Al}_2\text{O}_3$  because of a strong interaction between Ni and  $\text{K}_{2-x}\text{Ca}_{x/2}\text{Ti}_y\text{O}_z\text{-Al}_2\text{O}_3$  support.

Especially, for the  $x=0.6$  sample, interaction between Ni and the support is the strongest (Fig. 5.2) as well as its crystalline phases are so complicated, having unknown peaks (Fig. 5.1). In addition, its surface area is also the smallest. Therefore, physicochemical property of the  $x=0.6$  sample is not proper to be applied by a catalyst.



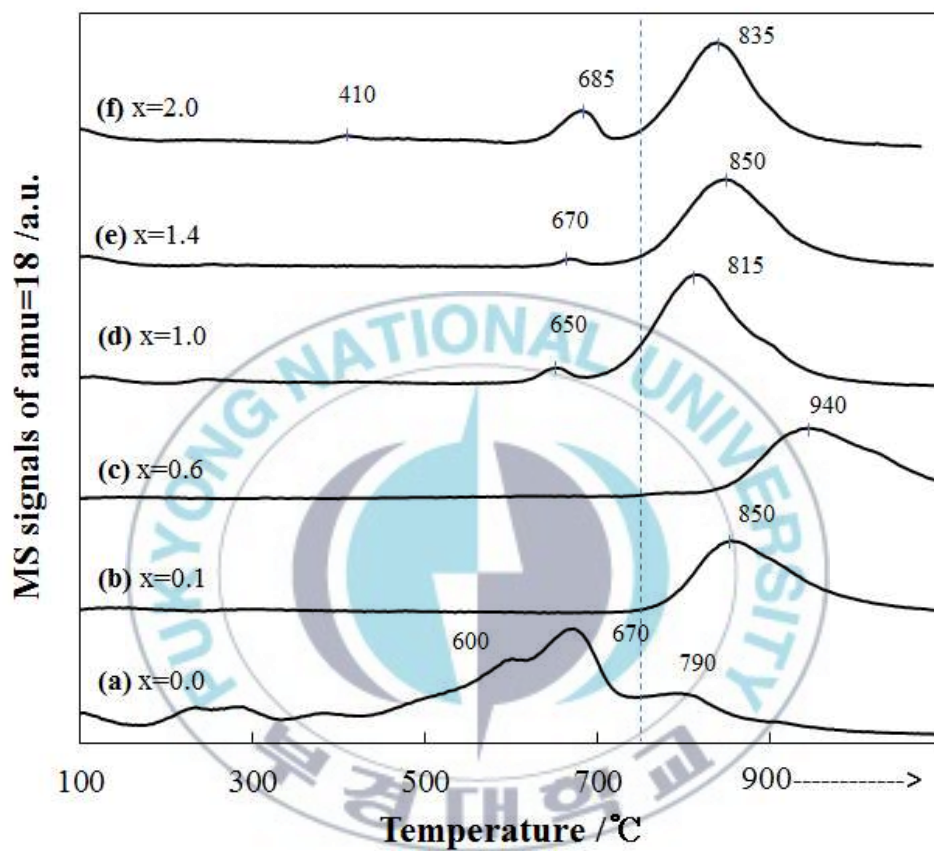


Fig. 5.2. H<sub>2</sub> temperature-programmed reduction (TPR) profiles for NiO/K<sub>2-x</sub>Ca<sub>x/2</sub>Ti<sub>y</sub>O<sub>z</sub>-Al<sub>2</sub>O<sub>3</sub> catalysts with Ca contents.

## 5.2. Activity of $\text{Ni/K}_{2-x}\text{Ca}_{x/2}\text{Ti}_y\text{O}_z\text{-Al}_2\text{O}_3$ catalyst

Activity for steam methane reforming over  $\text{Ni/K}_{2-x}\text{Ca}_{x/2}\text{Ti}_y\text{O}_z\text{-Al}_2\text{O}_3$  catalysts was tested under the mild reaction condition and the average results in steady state after 1 hour reaction were listed in Table 5.3 and plotted in Fig. 5.3. With increasing Ca content, the catalytic activities over  $\text{Ni/K}_{2-x}\text{Ca}_{x/2}\text{Ti}_y\text{O}_z\text{-Al}_2\text{O}_3$  catalysts slightly decrease (Fig. 5.3). All of tested samples show acceptable methane conversions of about 94 to 97%. compared with reference catalysts such as FCR-4 (97.5%) and  $\text{Ni/Al}_2\text{O}_3$  (96.9%). The activity of  $\text{Ni/K}_{2-x}\text{Ca}_{x/2}\text{Ti}_y\text{O}_z\text{-Al}_2\text{O}_3$  samples having lower Ca content ( $x=0.0\text{-}0.6$ ) are somewhat better than those of them having higher it ( $x=1.0\text{-}2.0$ ).

Apart from this activity test under the mild reaction condition, a severe reaction condition can be applied for investigating catalytic stability of the catalyst, which is a experimental condition easy to cause deactivation on the catalyst surface (i.e., feed composition of lower S/C ratio than 1.0, higher reaction temperature, and long time-on-stream). Therefore, in the next paragraph, results for the stability activity for the catalysts are discussed.

Table 5.3 Activities of steam methane reforming over Ni/K<sub>2-x</sub>Ca<sub>x/2</sub>Ti<sub>y</sub>O<sub>z</sub>-Al<sub>2</sub>O<sub>3</sub> catalysts

x of K <sub>2-x</sub> Ca <sub>x/2</sub> Ti <sub>y</sub> O <sub>z</sub> -Al <sub>2</sub> O <sub>3</sub>	X <sub>CH4</sub> (%)	S <sub>H2/CH4</sub>	S <sub>CO/CH4</sub>	S <sub>CO2/CH4</sub>
0.0	97.2	3.01	0.77	0.18
0.1	97.0	2.97	0.79	0.15
0.6	96.6	3.00	0.73	0.20
1.0	94.4	2.87	0.70	0.19
1.4	95.0	2.89	0.72	0.18
2.0	94.5	2.82	0.72	0.17

The reaction conditions: S/C=2.5, GHSV=15,000 h<sup>-1</sup>, T=750°C, and time-on-stream=20 h.

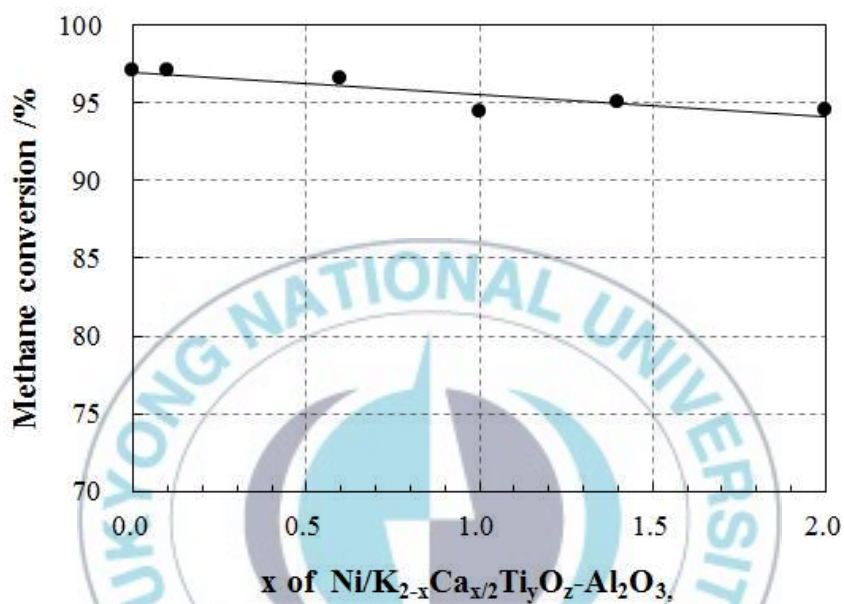


Fig. 5.3 Activity change of steam methane reforming over  $\text{Ni/K}_{2-x}\text{Ca}_{x/2}\text{Ti}_y\text{O}_z\text{-Al}_2\text{O}_3$  catalysts with Ca content. (Reaction conditions: S/C=2.5, GHSV=15,000  $\text{h}^{-1}$ ,  $T=750^\circ\text{C}$ , and time-on-stream=20 h)

Catalytic stability test of steam methane reforming over the  $\text{Ni/K}_{2-x}\text{Ca}_{x/2}\text{Ti}_y\text{O}_z\text{-Al}_2\text{O}_3$  catalysts was tested under the severe reaction condition for 100 h, shown in Table 5.4 and Fig 5.4. According to the results, deactivation degree of the  $\text{Ni/K}_{1.0}\text{Ca}_{0.5}\text{Ti}_y\text{O}_z(20)\text{-Al}_2\text{O}_3(80)$  and  $\text{Ni/CaTi}_y\text{O}_z(20)\text{-Al}_2\text{O}_3(80)$  were 7.2 and 1.3%, respectively. The catalysts containing Ca have more catalytic stability as well as better activity for this reaction than the other catalysts such as  $\text{Ni/Al}_2\text{O}_3$ , FCR-4 (Table 4.4), and  $\text{Ni/K}_2\text{Ti}_y\text{O}_z(20)\text{-Al}_2\text{O}_3(80)$ . In particular,  $\text{Ni/CaTi}_y\text{O}_z(20)\text{-Al}_2\text{O}_3(80)$  catalyst showed the best catalytic stability among all of catalysts tested. Since its amount of deposited carbon is also low, 1.67 wt.%,  $\text{Ni/CaTi}_y\text{O}_z(20)\text{-Al}_2\text{O}_3(80)$  have a good resistance to coking.

Table 5.4 Catalytic stability results of  $\text{Ni/K}_{2-x}\text{Ca}_{x/2}\text{Ti}_y\text{O}_z\text{-Al}_2\text{O}_3$  and  $\text{Ni/Al}_2\text{O}_3$  catalysts

Catalyst	Terminal $X_{\text{CH}_4}$ (%) <sup>a</sup>	Deactivation degree (%) <sup>b</sup>
$\text{Ni/Al}_2\text{O}_3$	68.3	7.1
$x=2.0$ , $\text{Ni/CaTi}_y\text{O}_z(20)\text{-Al}_2\text{O}_3(80)$	79.0	1.3
$x=1.0$ , $\text{Ni/K}_{1.0}\text{Ca}_{0.5}\text{Ti}_y\text{O}_z(20)\text{-Al}_2\text{O}_3(80)$	69.6	7.2
$x=0.0$ , $\text{Ni/KTi}_y\text{O}_z(20)\text{-Al}_2\text{O}_3(80)$	70.6	8.1

Same as Table 4.4.

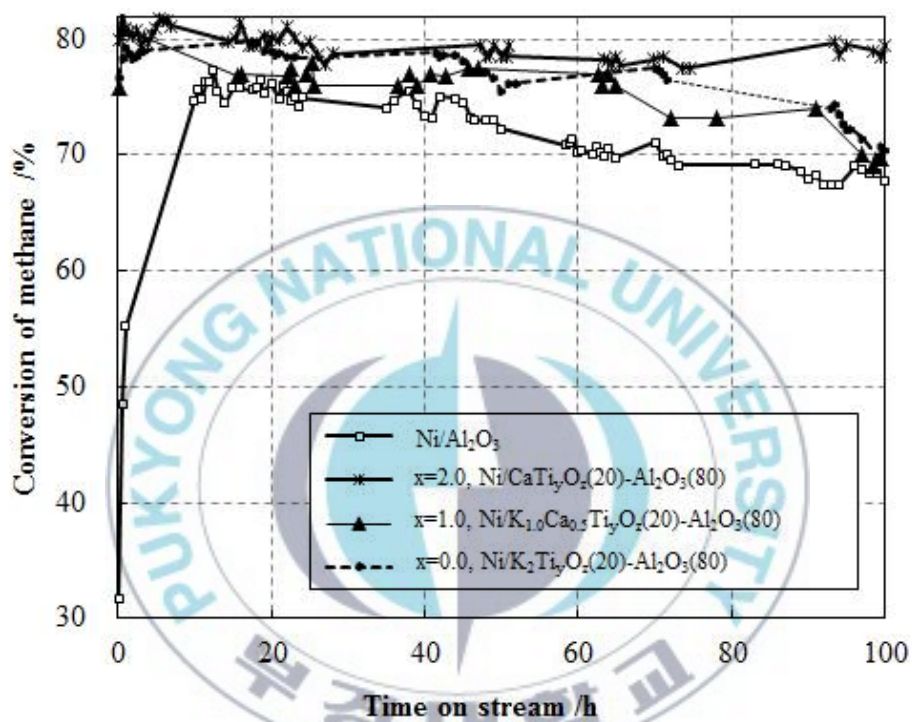


Fig. 5.4 Change in activity of  $\text{Ni}/\text{Al}_2\text{O}_3$  and  $\text{Ni}/\text{K}_{2-x}\text{Ca}_{x/2}\text{Ti}_{0.5}\text{O}_7\text{-Al}_2\text{O}_3$  catalysts with different Ca content for steam methane reforming. (Reaction conditions as Fig. 4.10)



### 5.3. Role of $\text{CaTiO}_3$ on $\text{Ni}/\text{Al}_2\text{O}_3$ catalyst for steam methane reforming

In summary for this chapter, all  $\text{Ni}/\text{K}_{2-x}\text{Ca}_{x/2}\text{Ti}_y\text{O}_z\text{-Al}_2\text{O}_3$  catalysts containing Ca ( $x=0.1\text{-}2.0$ ) show acceptable activity as well as superior catalytic stability (i.e.,  $\text{Ni}/\text{CaTi}_y\text{O}_z(20)\text{-Al}_2\text{O}_3(80)$  catalyst) for steam methane reforming. All the samples also have crystalline of  $\text{CaTiO}_3$ , which corresponds to a kind of perovskite. According to Takehira group's researches [72-75] reported, the perovskite-type oxides such as  $\text{SrO}_3$ ,  $\text{CaTiO}_3$ , and  $\text{BaTiO}_3$  that contain a small amount of nickel in the titanium sites show high catalytic activities with high resistance to coking in both partial oxidation and dry reforming of methane, because of the high dispersion of nickel. They also examined oxygen mobility in perovskites and found that high resistance to coking might be partly due to the migration of mobile oxygen from the perovskite support to the metallic nickel particles.

Since perovskites have so low surface area to be applied to support, hence, use of perovskite as an additive may be a promising method for modification of alumina-supported nickel steam reforming catalyst. It is mechanistically expected that oxidation of  $\text{CH}_x$  fragments adsorbed on metallic nickel would be promoted by the lattice oxygen in perovskite oxides, as proposed for CO oxidation

[76,77] and dry reforming of methane [78-81]. Consequently, the addition of calcium titanate to Ni/Al<sub>2</sub>O<sub>3</sub> effectively inhibit their deactivation through carbon deposition.



## **6. Catalytic Activity and Characterization of Ni/CaTi<sub>x</sub>O<sub>y</sub>-Al<sub>2</sub>O<sub>3</sub>**

### **Catalyst for Steam Methane Reforming**

The work described in this chapter are the effect of CaTi<sub>x</sub>O<sub>y</sub> content, reaction temperature condition, and CaTi<sub>x</sub>O<sub>y</sub> additives on the activity and sulfur-tolerance ability of Ni/CaTi<sub>x</sub>O<sub>y</sub>-Al<sub>2</sub>O<sub>3</sub> for steam methane reforming. The catalyst preparation methods, experimental apparatus, and analytical equipment are presented in the Chapter 3. The correlation between characteristics of the catalyst surface and its catalytic activity is also discussed.

#### **6.1. Characteristics of Ni/CaTi<sub>x</sub>O<sub>y</sub>-Al<sub>2</sub>O<sub>3</sub> catalyst**

X-ray diffraction patterns of  $\gamma$ -Al<sub>2</sub>O<sub>3</sub>, NiO/Al<sub>2</sub>O<sub>3</sub>, and NiO/K<sub>2</sub>Ti<sub>x</sub>O<sub>y</sub>-Al<sub>2</sub>O<sub>3</sub> catalysts are presented in Fig 6.1. The patterns displayed several distinctive features. First, for all the samples including CaTi<sub>x</sub>O<sub>y</sub> (Fig. 6.1, a to d), nickel oxide phase is well-dispersed and titanium component is isolated on the catalysts. Next, for the catalysts having higher contents of CaTi<sub>x</sub>O<sub>y</sub> (Fig. 6.1, c and d), these samples have solid state oxides derived from M-Ti-O

system such as  $\text{CaTiO}_3$  and  $\text{NiTiO}_3$ . With increase of the  $\text{CaTi}_x\text{O}_y$  amount, the peak intensities of these solid state phases are increased obviously, indicating the strong interaction between  $\text{NiO}$  and  $\text{CaTi}_x\text{O}_y$  additive onto the supports.

Table 6.1 shows the surface areas, crystalline sizes, and retained phases of the  $\text{NiO}/\text{CaTi}_x\text{O}_y\text{-Al}_2\text{O}_3$  catalysts. The crystalline diameters of  $\text{NiO}$  on  $\text{CaTi}_x\text{O}_y\text{-Al}_2\text{O}_3$  catalysts are calculated to be 11.0 to 14.5 nm (Table 6.1) unlike the size of  $\text{NiO}$  increases with increasing  $\text{K}_2\text{Ti}_x\text{O}_y$  content in the samples (Table 4.1). Table 6.1 compares the surface areas of the  $\text{NiO}/\text{CaTi}_x\text{O}_y\text{-Al}_2\text{O}_3$  catalysts with different content of  $\text{CaTi}_x\text{O}_y$ . After the  $\text{CaTi}_x\text{O}_y$  loading, the surface areas (51-73  $\text{m}^2/\text{g}$ ) of the nickel catalysts were smaller than that (106  $\text{m}^2/\text{g}$ , in Table 4.1) of  $\text{NiO}/\text{Al}_2\text{O}_3$ . The reason is that some of the pores may be blocked by  $\text{CaTi}_x\text{O}_y$  nanoparticles like  $\text{K}_2\text{Ti}_x\text{O}_y$ . However, between  $\text{CaTi}_x\text{O}_y$  and  $\text{K}_2\text{Ti}_x\text{O}_y$ ,  $\text{CaTi}_x\text{O}_y$  less affects diminish of the surface area of the modified nickel catalyst. Like case of  $\text{K}_2\text{Ti}_x\text{O}_y$ ,  $\text{CaTi}_x\text{O}_y$  is likely that appropriate amount, approximately 20 wt.%, can induce dispersing nickel component onto a support. Thus, it found that  $\text{NiO}$  particles do not be isolated and can be well-dispersed onto the  $\text{CaTi}_x\text{O}_y\text{-Al}_2\text{O}_3$  supports.

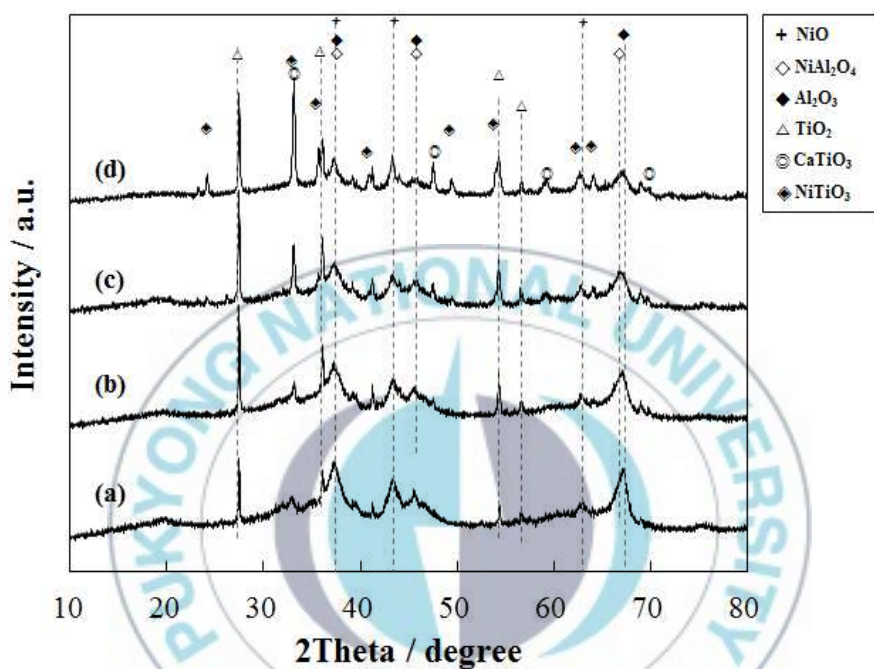


Fig. 6.1 X-ray diffraction patterns of NiO/CaTi<sub>x</sub>O<sub>y</sub>-Al<sub>2</sub>O<sub>3</sub> catalysts with CaTi<sub>x</sub>O<sub>y</sub> loading: (a) NiO/CaTi<sub>x</sub>O<sub>y</sub>(5)-Al<sub>2</sub>O<sub>3</sub>(95), (b) NiO/CaTi<sub>x</sub>O<sub>y</sub>(11)-Al<sub>2</sub>O<sub>3</sub>(89), (c) NiO/CaTi<sub>x</sub>O<sub>y</sub>(20)-Al<sub>2</sub>O<sub>3</sub>(80), and (d) NiO/CaTi<sub>x</sub>O<sub>y</sub>(30)-Al<sub>2</sub>O<sub>3</sub>(70).

Table 6.1 Physical properties of NiO/CaTi<sub>x</sub>O<sub>y</sub>-Al<sub>2</sub>O<sub>3</sub> catalysts

Catalyst	BET surface area (m <sup>2</sup> ·g <sub>cat</sub> <sup>-1</sup> )	Crystallite size <sup>a</sup> (nm)	Crystallite phases <sup>b</sup>
NiO/CaTi <sub>x</sub> O <sub>y</sub> (5)-Al <sub>2</sub> O <sub>3</sub> (95)	51.3	11.0	NiO, TiO <sub>2</sub> , NiAl <sub>2</sub> O <sub>4</sub> , γ-Al <sub>2</sub> O <sub>3</sub>
NiO/CaTi <sub>x</sub> O <sub>y</sub> (11)-Al <sub>2</sub> O <sub>3</sub> (89)	53.9	14.0	NiO, CaTiO <sub>3</sub> , TiO <sub>2</sub> , NiAl <sub>2</sub> O <sub>4</sub> , γ-Al <sub>2</sub> O <sub>3</sub>
NiO/CaTi <sub>x</sub> O <sub>y</sub> (20)-Al <sub>2</sub> O <sub>3</sub> (80)	73.6	14.5	NiO, CaTiO <sub>3</sub> , TiO <sub>2</sub> , NiTiO <sub>3</sub> , NiAl <sub>2</sub> O <sub>4</sub> , γ-Al <sub>2</sub> O <sub>3</sub>
NiO/CaTi <sub>x</sub> O <sub>y</sub> (50)-Al <sub>2</sub> O <sub>3</sub> (50)	65.2	12.8	NiO, CaTiO <sub>3</sub> , TiO <sub>2</sub> , NiTiO <sub>3</sub> , NiAl <sub>2</sub> O <sub>4</sub> , γ-Al <sub>2</sub> O <sub>3</sub>

<sup>a</sup> Calculated from NiO (220) plane using Scherrer equation from XRD for calcined samples.

<sup>b</sup> From XRD patterns in Fig. 6.1.



In order to investigate between nickel species and  $\text{CaTi}_x\text{O}_y\text{-Al}_2\text{O}_3$  support., TPR measurements are carried out for the  $\text{NiO/CaTi}_x\text{O}_y\text{-Al}_2\text{O}_3$  catalysts. Fig. 6.2 shows  $\text{H}_2$ -TPR profiles of calcined catalyst samples with various  $\text{CaTi}_x\text{O}_y$  contents. The  $\text{H}_2\text{O}$  ( $\text{amu}=18$ ) generating curves are derived from  $\text{H}_2$  consumption. As a results,  $\gamma$ - and  $\beta$ -type  $\text{NiO}$  is found in all samples. Particularly,  $\beta$ -type  $\text{NiO}$  becomes dominant for the  $\text{NiO/CaTi}_x\text{O}_y(20)\text{-Al}_2\text{O}_3(80)$  in Fig. 6.2c. For samples of Fig. 6.2, (a), (b), and (d), a dominant reduction band at higher than  $750^\circ\text{C}$ , indicating the existence of solid state phase with nickel such as  $\text{NiAl}_2\text{O}_4$  and  $\text{NiTiO}_3$ . It is known that  $\text{NiO}$  can react with  $\text{Al}_2\text{O}_3$  to form a highly stable  $\text{NiAl}_2\text{O}_4$  phase which has a lower reducibility than that of  $\text{NiO}$  [59].  $\text{NiO/CaTi}_x\text{O}_y(20)\text{-Al}_2\text{O}_3(80)$  and  $\text{NiO/CaTi}_x\text{O}_y(30)\text{-Al}_2\text{O}_3(70)$  catalysts have also  $\alpha$ -type (weak interaction between the  $\text{NiO}$  and support,  $300\text{-}475^\circ\text{C}$ )  $\text{NiO}$ .

Like case of  $\text{NiO/K}_2\text{Ti}_x\text{O}_y\text{-Al}_2\text{O}_3$ , the metal-support interaction in  $\text{NiO/CaTi}_x\text{O}_y\text{-Al}_2\text{O}_3$  is also weaker than that of  $\text{NiO/Al}_2\text{O}_3$ . It means that  $\text{CaTi}_x\text{O}_y$  in a  $\text{Al}_2\text{O}_3$ -supported  $\text{Ni}$  catalyst played a role in varying  $\text{NiO}$  species with weaker interaction between metal and support. This is consistent with a previous finding that  $\text{NiO}$  can be reduced easily in the presence of an additive [34].

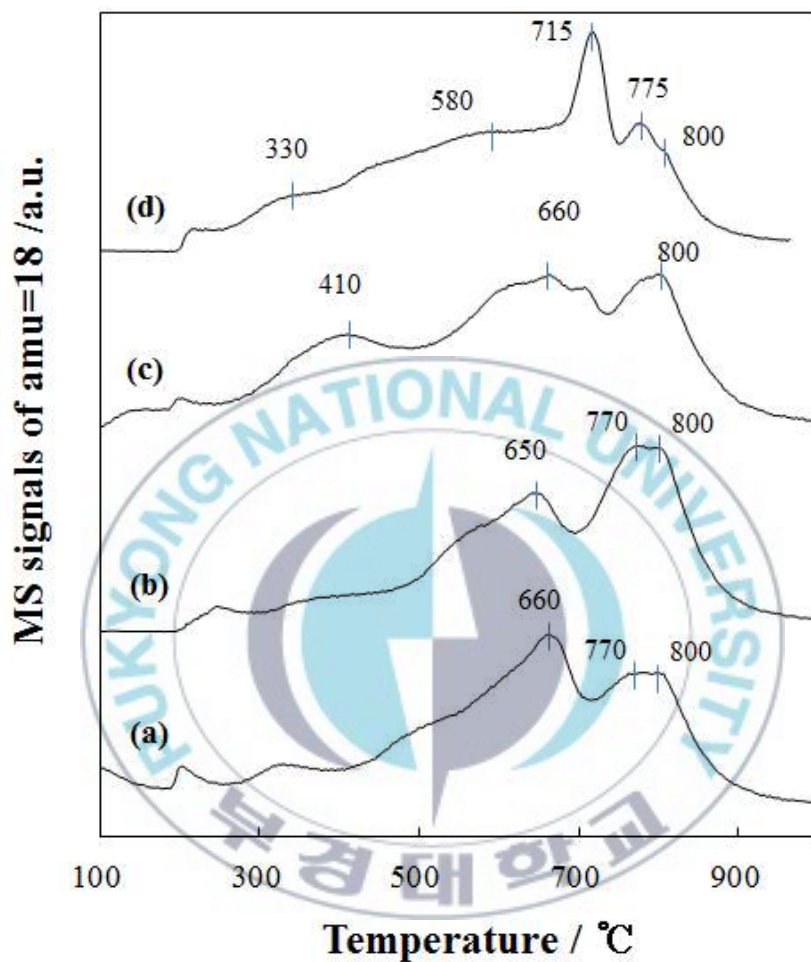


Fig. 6.2. H<sub>2</sub> temperature-programmed reduction (TPR) profiles for NiO/CaTi<sub>x</sub>O<sub>y</sub>-Al<sub>2</sub>O<sub>3</sub> catalysts with CaTi<sub>x</sub>O<sub>y</sub> loading: (a) NiO/CaTi<sub>x</sub>O<sub>y</sub>(5)-Al<sub>2</sub>O<sub>3</sub>(95), (b) NiO/CaTi<sub>x</sub>O<sub>y</sub>(11)-Al<sub>2</sub>O<sub>3</sub>(89), (c) NiO/CaTi<sub>x</sub>O<sub>y</sub>(20)-Al<sub>2</sub>O<sub>3</sub>(80), and (d) NiO/CaTi<sub>x</sub>O<sub>y</sub>(30)-Al<sub>2</sub>O<sub>3</sub>(70).

SEM images and elemental mapping by EDS for NiO/CaTi<sub>x</sub>O<sub>y</sub>-Al<sub>2</sub>O<sub>3</sub> catalysts are shown in Figs. 6.3 and 6.4. NiO/CaTi<sub>x</sub>O<sub>y</sub>-Al<sub>2</sub>O<sub>3</sub> possesses larger particles with relatively uniform size in range of 50 to 100 μm in diameter, unlike case of NiO/K<sub>2</sub>Ti<sub>x</sub>O<sub>y</sub>-Al<sub>2</sub>O<sub>3</sub> catalysts (Fig. 4.3, b to f), showing similar shape to NiO/Al<sub>2</sub>O<sub>3</sub> (Fig. 4.3a). Fig. 6.4 presents the distribution of each Ni, O, Al, Ca and Ti element on Al<sub>2</sub>O<sub>3</sub> indicating well-dispersed both Ni and CaTi<sub>x</sub>O<sub>y</sub> on the substrate, Al<sub>2</sub>O<sub>3</sub>. The mapping results of Ni and Ca element in Fig. 6.4 show that the NiO particles as well as Ca are well-dispersed on the support for all samples. However, Ti element were partially aggregated on the samples with CaTi<sub>x</sub>O<sub>y</sub> of high loading (Fig. 6.4, c and d). Accordingly, the SEM-EDS results for NiO/CaTi<sub>x</sub>O<sub>y</sub>-Al<sub>2</sub>O<sub>3</sub> catalysts present some inhomogeneity in the dispersion of Ni species, which corresponds to the XRD results (Fig. 6.1 and Table 6.1).

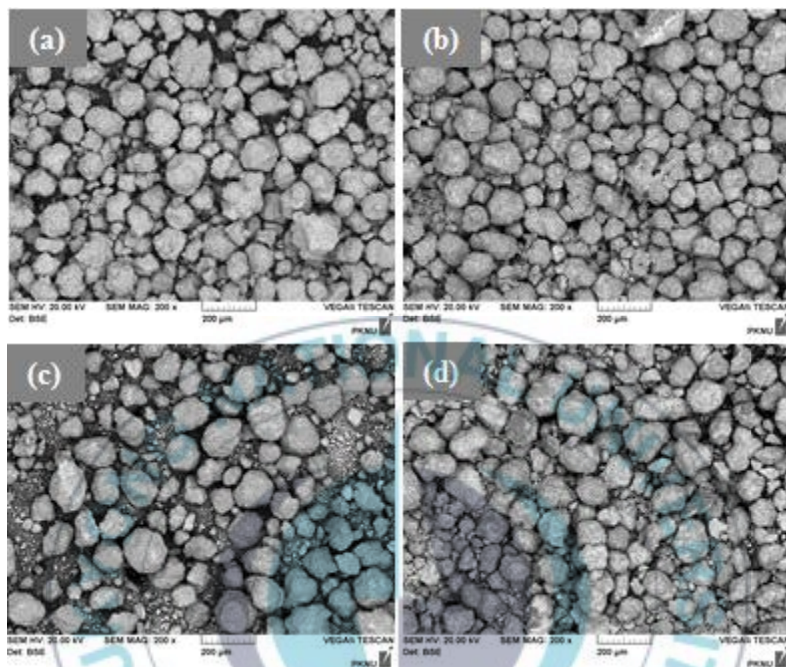


Fig. 6.3. Scanning electron microscopy (SEM) images of  $\text{NiO}/\text{CaTi}_x\text{O}_y\text{-Al}_2\text{O}_3$  catalysts with  $\text{CaTi}_x\text{O}_y$  loading: (a)  $\text{NiO}/\text{CaTi}_x\text{O}_y(5)\text{-Al}_2\text{O}_3(95)$ , (b)  $\text{NiO}/\text{CaTi}_x\text{O}_y(11)\text{-Al}_2\text{O}_3(89)$ , (c)  $\text{NiO}/\text{CaTi}_x\text{O}_y(20)\text{-Al}_2\text{O}_3(80)$ , and (d)  $\text{NiO}/\text{CaTi}_x\text{O}_y(30)\text{-Al}_2\text{O}_3(70)$ .

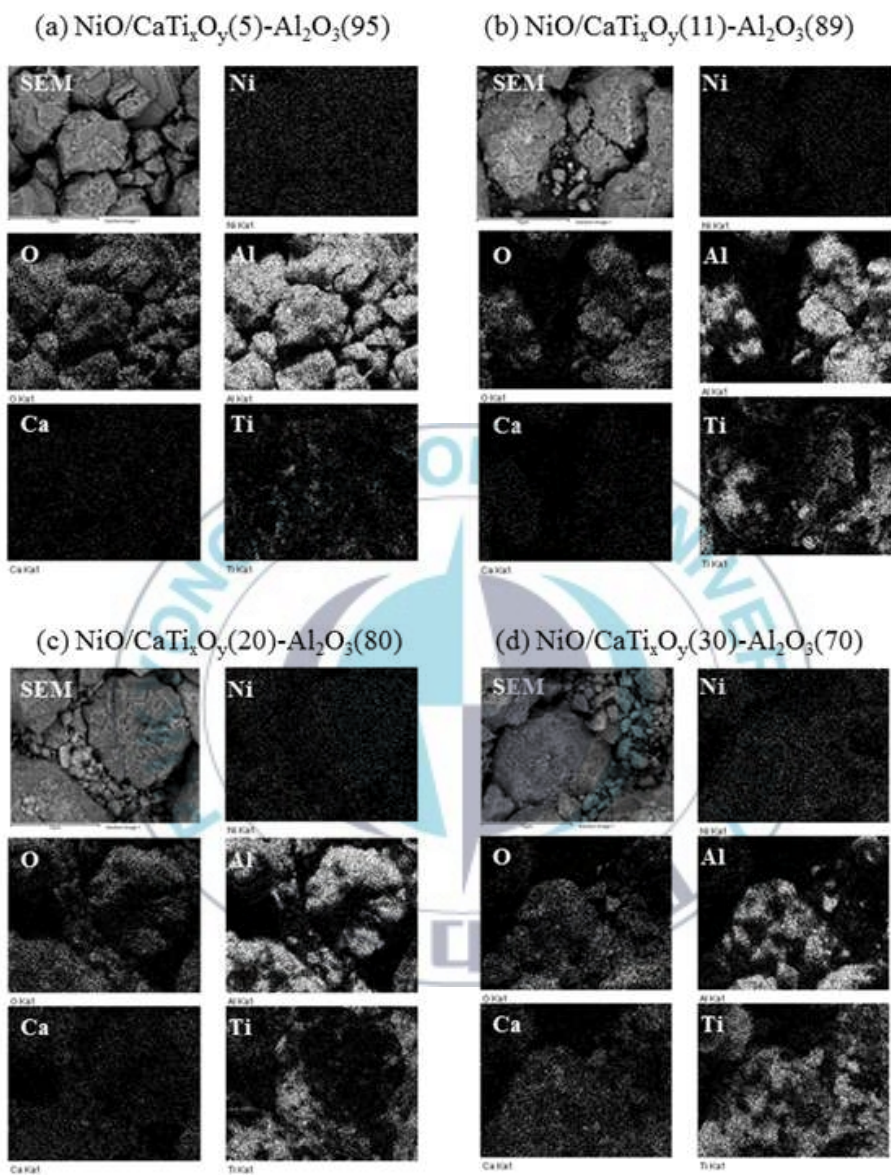


Fig. 6.4 Scanning electron spectroscopy (SEM) and electron dispersive spectroscopy (EDS) mapping images for Ni, O, Al, Ca, and Ti element on the  $\text{NiO}/\text{CaTi}_x\text{O}_y\text{-Al}_2\text{O}_3$  catalysts: (a)-(d) are same as in Fig. 6.3.



## 6.2. Activity of Ni/CaTi<sub>x</sub>O<sub>y</sub>-Al<sub>2</sub>O<sub>3</sub> catalyst

In order to examine the effect of reaction temperature condition over Ni/CaTi<sub>x</sub>O<sub>y</sub>-Al<sub>2</sub>O<sub>3</sub> catalysts for the steam methane reforming, Ni/CaTi<sub>x</sub>O<sub>y</sub>(20)-Al<sub>2</sub>O<sub>3</sub>(80) catalyst was tested at several different temperature. Thermodynamic equilibrium calculations were carried out by HSC Chemistry 5 software, compared to the experimental activity in Fig. 6.5. The experimental methane conversion increased with increasing reaction temperature like the thermodynamic equilibrium conversion was smaller with a higher temperature. These gaps are smaller than those of Ni/K<sub>2</sub>Ti<sub>x</sub>O<sub>y</sub>-Al<sub>2</sub>O<sub>3</sub> in Fig. 4.9(a) at the higher temperature (800-850 °C).



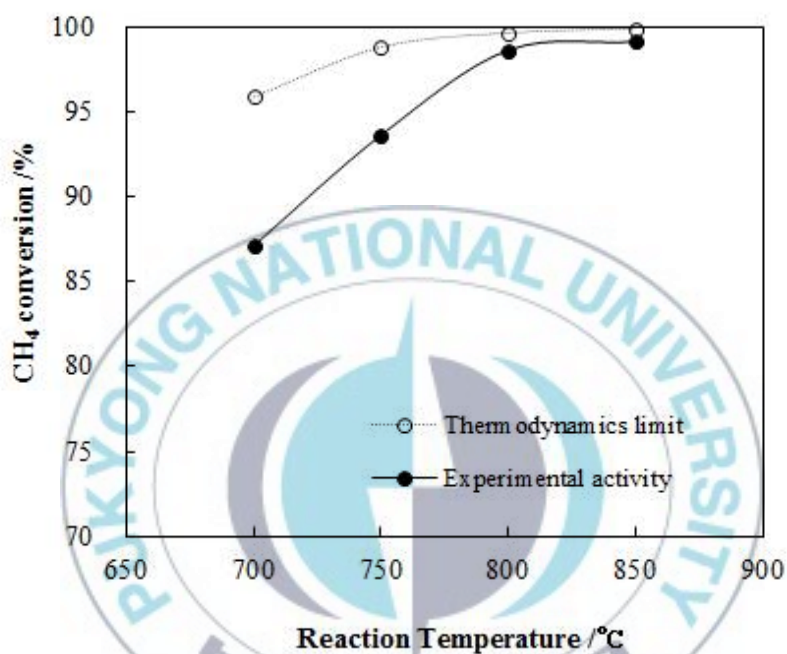


Fig. 6.5 Reaction temperature effect for steam methane reforming over Ni/CaTi<sub>x</sub>O<sub>y</sub>(20)-Al<sub>2</sub>O<sub>3</sub>(80) catalyst under the reaction condition: GHSV=15,000 h<sup>-1</sup>, and time on stream=20 h.

The activity for steam methane reforming over  $\text{Ni/CaTi}_x\text{O}_y\text{-Al}_2\text{O}_3$  catalysts was tested under the mild reaction condition and the average results in steady state after 1 hour reaction were listed in Table 6.2. With increasing the  $\text{CaTi}_x\text{O}_y$  content, the catalytic activities over  $\text{Ni/CaTi}_x\text{O}_y\text{-Al}_2\text{O}_3$  catalysts slightly decreased, being almost negligible. The  $\text{Ni/CaTi}_x\text{O}_y\text{-Al}_2\text{O}_3$  catalysts showed lower activity than those (Table 4.3) of  $\text{Ni/K}_2\text{Ti}_x\text{O}_y\text{-Al}_2\text{O}_3$  catalysts for steam methane reforming under the mild reaction conditions ( $\text{S/C}=2.5$ ,  $\text{GHSV}=15,000 \text{ h}^{-1}$ , and  $750^\circ\text{C}$ ). Moreover,  $\text{Ni/CaTi}_x\text{O}_y\text{-Al}_2\text{O}_3$  catalysts exhibited little poor performances for the steam methane reforming under the reaction condition, compared to FCR-4 catalyst and  $\text{Ni/Al}_2\text{O}_3$  (Table 4.3). Therefore, the  $\text{Ni/CaTi}_x\text{O}_y\text{-Al}_2\text{O}_3$  catalysts shows good performance at a reaction temperature higher than  $800^\circ\text{C}$ .

Table 6.2 Activities of steam methane reforming over Ni/CaTi<sub>x</sub>O<sub>y</sub>-Al<sub>2</sub>O<sub>3</sub> catalysts

Catalyst	X <sub>CH4</sub> (%)	S <sub>H2/CH4</sub>	S <sub>CO/CH4</sub>	S <sub>CO2/CH4</sub>
Ni/CaTi <sub>x</sub> O <sub>y</sub> (5)-Al <sub>2</sub> O <sub>3</sub> (95)	94.8	2.85	0.74	0.16
Ni/CaTi <sub>x</sub> O <sub>y</sub> (11)-Al <sub>2</sub> O <sub>3</sub> (89)	93.4	2.75	0.75	0.12
Ni/CaTi <sub>x</sub> O <sub>y</sub> (20)-Al <sub>2</sub> O <sub>3</sub> (80)	93.6	2.76	0.75	0.13
Ni/CaTi <sub>x</sub> O <sub>y</sub> (30)-Al <sub>2</sub> O <sub>3</sub> (70)	91.6	2.75	0.71	0.16

The reaction conditions: S/C=2.5, GHSV=15,000 h<sup>-1</sup>, T=750°C, and time-on-stream=10 h.

### 6.3. Sulfur-tolerance ability of Ni/CaTi<sub>x</sub>O<sub>y</sub>-Al<sub>2</sub>O<sub>3</sub> catalyst

The existence of a few sulfur compounds can irreversibly deactivate fuel processing catalysts, especially to supported Ni catalysts [82]. Used as one of the primary fuels to convert into hydrogen, pipeline natural gas (called ‘city gas’) contains several parts per million (ppm) of organic sulfur compounds such as tetrahydrothiophene (THT), tert-butylmercaptan (TBM), and dimethyl sulfide (DMS). In particular, for fuel cell applications, the pipeline natural gas is dominantly applied as a starting reactant. Thus, steam reforming catalysts in this work, need to have sulfur-tolerance to be guarantee their catalytic stabilities.

Sulfur-tolerance test for steam methane reforming over the Ni/CaTi<sub>x</sub>O<sub>y</sub>-Al<sub>2</sub>O<sub>3</sub> catalysts was performed under a mild condition of reaction containing sulfur compounds (Fig. 6.6). We applied FCR-4 and Ni/Al<sub>2</sub>O<sub>3</sub> as reference catalysts to this sulfur-tolerance test and compared their activities with those of Ni/CaTi<sub>x</sub>O<sub>y</sub>-Al<sub>2</sub>O<sub>3</sub> catalysts. As shown in Fig. 6.6, significant loss in activity was observed over the Ni/Al<sub>2</sub>O<sub>3</sub> catalyst during SMR of methane gas containing TBM and THT for 300 min. Same experiments were carried out on the Ni/CaTi<sub>x</sub>O<sub>y</sub>-Al<sub>2</sub>O<sub>3</sub> catalysts with different CaTi<sub>x</sub>O<sub>y</sub> loading and the results are also presented in Fig. 6.6. It is clear from these plots that most of the catalysts exhibit resistance to sulfur poisoning in contrast

to the activity decay observed over the reference catalysts, FCR-4 and Ni/Al<sub>2</sub>O<sub>3</sub>.

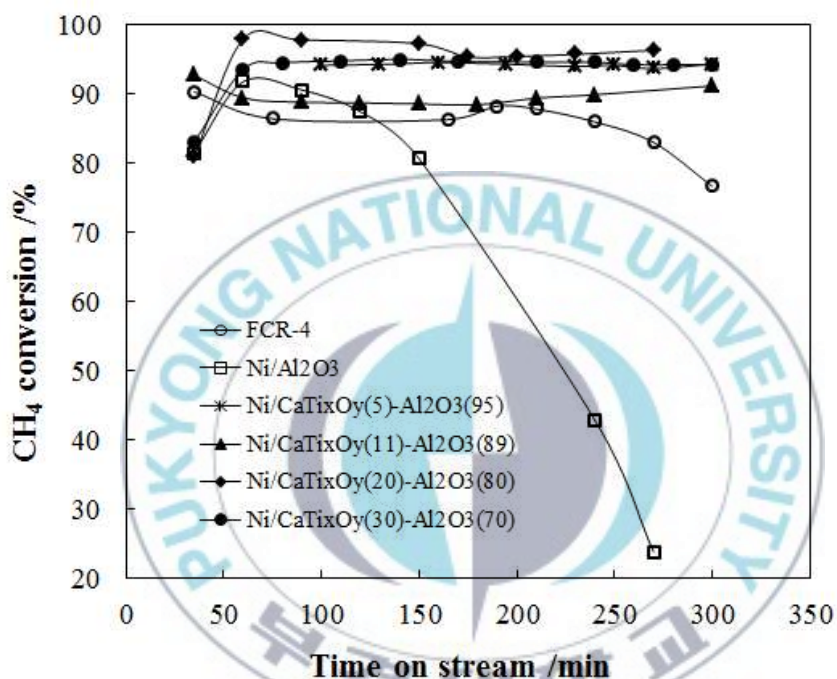


Fig. 6.6 Sulfur-tolerance performances over Ni/CaTi<sub>x</sub>O<sub>y</sub>-Al<sub>2</sub>O<sub>3</sub> catalysts and reference catalysts for steam methane reforming. (Reaction condition: S/C=2.5, GHSV=15,000 h<sup>-1</sup>, T=750 °C, time-on-stream=300 min, and sulfur concentration of 7 ppmv)

#### 6.4. Role of $\text{CaTi}_x\text{O}_y$ additive on $\text{Ni}/\text{Al}_2\text{O}_3$ catalyst for steam methane reforming stability

Sulfur tolerance of the  $\text{Ni}/\text{CaTi}_x\text{O}_y\text{-Al}_2\text{O}_3$  catalysts can be studied by conducting surface characterization studies in order to explain the phenomenon involved in the improved performance and the results are presented below.

Fig. 6.7 shows the XRD patterns of reduced  $\text{Ni}/\text{CaTi}_x\text{O}_y\text{-Al}_2\text{O}_3$  catalysts before and after the sulfur-tolerance test. Crystalline phase change and nickel crystal size of the  $\text{Ni}/\text{CaTi}_x\text{O}_y\text{-Al}_2\text{O}_3$  catalyst and the reference catalyst are listed in Table 6.3. For the  $\text{Ni}/\text{Al}_2\text{O}_3$  catalyst, the diffraction peaks of nickel metal ( $2\theta=44.5, 51.7,$  and  $76.7^\circ$ ) were almost disappeared, indicating oxidation of nickel. For almost  $\text{Ni}/\text{CaTi}_x\text{O}_y\text{-Al}_2\text{O}_3$  samples, nickel metal phases were retained and their amount decreased, indicating larger Ni particles than those of before the reaction. However, for the  $\text{Ni}/\text{CaTi}_x\text{O}_y(20)\text{-Al}_2\text{O}_3(80)$  catalyst, particle size of Ni metal was maintained to be same during the sulfur-tolerance test.

As reported in the previous research [83], on the Ni catalyst, sulfur was adsorbed on the catalyst as  $\text{SO}_4^{2-}$  and Ni was oxidized to NiO. Therefore, the  $\text{Ni}/\text{Al}_2\text{O}_3$  catalyst did not inhibit the oxidation of active metal, nickel, during SMR with the methane stream containing



the organic sulfur compounds.

According to Sato and Fujimoto [84], sulfur resistance in the reforming on a Ni/MgO-CaO catalyst promoted with  $\text{WO}_3$  was examined. The study showed that increased  $\text{WO}_3$  loading led to improved resistance to  $\text{H}_2\text{S}$  deactivation. The proposed mechanism involved the reaction of W with Ni-S to form W-S, which can then react with hydrogen to form and desorb  $\text{H}_2\text{S}$  from the catalyst surface. Ni-W catalyst is known to be significantly active for hydrodesulfurization (HDS). In HDS process,  $\text{WS}_x$  on nickel catalyst promotes conversion of organic sulfur compounds to  $\text{H}_2\text{S}$  [85, 86]. It is also confirmed that  $\text{H}_2\text{S}$  desorbs from sulfided nickel catalyst in presence of hydrogen at high temperature [85].

Similarly, this explains that the presence of  $\text{CaTi}_x\text{O}_y$  prevents the Ni/ $\text{Al}_2\text{O}_3$  from sulfur poisoning. It can be proposed that the  $\text{CaTi}_x\text{O}_y$  additive promoting the dissociation of Ni-S accelerates the reaction of a metal (M) of additive with Ni-S to form M-S and then reconvert to  $\text{H}_2\text{S}$  in presence of hydrogen, presumably retaining the active nickel.

As XRD results (Fig. 6.1 and Table 6.1), all the samples also have crystalline of  $\text{CaTiO}_3$ , which corresponds to a kind of perovskite. As I mentioned, since the perovskite-type oxides such as  $\text{CaTiO}_3$  have oxygen mobility it makes specially high resistance to deactivation.

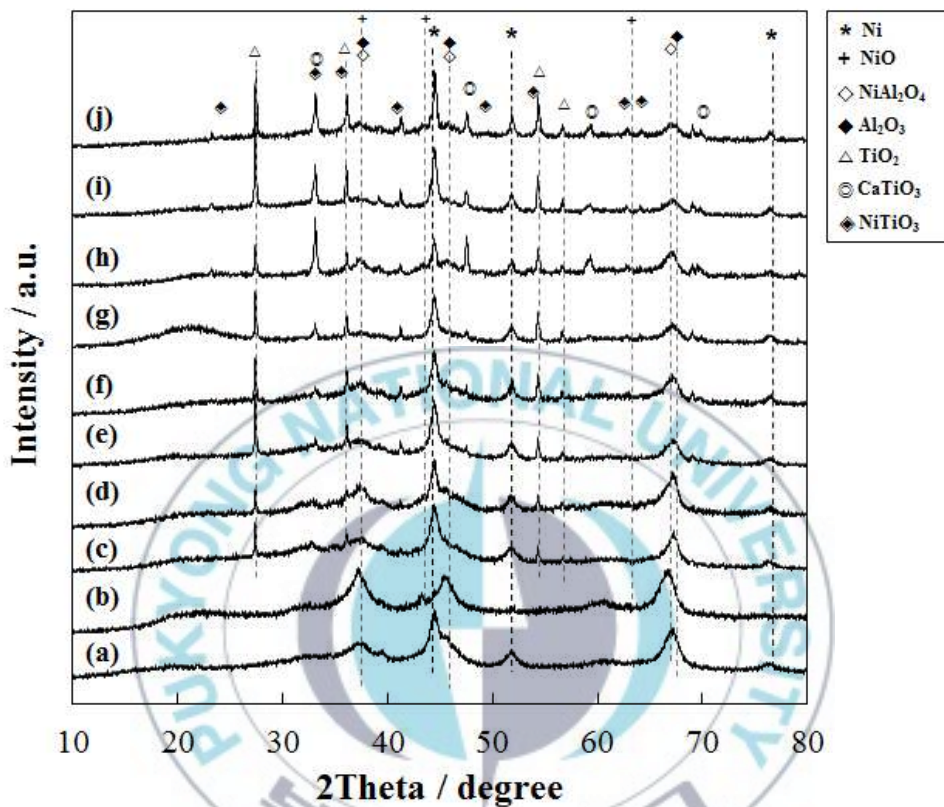


Fig. 6.7 X-ray diffraction patterns of fresh and spent samples of  $\text{Ni}/\text{CaTi}_x\text{O}_y\text{-Al}_2\text{O}_3$  catalysts: (a) fresh and (b) spent  $\text{Ni}/\text{Al}_2\text{O}_3$ , (c) fresh and (d) spent  $\text{Ni}/\text{CaTi}_x\text{O}_y(5)\text{-Al}_2\text{O}_3(95)$ , (e) fresh and (f) spent  $\text{Ni}/\text{CaTi}_x\text{O}_y(11)\text{-Al}_2\text{O}_3(89)$ , (g) fresh and (h) spent  $\text{Ni}/\text{CaTi}_x\text{O}_y(20)\text{-Al}_2\text{O}_3(80)$ , (i) fresh and (j) spent  $\text{Ni}/\text{CaTi}_x\text{O}_y(30)\text{-Al}_2\text{O}_3(70)$ . (Fresh samples were after the reduction pretreatment and spent samples were after the sulfur-tolerance test with reaction conditions as in Fig. 6.6)

Table 6.3 Crystalline phases change and Ni metal sizes of the catalysts before and after the sulfur-tolerance test

Sample	Crystalline phases		Crystalline size of Ni (nm) <sup>c</sup>	
	Retained <sup>a</sup>	Changed <sup>b</sup>	Before test	After test
Ni/Al <sub>2</sub> O <sub>3</sub>	Ni, NiAl <sub>2</sub> O <sub>4</sub> , $\gamma$ -Al <sub>2</sub> O <sub>3</sub>	$\uparrow$ NiO, $\downarrow$ Ni	8.7	–
Ni/CaTi <sub>x</sub> O <sub>y</sub> (5)-Al <sub>2</sub> O <sub>3</sub> (95)	Ni, TiO <sub>2</sub> , NiAl <sub>2</sub> O <sub>4</sub> , $\gamma$ -Al <sub>2</sub> O <sub>3</sub>	–	9.3	12.4
Ni/CaTi <sub>x</sub> O <sub>y</sub> (11)-Al <sub>2</sub> O <sub>3</sub> (89)	Ni, CaTiO <sub>3</sub> , TiO <sub>2</sub> , NiAl <sub>2</sub> O <sub>4</sub> , $\gamma$ -Al <sub>2</sub> O <sub>3</sub>	$\downarrow$ TiO <sub>2</sub>	11.1	15.3
Ni/CaTi <sub>x</sub> O <sub>y</sub> (20)-Al <sub>2</sub> O <sub>3</sub> (80)	Ni, CaTiO <sub>3</sub> , TiO <sub>2</sub> , NiTiO <sub>3</sub> , NiAl <sub>2</sub> O <sub>4</sub> , $\gamma$ -Al <sub>2</sub> O <sub>3</sub>	$\downarrow$ TiO <sub>2</sub>	15.3	16.6
Ni/CaTi <sub>x</sub> O <sub>y</sub> (30)-Al <sub>2</sub> O <sub>3</sub> (70)	Ni, CaTiO <sub>3</sub> , TiO <sub>2</sub> , NiTiO <sub>3</sub> , NiAl <sub>2</sub> O <sub>4</sub> , $\gamma$ -Al <sub>2</sub> O <sub>3</sub>	$\downarrow$ TiO <sub>2</sub>	15.3	24.2

<sup>a</sup> For reduced samples.

<sup>b</sup> After the test with reaction conditions as in Fig. 6.6.

<sup>c</sup> Calculated from Ni metal (200) plane using Scherrer equation by XRD.

## 7. Conclusions

The objective of this work was to get information on the fundamental principles of steam methane reforming over Ni/MTi<sub>x</sub>O<sub>y</sub>-Al<sub>2</sub>O<sub>3</sub> (M=K and/or Ca) catalysts through the activity test and the characterization of the catalysts. From the results obtained, the following conclusions can be described.

The catalytic activities of Ni/K<sub>2</sub>Ti<sub>x</sub>O<sub>y</sub>-Al<sub>2</sub>O<sub>3</sub> catalysts were comparable to that of FCR-4 under the mild reaction condition: at 750°C, in a reactant flow with S/C feed ratio of 2.5, at a GHSV of 15,000 h<sup>-1</sup>, and under atmospheric pressure. A stability test result for the Ni/K<sub>2</sub>Ti<sub>x</sub>O<sub>y</sub>-Al<sub>2</sub>O<sub>3</sub> catalysts under a severe reaction condition: at 800°C, in a reactant flow with S/C feed ratio of 1.0, at a GHSV of 200,000 h<sup>-1</sup> demonstrated that the Ni/K<sub>2</sub>Ti<sub>x</sub>O<sub>y</sub>-Al<sub>2</sub>O<sub>3</sub> catalysts with less than 11 wt.% K<sub>2</sub>Ti<sub>x</sub>O<sub>y</sub> in the support maintained their good stability for the reaction time of 100 hours. It was also found that the main factors accounting for the better catalytic performance over the Ni/K<sub>2</sub>Ti<sub>x</sub>O<sub>y</sub>-Al<sub>2</sub>O<sub>3</sub> catalysts than Ni/Al<sub>2</sub>O<sub>3</sub> were the medium interaction strength between nickel and the support, the proper amount of K<sub>2</sub>Ti<sub>x</sub>O<sub>y</sub> additive, and their superior stability. This work demonstrates that proper K<sub>2</sub>Ti<sub>x</sub>O<sub>y</sub> phases with a surface monolayer coverage achieved at ca. 15 wt.% loading in the support would be promising

additive material for alumina supported nickel catalyst used in a steam methane reforming process.

The  $\text{Ni/K}_{2-x}\text{Ca}_{x/2}\text{Ti}_y\text{O}_z(20)\text{-Al}_2\text{O}_3(80)$  catalysts have complex phases of K-Ca-Ti-O system and their nickel species were strongly interacted with the  $\text{K}_{2-x}\text{Ca}_{x/2}\text{Ti}_y\text{O}_z(20)\text{-Al}_2\text{O}_3(80)$  support, indicating their low reducibilities. The  $\text{Ni/K}_{2-x}\text{Ca}_{x/2}\text{Ti}_y\text{O}_z(20)\text{-Al}_2\text{O}_3(80)$  catalysts showed acceptable activities for steam methane reforming under the mild reaction condition. For the catalytic stability test, the  $\text{Ni/CaTi}_y\text{O}_z(20)\text{-Al}_2\text{O}_3(80)$  represented the superior stability than FCR-4,  $\text{Ni/Al}_2\text{O}_3$ , and any other catalysts in this work. For the  $\text{Ni/K}_{2-x}\text{Ca}_{x/2}\text{Ti}_y\text{O}_z\text{-Al}_2\text{O}_3$  catalyst (having higher than  $x$  of 0.6), the presence of perovskite oxide ( $\text{CaTiO}_3$ ) on the catalyst may derive acceptable catalytic activity with high resistance to coking due to its oxygen mobility.

The  $\text{Ni/CaTi}_x\text{O}_y\text{-Al}_2\text{O}_3$  catalysts have the medium interaction strength between nickel and support, weaker than that of  $\text{NiO/Al}_2\text{O}_3$ , and their nickel species were well-dispersed in the support. They showed relatively lower activities for steam methane reforming under the mild reaction condition. However, the  $\text{Ni/CaTi}_x\text{O}_y\text{-Al}_2\text{O}_3$  catalysts presented good performance at a reaction temperature higher than 80  $^{\circ}\text{C}$ , closed to thermodynamic limit. A sulfur-tolerance test result for the  $\text{Ni/CaTi}_x\text{O}_y\text{-Al}_2\text{O}_3$  catalysts under a severe reaction condition: at

750°C, in a reactant flow with S/C feed ratio of 2.5 containing sulfur compounds of 7 ppmv, and at a GHSV of 15,000 h<sup>-1</sup> demonstrated that they maintained their good stability for the reaction time of 300 min. On the other side, significant loss in activity was observed over the Ni/Al<sub>2</sub>O<sub>3</sub> catalyst. In particular, over the Ni/CaTi<sub>x</sub>O<sub>y</sub>(20)-Al<sub>2</sub>O<sub>3</sub>(80) catalyst, particle size of Ni metal was maintained to be same during the sulfur-tolerance test, indicating its superior resistance to sulfur.

Consequently, both potassium titanate (K<sub>2</sub>Ti<sub>x</sub>O<sub>y</sub>) and calcium titanate (CaTi<sub>y</sub>O<sub>z</sub>, specially CaTiO<sub>3</sub>) would be a promising additive material of alumina supported nickel catalyst for steam methane reforming reaction, effectively inhibiting deactivation from sintering of catalyst or sulfur poisoning.



# **Ni/MTi<sub>x</sub>O<sub>y</sub>-Al<sub>2</sub>O<sub>3</sub> (M=K, Ca) 촉매의 메탄 수증기 개질 반응활성 및 특성분석**

이 소 연

부 경 대 학 교 대 학 원 화 학 공 학 과

## **요 약**

연료전지는 화학적 에너지를 직접 전기에너지로 전환하는 장치로, 효율성이 높고 오염물질을 배출하지 않는 장점으로 인해 상용화 단계에 있는 신재생 에너지 기술로 여겨지고 있다. 연료전지 시스템의 연료인 수소는 탄화수소의 수증기 개질 반응으로 대부분 생성된다. 이 반응을 위한 수많은 촉매 연구가 보고되고 있지만, 촉매비활성화는 이 기술적 진보의 주요한 걸림돌로 여겨지고 있다. 따라서 본 연구의 목적은 니켈 촉매에 티타늄 산화물을 첨가하여 변형하고 메탄 수증기 개질반응에서의 촉매적 안정성을 평가하는 것이다. 이 티타늄 산화물 첨가제에는 칼륨과 칼슘 성분이 포함되며, 이로써 변형된 니켈 촉매의 수증기 개질 활성을 평가하고자 하였다. 니켈 촉매의 촉매적 활성 뿐 아니라 촉매의 물리·화학적 특성을 조사하고, 이 반응에 사용되는 기준촉매(Ni/Al<sub>2</sub>O<sub>3</sub>)와 상용 촉매(FCR-4)와의 비교연구를 수행하였다.

티타늄 산화물이 첨가된 변형 니켈 촉매는 단계적 함침법을 적용하여 제조하였고, 메탄의 수증기 개질 활성을 평가하였다. 촉매의 물리 화학적 특성분석을 위해 X선 회절, 질소흡착, 주사현미경, 수소 승온환원, 광전자분석, 원소분석 기법 등을 이용하였다.

Ni/K<sub>2</sub>Ti<sub>x</sub>O<sub>y</sub>-Al<sub>2</sub>O<sub>3</sub>(M=K) 촉매의 반응 활성은 일반적인 수증기 개질 운전 조건(S/C=2.5, T=750℃, GHSV=15,000 h<sup>-1</sup>)에서 상용촉매 FCR-4와 비견할 정도로 우수하게 나타났다. 특히, 이 촉매는 가혹한 반응조건(S/C=1.0, GHSV=200,000 h<sup>-1</sup>, T=800℃, time-on-stream=100 h)에서 변형되지 않은 기준촉매(Ni/Al<sub>2</sub>O<sub>3</sub>)보다 높은 활성과 열적 안정성을 보여주어 비활성화에 저항성을 나타냈다. 이는 촉매에서의 니켈과 변형된 지지체 간의 적절한 상호인력에 기인하는 것으로 여겨진다. 더불어 K<sub>2</sub>Ti<sub>x</sub>O<sub>y</sub> 첨가제는 지지체의 15 wt.% 정도의 함량을 가질 때 알루미나에 단층으로 분산되어 적절한 결정상으로 분포되는 것으로써 이 또한 이 Ni/K<sub>2</sub>Ti<sub>x</sub>O<sub>y</sub>-Al<sub>2</sub>O<sub>3</sub> 촉매의 높은 반응 안정성에 기여하고 촉매의 소결을 막아주는 중요한 역할을 하는 것으로 판단된다.

상기 촉매에서 칼슘이 칼륨자리를 일정비율만큼 대체한 형태인 Ni/K<sub>2-x</sub>Ca<sub>x/2</sub>Ti<sub>y</sub>O<sub>z</sub>(20)-Al<sub>2</sub>O<sub>3</sub>(80) 촉매는 매우 복잡한 결정상으로 이루어져 있고 촉매에 분산된 니켈 성분이 변형된 지지체인 K<sub>2-x</sub>Ca<sub>x/2</sub>Ti<sub>y</sub>O<sub>z</sub>-Al<sub>2</sub>O<sub>3</sub> 과 매우 강하게 결합하고 있어 환원성이 낮은 특성을 보인다. 이 촉매 또한 일반적인 수증기 개질 운전 조건에서는 적용가능한 활성을 보여준다. 앞서 적용한 것과 같은 가혹한 반응 조건에서는 Ni/CaTi<sub>y</sub>O<sub>z</sub>(20)-Al<sub>2</sub>O<sub>3</sub>(80) 촉매가 다른 모든 비교 촉매보다도 우월한 반응 안정성을 보여주었다. 이 촉매에서 칼슘의 비율인 x 가 0.6 을 넘으면 CaTiO<sub>3</sub> 페로브스카이트 결정상과 TiO<sub>2</sub> 상이 두드러지게 나타나는 결정 성상을 나타내는데, 페로브스카이트 산화물이 표면의

활성산소를 가짐으로써 표면에 형성될 수 있는 코크에 대한 저항력으로 작용하는 것으로 보인다.

Ni/CaTi<sub>x</sub>O<sub>y</sub>-Al<sub>2</sub>O<sub>3</sub>(M=Ca) 촉매는 니켈 금속과 변형 지지체 사이의 중간 크기의 상호력을 가지고 있으며, 촉매의 니켈 성분은 CaTi<sub>x</sub>O<sub>y</sub> 함량과 관계없이 지지체에 잘 분산되는 것으로 관찰된다. 이 촉매는 일반적인 수증기 개질 반응 조건에서는 다소 낮은 촉매 활성을 보였으나, 800℃ 이상의 반응온도에서 열역학적 평형치에 거의 다다를 정도의 우수한 활성을 나타냈다. 황에 대한 피독 저항성을 조사하기 위해, 7 ppmv 정도의 유기황화합물을 포함하는 일반적인 개질 반응 운전 조건(S/C=2.5, T=750℃, GHSV=15,000 h<sup>-1</sup>)에서 반응 활성을 평가하였다. 이 조건에서 기준촉매(Ni/Al<sub>2</sub>O<sub>3</sub>)에서는 현저한 비활성화가 일어났으나 Ni/CaTi<sub>x</sub>O<sub>y</sub>-Al<sub>2</sub>O<sub>3</sub> 촉매는 뛰어난 황 저항성을 보여주었다. 특히 Ni/CaTi<sub>x</sub>O<sub>y</sub>(20)-Al<sub>2</sub>O<sub>3</sub>(80) 촉매는 반응 후에도 니켈 금속을 여전히 보유하고 있었으며 그 크기 또한 변함이 없어 내황성 및 내소결성을 동시에 나타내었다.

결론적으로, 칼륨과 또는 칼슘과 공존하는 티타늄 산화물은 알루미늄에 담지된 니켈 촉매의 소결, 코킹, 황피독으로 기인되는 비활성화 문제를 해결할 수 있는 유망한 첨가제가 된다.

## REFERENCES

1. R. R. Davda, J. W. Shabaker, G. W. Huber, R. D. Cortright, and J.A. Dumesic, "A review of catalytic issues and process conditions for renewable hydrogen and alkanes by aqueous-phase reforming of oxygenated hydrocarbons over supported metal catalysts", *Appl. Catal. B: Environ.*, 56 (2005) 171–186.
2. W. J. Piel, "Transportation fuels of the future?", *Fuel Processing Technol.*, 71 (2001) 167–179.
3. U.S. Department of Energy Hydrogen, Fuel Cells and infrastructure Technologies Program, Hydrogen Posture Plan, U.S. Department of Energy, 2006.
4. E. Yuzugullu, Record 5017: Air Quality and Population, U.S. Department of Energy, 2006.
5. S. C. Davis, and S. W. Diegel, Transportation Energy Data Book, 25th ed., Oak Ridge National Laboratory, 2006.
6. J. D. Holladay, J. Hu, D. L. King, and Y. Wang, "An overview of hydrogen production technologies", *Catal. Today*, 139 (2009) 244-260.
7. J.R. Rostrup-Nielsen, in: J.R. Anderson, M. Boudart (Eds.), *Catalysis, Science, and Technology*, vol. 5, Springer-Verlag, Berlin, 1984, chap. 1.

8. J. R. Rostrup-Nielsen, J. Sehested, and J. K. Norskov, "Hydrogen and Synthesis Gas by Steam- and CO<sub>2</sub>Reforming", *Adv. Catal.*, 47, (2002) 65-139.
9. J. Rostrup-Nielsen, in: I.T. Horvath (Ed.), *Encyclopedia of Catalysis*, Wiley Interscience, (2003) 4.
10. M. W. Twigg (Ed.), *Catalyst Handbook*, Wolfe Publishing Ltd., London, 1989.
11. Q. Wang, J. H. Sohn, and J. S. Chung, "Thermally stable Pt/K<sub>2</sub>Ti<sub>2</sub>O<sub>5</sub> as high-temperature NO<sub>x</sub> storage and reduction Catalyst", *Appl. Catal. B: Environ.*, 89 (2009) 97-103.
12. I. Hachisuka, T. Yoshida, H. Ueno, N. Takahashi, A. Suda, and M. Sugiura, "Improvement of NO<sub>x</sub> Storage-Reduction Catalyst", *SAE*, 2002-01-0732.
13. H.-R. Kim, J. E. Choi, H.-K. Youn, and J.-S. Chung, "Promoter Effect on Ni/YSZ Anode Catalyst of Solid Oxide Fuel Cell for Suppressing Coke Formation in the Methane Internal Reforming", *Korean Chem. Eng. Res.*, 46 (2008) 813-818.
14. Larminie, J. and A. Dicks, *Fuel cell systems explained 2000*, New York John Wiley & Sons. 308.
15. Joensen, F. and J.R. Rostrup-Nielsen, "Conversion of hydrocarbons and alcohols for fuel cells." *J. Power Sources*, 105 (2002) 195-201.
16. Rostrup-Nielsen, J.R. and J.-H. Bak Hansen, "CO<sub>2</sub>-reforming of

- methane over transition metals”, *J Catal.*, 144 (1993) 38-49.
17. J. Sehested, A. Carlson, T.V.W. Janssens, P.L. Hansen, and A.K. Datye, “Sintering of nickel steam-reforming catalysts on MgAl<sub>2</sub>O<sub>4</sub> spinel supports”, *J Catal.*, 197 (2001) 200.
18. D. J. Smith, and L. D. Marks, *Philosophical Magazine A* 44: 735, 1981.
19. J. Wei, and E. Iglesia, “Structural requirements and reaction pathways in methane activation and chemical conversion catalyzed by rhodium”, *J. Catal.*, 225 (2004) 116-127.
20. H. S. Bengaard, J. K. Nørskov, J. Sehested, B. S. Clausen, L. P. Nielsen, A. M. Molenbroek, and J. R. Rostrup-Nielsen, “Steam reforming and graphite formation on Ni catalysts”, *J Catal.*, 209 (2002) 365-384.
21. Rostrup-Nielsen, J.R., J. Sehested and J.K. Nørskov, “Hydrogen and synthesis gas by steam- and CO<sub>2</sub> reforming”, *Adv. Catal.*, 47 (2002) 65-139.
22. A. Frennet, G. Lienard, A. Crucq, and L. Degols, “Effect of multiple sites and competition in adsorption on the kinetics of reactions catalyzed by metals”, *J Catal.*, 53 (1978) 150-163.
23. S. Yokota, K. Okumura, and M. Niwa, “Support effect of metal oxide on Rh catalysts in the CH<sub>4</sub>-CO<sub>2</sub> reforming reaction”, *Catal. Lett.*, 84 (2002) 131-134.
24. Z. Hou, and T. Yashima, “Small amounts of Rh-promoted Ni



- catalysts form methane reforming with CO<sub>2</sub>”, *Catal. Lett.*, 89 (2003) 193-197.
25. N.A. Jarrah, J.G. van Ommen, and L. Lefferts, “Mechanistic aspects of the formation of carbon-nanofibers on the surface of Ni foam: A new microstructured catalyst support”, *J. Catal.*, 239 (2006) 460-469.
26. F. Besenbacher, I. Chorkendorff, B. S. Clausen, B. Hammer, A. M. Molenbroek, J. K. Nørskov, and I. Stensgaard, “Design of a Surface Alloy Catalyst for Steam Reforming”, *Science*, 279 (1998) 1913-1915.
27. D. A. Porter, and K. E. Easterling, *Phase Transformations in Metals and Alloys*, 2<sup>nd</sup>ed., Chapman and Hall, London, 1992.
28. N. V. Parizotto, K.O. Rocha, S. Damyanova, F.B. Passos, D. Zanchet, C.M.P. Marques, and J.M.C. Bueno, “Alumina-supported Ni catalysts modified with silver for the steam reforming of methane: Effect of Ag on the control of coke formation”, *Appl. Catal. A:Gen.*, 330 (2007) 12-22.
29. B. Li, S. Kado, Y. Mukainakano, T. Miyazawa, T. Miyao, S. Naito, K. Okumura, K. Kunimori, and K. Tomishige, “Surface modification of Ni catalysts with trace Pt for oxidative steam reforming of methane”, *J. Catal.*, 245 (2007) 144-155.
30. Y. Mukainakano, B. Li, S. Kado, T. Miyazawa, K. Okumura, T. Miyao, S. Naito, K. Kunimori, and K. Tomishige, “Surface

- modification of Ni catalysts with trace Pd and Rh for oxidative steam reforming of methane, *Appl. Catal. A: Gen.*, 318 (2007) 252-264.
31. K. Tomishige, M. Asadullah, and K. Kunimori, "Novel catalysts for gasification of biomass with high conversion efficiency", *Catal. Surv. Asia*, 7 (2003) 219-233.
32. S. Wang, and G. Q. M. Lu, "CO<sub>2</sub> reforming of methane on Ni catalysts: Effect of the support phase and preparation technique", *Appl. Catal. B Environ.*, 16 (1998) 269-277.
33. R. Cracium, W. Daniell, and H. Knozinger, "The effect of CeO<sub>2</sub> structure on the activity of supported Pd catalysts used for methane steam reforming", *Appl. Catal. A : Gen.*, 230 (2002) 153-168.
34. H. -S. Roh, K. Y. Koo, J. H. Jeong, Y. T. Seo, D. J. Seo, Y. - S. Seo, W. L. Yoon, and S. B. Park, "Combined reforming of methane over supported Ni catalysts", *Catal. Lett.*, 117 (2007) 85-90.
35. P. K. Cheekatamarla, and A. M. Lane, "Efficient sulfur-tolerant bimetallic catalysts for hydrogen generation from diesel fuel", *J. Power Sources*, 153 (2006) 157-164.
36. E. Ochoa-Fernandez, C. Lacalle-Vila, K.O. Christensen, J.C. Walmsle, M. Rønning, A. Holmen, and D. Chen, "Ni catalysts for sorption enhanced steam methane reforming", *Top Catal.*, 45,

- 2007, 3-9.
37. K. Urasaki, Y. Sekine, S. Kawabe, E. Kikchi, and M. Matsukata, “Catalytic activities and coking resistance of Ni/perovskites in steam reforming of methane”, *Appl. Catal. A: Gen.*, 286 (2005) 23.
  38. M. C. J. Bradford, and M. A. Vannice, “Catalytic reforming of methane with carbon dioxide over nickel catalysts. I. Catalyst characterization and activity”, *Appl. Catal. A : Gen.*, 142 (1996) 73-96.
  39. Z. Zhang, and X. E. Verykios, “Carbon dioxide reforming of methane to synthesis gas over Ni/La<sub>2</sub>O<sub>3</sub> catalysts”, *Appl. Catal. A : Gen.*, 138 (1996) 109-133.
  40. S. Takatani, and Y. W. Chung, “Strong metal-support interaction in Ni/TiO<sub>2</sub>: Auger and vibrational spectroscopy evidence for the segregation of TiO<sub>x</sub> (x~1) on Ni and its effects on CO chemisorption”, *J Catal.*, 90 (1984) 75-83.
  41. O. Yamazaki, T. Nozaki, K. Omata, and K. Fujimoto, “Reduction of carbon dioxide by methane with Ni-on-MgO-CaO containing catalysts”, *Chemistry Letters*, 21 (1992) 1953-1954.
  42. S. Wang, and G. Q. Lu, “Catalytic activities and coking characteristics of oxides supported Ni catalysts for CH<sub>4</sub> reforming with carbon dioxide”, *Energy & Fuels*, 12 (1998) 248-256.
  43. S. Wang, and G. Q. M. Lu, “Role of CeO<sub>2</sub> in Ni/CeO<sub>2</sub>-Al<sub>2</sub>O<sub>3</sub> catalysts for carbon dioxide reforming of methane”, *Appl. Catal. B*

- : *Environ.*, 19 (1998) 267-277.
44. S. L. Swartz, Nano-scale water-gas-shift catalysts, *DOE CARAT Program*, 2003.
45. W. S. Dong, H. S. Roh, K. W. Jun, S. E. Park, and Y. S. Oh, "Methane reforming over Ni/Ce-ZrO<sub>2</sub> catalysts: effect of nickel content", *Appl. Catal. A : Gen.*, 226 (2002) 63-72.
46. X. E. Verykios, "Catalytic dry reforming of natural gas for the production of chemicals and hydrogen", *Int. J. Hydrogen Energy*, 28 (2003) 1045-1063.
47. Xu, and G.F. Froment, "Methane steam reforming, methanation and water-gas shift: I. Intrinsic kinetics", *AIChE Journal*, 35 (1) (1989) 88-96.
48. B. Nielsen, A. C. Luntz, P. M. Holmblad, and I. Chorkendorff, "Activated dissociative chemisorption of methane on Ni(100): a direct mechanism under thermal conditions", *Catal. Lett.*, 32 (1995) 15-30.
49. Y. Matsumura, and T. Nakamori, "Steam reforming of methane over nickel catalysts at low reaction temperature," *Appl. Catal. A : Gen.*, 258 (2004) 107-114.
50. S. Ayabe, H. Omoto, T. Utaka, R. Kikuchi, K. Sasaki, Y. Teraoka, and K. Eguchi, "Catalytic autothermal reforming of methane and propane over supported metal catalysts", *Appl. Catal. A : Gen.*, 241 (2003) 261-269.

51. G. A. Somorjai, Introduction to surface chemistry and catalysis, Wiley Interscience, New York, 1994.
52. P. van Beurden, On the catalytic aspects of steam-methane reforming, Report No. ECN-1-04-003, December 2004
53. M. V. Twigg, *Catalyst Handbook*, Wolfe Publishing Ltd., 1989.
54. N. R. Udengaard, J. -H. B. Hansen, and D. C. Hanson, *Oil & Gas Journal*, 90 (1992) 62.
55. T. Borowiecki, A. Gołćbiowski, and B. Stasińska, “Effects of small MoO<sub>3</sub> additions on the properties of nickel catalysts for the steam reforming of hydrocarbons”, *Appl. Catal. A : Gen.*, 153 (1997) 141-156.
56. J. S. Choi, K. I. Moon, Y. G. Kim, J. S. Lee, C. H. Kim, and D. L. Trimm, “Stable carbon dioxide reforming of methane over modified Ni/Al<sub>2</sub>O<sub>3</sub> catalysts”, *Catal. Lett.*, 52 (1998) 43-47.
57. C. Lee et al, *J Korean Ind. Eng. Chemistry*, 5 (1994) 160.
58. J. M. Rynkowski, T. Paryjczak, and M. Lenik, “On the nature of oxidic nickel phases in NiO/γ-Al<sub>2</sub>O<sub>3</sub> catalysts”, *Appl. Catal. A: Gen.*, 106, 1993, 73-82.
59. W. O. Milligan, L. Merten, *J. Am. Chem. Soc.*, 55 (1946) 527.
60. J. Zhang, H. Xu, X. Jin, Q. Ge, and W. Li, “Characterizations and activities of the nano-sized Ni/Al<sub>2</sub>O<sub>3</sub> and Ni/La–Al<sub>2</sub>O<sub>3</sub> catalysts for NH<sub>3</sub> decomposition”, *Appl. Catal. A: Gen.*, 290, 2005, 87-96.

61. A. Zhao, W. Ying, H. Zhang, H. Ma, and D. Fang, "Ni-Al<sub>2</sub>O<sub>3</sub> catalysts prepared by solution combustion method for syngas methanation", *Catal. Commun.*, 17 (2012) 34-38.
62. I. E. Wachs, and L. E. Fitzpatrick, *Characterization of Catalytic Materials*, Manning Publications Co., Greenwich, 1992, pp73-75.
63. Z. Hou, O. Yokota, T. Tanaka, and T. Yashima, "Characterization of Ca-promoted Ni/ $\alpha$ -Al<sub>2</sub>O<sub>3</sub> catalyst for CH<sub>4</sub> reforming with CO<sub>2</sub>", *Appl. Catal. A: Gen.*, 253 (2003) 381-387.
64. R. B. Shalvoy, P. J. Reucroft and B. H. Davis, *J. Vac. Sci. Technol.*, 17 (1980) 209.
65. L. Salvati, L. E. Makovsky, J. M. Stencel, F. R. Brown, and D. M. Hercules, "Surface spectroscopic study of tungsten-alumina catalyst using x-ray photoelectron, ion scattering, and raman spectroscopies", *J. Phys. Chem.*, 85 (1981) 3700.
66. J. G. Seo, M. H. Youn, J. C. Jung, and I. K. Song, "Effect of preparation method of mesoporous Ni-Al<sub>2</sub>O<sub>3</sub> catalysts on their catalytic activity for hydrogen production by steam reforming of liquefied natural gas (LNG)", *Int. J Hydrogen Energy*, 34 (2009) 5409.
67. K. Urasaki, Y. Sekine, S. Kawabe, E. Kikchi, and M. Matsukata, "Catalytic activities and coking resistance of Ni/perovskites in steam reforming of methane", *Appl. Catal. A: Gen.*, 286 (2005) 23-29.



68. J. Escobar, J. A. De Los Reyes and T. Viveros, *Appl. Catal. A: Gen.*, 253 (2003) 381.
69. Y.-J. Huang, J. A. Schwarz, J. R. Diehl, and J. P. Baltrus, "Effect of catalyst preparation on catalytic activity: VII. The Chemical Structures on Nickel/Alumina Catalysts: Their Impact on the Formation of Metal—Support Interactions", *Appl. Catal.*, 37, 1988, 229-245.
70. S. M. Fang, J. M. White, T. J. Campione, and J. G. Ekerdt, "CO hydrogenation and adsorption studies on supported-nickel SMSI catalysts", *J. Catal.*, 96 (1985) 491-498.
71. J. Sehested, "Four challenges for nickel steam-reforming catalysts", *Catal. Today*, 111 (2006) 103-110.
72. K. Takehira, T. Shishido, and M. Kondo, "Partial oxidation of CH<sub>4</sub> over Ni/SrTiO<sub>3</sub> catalysts prepared by a solid-phase crystallization method", *J. Catal.*, 207 (2002) 307-316.
73. K. Takehira, T. Hayakawa, H. Harihara, A.G. Andersen, K. Suzuki, and M. Shimizu, "Partial oxidation of methane to synthesis gas over (Ca,Sr)(Ti,Ni) oxide", *Catal. Today*, 24 (1995) 237-242.
74. T. Hayakawa, H. Harihara, A.G. Andersen, K. Suzuki, H. Yasuda, T. Tsunoda, S. Hamakawa, A.P.E. York, Y.S. Yoon, M. Shimizu, and K. Takehira, "Sustainable Ni/Ca<sub>1-x</sub>Sr<sub>x</sub>TiO<sub>3</sub> catalyst prepared in situ for the partial oxidation of methane to synthesis gas", *Appl. Catal. A: Gen.*, 149 (1997) 391.

75. T. Hayakawa, S. Suzuki, J. Nakamura, T. Uchijima, T. Hamakawa, K. Suzuki, T. Shishido, K. Takehira, *Appl. Catal. A: Gen.*, 183 (1999) 273.
76. G. S. Zafiris, and R. J. Gorte, "Evidence for low temperature oxygen migration from ceria to Rh", *J. Catal.*, 139 (1993) 561-567.
77. G. S. Zafiris, and R.J. Gorte, "Evidence for a second CO oxidation mechanism on Rh/Ceria", *J. Catal.*, 143 (1993) 86-91.
78. J.H. Bitter, W. Hally, K. Seshan, J.G. van Ommen, J.A. Lercher, "The role of the oxidic support on the deactivation of Pt catalysts during the CO<sub>2</sub> reforming of methane", *Catal. Today*, 29 (1996) 349-353.
79. F. B. Noronha, E. C. Fendley, R. R. Soares, W. E. Alvarez, and D. E. Resasco, "Correction between catalytic activity and support reducibility in the CO<sub>2</sub> reforming of methane over Pt/Ce<sub>x</sub>Zr<sub>1-x</sub>O<sub>2</sub> catalysts", *Chem. Eng. J.*, 82 (2001) 21.
80. R. Craciun, W. Daniell, and H. Knözinger, "The effect of CeO<sub>2</sub> structure on the activity of supported Pd catalysts used for ethane steam reforming", *Appl. Catal. A: Gen.*, 230, 2002, 153-168.
81. J. B. Wang, Y. L. Tai, W. P. Dow, and T. J. Huang, "Study of ceria-supported nickel catalyst and effect of yttria doping on carbon dioxide reforming of methane", *Appl. Catal. A: Gen.*, 218 (2001) 69-79.

82. S. M. Haile, "Fuel cell materials and components", *Acta Mater.*, 51 (2003) 5981-6000.
83. K. Tomishige, T. Miyazawa, T. Kimura, K. Kunimori, N. Koizumi, and M. Yamada, "Resistance to sulfur poisoning of hot gas cleaning catalysts for the removal of tar from the pyrolysis of cedar wood", *Appl. Catal. B: Environ.*, 60 (2005) 299-307.
84. K. Sato, and K. Fujimoto, "Development of new nickel based catalyst for tar reforming with superior resistance to sulfur poisoning and coking in biomass gasification", *Catal. Commun.*, 8 (2007) 1697-1701.
85. I. Chen, and D. W. Shine, "Resistivity to sulfur poisoning of nickel-alumina catalysts", *Ind. Eng. Chem. Res.*, 27 (1988) 1391-1396
86. Y. Yoshimura, T. Sato, H. Shimada, N. Matsubayashi, M. Imamura, A. Nishijima, M. Higo, and S. Yoshitomi, "Preparation of nickel-tungstate catalysts by as novel impregnation method", *Catal. Today*, 29 (1996) 221-228.

## CURRICULUM VITAE

### Personal Information

Name: So Yun Lee

Birth of Date: July 3, 1980

Address: 309-510, Chungsol APT, Songgang-dong, Yuseong-gu, Daejeon, Korea

### Educations

2010. 9 – Present : Ph.D candidate in Department of Chemical Engineering,  
The Graduate School, Pukyong National University

2004. 3 – 2006. 2 : M.S in Department of Chemical Engineering,  
The Graduate School, Pukyong National University  
Thesis Topic : “A Study on the Preferential Oxidation  
of Carbon Monoxide over  $\text{Cu/Ce}_x\text{Zr}_{x-1}\text{O}_2$  Catalysts”  
(Advisor: Hee Chul Woo)

1999. 3 – 2004. 2 : B.S in Division of Applied Chemical Engineering,  
The College of Engineering, Pukyong National University

### Carrier

2010. 6 – 2010. 8 : Research Fellow,  
The Institute of Cleaner Production Technology,  
Pukyong National University, Busan, Korea  
2009. 5 – 2010. 5 : Research Fellow,  
Korea Institute of Ceramic Engineering and Technology (KICET),  
Seoul, Korea

2006. 4 – 2008. 4 : Research Fellow,  
Korea Institute of Science and Technology (KIST),  
Seoul, Korea

### **Publications in International Journals**

1. S. Y. Lee, H. Lim, and H. C. Woo, "Catalytic Activity and Characterizations of  $\text{Ni/K}_2\text{Ti}_x\text{O}_y\text{-Al}_2\text{O}_3$  Catalyst for Steam Methane Reforming" submitted to *Int. J. Hydrogen E.*
2. H. P. Ho, S. Y. Lee, D. Lee, and H. C. Woo, "Selective Adsorption of tert-Butylmercaptan and Tetrahydrothiophene on Modified Activated Carbons for Fuel Processing in Fuel Cell Applications" submitted to *Int. J. Hydrogen E.*
3. S. Y. Lee, Y. K. Lee, S. T. Oyama, S. H. Lee, and H. C. Woo, "Preparation of Silica-Supported Nickel Molybdenum Phosphides by Temperature-programmed Reduction Technique" *Solid State Phenomena*, **124-126**, 2007, 1765-1768.

### **Publications in Domestic Journals**

1. S. Y. Lee, S. H. Lee, and H. C. Woo, "Catalytic Performance of Nickel-based Catalysts Containing Calcium Titanate for Methane Steam Reforming" *Chemical Industry and Technology*, **11**(1), 2011, 126-128.
2. S. Y. Lee, M. J. Moon, K. Huh, and H. C. Woo, "Activities of Various Ni-based Catalysts for Production of Fuel Cell Hydrogen" *Chemical Industry and Technology*, **10**(1), 2010, 90-93.
3. S. Y. Lee, S. H. Lee, J. K. Chun, and H. C. Woo, "Synthesis of  $\text{Cu/Ce}_x\text{Zr}_{x-1}\text{O}_2$  Catalysts for Selective Oxidation of Carbon Monoxide" *Chemical Industry and Technology*, **7**(1), 2007, 104-107.
4. S. Y. Lee, S. H. Lee, J. K. Chun, and H. C. Woo, "Preparation and Characterization of  $\text{Cu/Ce}_x\text{Zr}_{x-1}\text{O}_2$  Catalysts for Preferential Oxidation of Carbon Monoxide", *Clean Technology*, **13**(1), 2007, 54-63.
5. S. Y. Lee, S. H. Lee, and H. C. Woo, "An Evaluation on Catalytic Activity and Preparation of  $\text{Cu/Ce}_x\text{Zr}_{x-1}\text{O}_2$  for the Preferential Oxidation of Carbon Monoxide", *Chemical Industry and Technology*, **6**(1), 2005, 169-172.

6. S. Y. Lee, J. K. Chun, and H. C. Woo, "Preparation of Nanosized SnO<sub>2</sub> Particles by Microwave Heating" *Chemical Industry and Technology*, **6**(1), 2005, 173-176.

### Patents

1. H. C. Woo, W. G. Jeon, and S. Y. Lee, "The Adsorbent for Removing Organic Sulfur Compounds, The Method for Preparing The Same, and The Desulfurization System for Fuel Gas Using The Adsorbent", KR 10-1340114 B1. (Dec. 4, 2013)
2. H. C. Woo, S. Y. Lee, S. J. Choi, S. W. Park, and B. H. Yae, "Catalysts for Steam Reforming, Method for Fabricating the same and Hydrogen Production Method Using the Catalysts", KR 10-1337743 B1. (Nov. 29, 2013)
3. J. W. Yoo, H. S. Lee, S. Y. Lee, G. M. Lee, and J. K. Jung "Catalyst Composit for VOCs Oxidation and Preparation Process Thereof ", KR 10-1182755 B1. (Sept. 7, 2012)
4. J. W. Yoo, S. H. Lee, S. Y. Lee, D. S. Yoon, and M. S. Ha, "Oxygen Generating Composition", KR 10-1040742 B1. (Jun 3, 2011)

### Papers presented at international conference and meetings

1. S. Y. Lee, M. Song, and H. C. Woo, "Steam Methane Reforming over Modified Ni/Al<sub>2</sub>O<sub>3</sub> Catalysts: Effect of Loading Potassium Titanate" *14<sup>th</sup> Japan-Korea Symposium on Catalysis*, Japan, July 1-3, **2013**.
2. S. Y. Lee, K. Huh, and H. C. Woo, "Methane Steam Reforming Performance over Ni-based Catalysts Containing Potassium Titanate" *23<sup>rd</sup> North American Catalysis Society Meeting (NAM)*, USA, Jun 2-7, **2013**.
3. S. Y. Lee, K. Huh, and H. C. Woo, "Methane Steam Reforming Activity over Nickel-based Catalysts Containing Titanate" *PACCON2013*, Thailand, Jan. 23-25, **2013**.



4. S. Y. Lee, and H. C. Woo, "Catalytic Performance of Mixed Oxide-supported Nickel Catalysts for Methane Steam Reforming" *International Conference on Hydrogen Production (ICH2P) 2012*, Korea, Jun 24-27, **2012**.
5. S. Y. Lee, S. H. Lee, and H. C. Woo, "Nickel-based Composite Catalysts Containing Titanium for Methane Steam Reforming" *15<sup>th</sup> International Congress on Catalysis (ICC) 2012*, Germany, July 1-6, **2012**.
6. S. Y. Lee, K. Huh, S. H. Lee, and H. C. Woo, "Performance of Nickel-based Catalyst Containing Titanium for Steam Reforming" *2011 Korea/Japan/Taiwan Chemical Engineering Conference*, Korea, Nov 11, **2011**.
7. S. Y. Lee, and H. C. Woo, "Catalytic Activity of Ni/TiO<sub>2</sub>-Al<sub>2</sub>O<sub>3</sub> Catalyst for Methane Steam Reforming", *EuropaCat X*, Scotland, Aug 28-Sep 2, **2011**.
8. S. Y. Lee, and H. C. Woo, "Methane Steam Reforming over Alumina Supported Ni Catalyst: Potassium Titanate Promoter Effect" *13<sup>th</sup> Korea-Japan Symposium on Catalysis*, Korea, May 23-24, **2011**.
9. S. Y. Lee, Y. K. Lee, S. T. Oyama, S. H. Lee, and H. C. Woo, "Preparation of Silica-supported Nickel Molybdenum Phosphides by Temperature-programmed Reduction", *International Union of Materials Research Societies – International Conference in Asia (IUMRS-ICA) 2006*, Korea, Sep 10-14, **2006**.
10. S. Y. Lee, Y. K. Lee, S. T. Oyama, S. H. Lee, and H. C. Woo, "Preparation of NiMoP/SiO<sub>2</sub> by Temperature Programmed Reduction Procedure", *Materials Research Society (MRS) 2005 Spring Meeting*, USA, Mar 30-Apr 4, **2005**.
11. S. Y. Lee, S. H. Lee, H. C. Woo, and S. T. Oyama, "Preparation of Silica-supported Nickel Molybdenum Phosphides by Temperature-programmed Reduction Method", *2004 Korea/Japan/Taiwan Chemical Engineering Conference*, Korea, Nov 2-4, **2004**.

## **Projects involved for research and their technical reports**

1. "Development of Fuel Processing Catalysts in Fuel Cell System for Transportation",  
Jun 2013 - Jan 2014 (8 month),  
The "Leaders INdustry-university Cooperation" Project, supported by the Ministry of Education.
2. "The Preparation and Characterization of Highly Selective Adsorbents for the Removal for Sulfur Compounds in Fuel Diesel",  
Jun 2013 - May 2016 (36 month),  
Basic Science Research Program through the National Research Foundation of Korea (NRF) funded by the Ministry of Education.
3. "Measurement of Desulfurizer Performance for Fuel Cell Powered Vessel System",  
Oct 2012 - Mar 2013 (5 month),  
Funded by POSCO ENERGY Co., Ltd.
4. "Development of Desulfurization System for Fuel Cell Powered Vessel",  
Aug 2012 - Jan 2013 (6 month),  
The "Leaders INdustry-university Cooperation" Project, supported by the Ministry of Education, Science & Technology (MEST).
5. "Development of Hydrogen Production Techniques for Fuel Cells Electric Vehicle based on New & Renewable Energy",  
Aug 2011 - Feb 2012 (7 month),  
The "Bukyong Education center For vehicle Safety component Technology" Project, supported by the Ministry of Education, Science & Technology (MEST).
6. "Development of HC trap materials for gasoline engine exhaust gas stream",  
May 2011 - July 2014 (36 month),  
Funded by Hyundai & Kia Motors Co., Ltd.
7. "Development of Reformer and Reforming Catalysts",  
Oct 2009 - Apr 2012 (31 month),  
Leading Industry Development for Economic Region, financially supported by the Ministry of Knowledge Economy (MKE), Korea Institute for Advancement of Technology (KIAT) and Dae-Gyeong

Leading Industry Office through the Leading Industry Development for Economic Region.

8. “Development of Renewable Energy Components Technology”,  
Sep 2009 - Aug 2011 (24 month),  
Funded by Sewon Industries Co., Ltd.

### **Proposals submitted**

2013. 5. “Development of diesel fuel desulfurizer for MCFC”,  
New & Renewable Energy Program of the Korea Institute of  
Energy Technology Evaluation and Planning (KETEP)  
(한국에너지기술평가원의 신재생에너지기술개발 사업)
2013. 4. “Development of fuel processing catalysts in fuel cell system  
for transportation”,  
The "Leaders INdustry-university Cooperation" Project  
(산학협력선도대학 육성사업단 산학공동기술개발 과제)
2013. 2. “The Preparation and Characterization of Highly Selective Adsorbents  
for the Removal of Sulfur Compounds in Transportation Fuels”  
Basic Science Research Program through the National Research  
Foundation of Korea (NRF)  
(한국연구재단 이공분야 기초연구사업-중견연구자)
2013. 2. “The Preparation and Characterization of Highly Selective  
Adsorbents for the Removal of Sulfur Compounds in Fuel Diesel”,  
Basic Science Research Program through the National Research  
Foundation of Korea (NRF)  
(한국연구재단 이공분야 기초연구사업-일반연구자)
2012. 9. “Measurement of Desulfurizer Performance for Fuel Cell Powered  
Vessel System”,  
Project from POSCO ENERGY Co., Ltd.  
(포스코에너지 용역과제)
2012. 6. “Development of Desulfurization System for Fuel Cell Powered Vessel”,  
The "Leaders INdustry-university Cooperation" Project  
(산학협력선도대학 육성사업단 산학공동기술개발 과제)

2012. 2 “The Preparation and Characterization of Highly Selective Catalysts for the Oxidation of Sulfur Compounds in Hydrocarbon Gas”,  
Basic Science Research Program through the National Research Foundation of Korea (NRF)  
(한국연구재단 이공분야 기초연구사업)
2011. 7. “Development of Hydrogen Production Techniques for Fuel Cells Electric Vehicle based on New & Renewable Energy”,  
The "Bukyoung Education center For vehicle Safety component Technology" Project  
(수송기계안전편의융합부품소재 인재양성센터 산학공동연구과제)
2011. 3. “Development of HC trap materials for gasoline engine exhaust gas stream”,  
Project from Hyundai & Kia Motors Co., Ltd.  
(현대자동차 산학협동 연구과제)
2011. 1. “Experts Training Program for Advanced Clean Fuel Research”,  
The Human Resource Training Project for Regional Innovation through National Research Foundation of Korea(NRF)  
(한국연구재단의 지역혁신인력양성사업)

## 감사의 글

무엇보다도 이 모든 것을 가능하게 하신 하나님께 감사드립니다.

철없는 막내딸이 하고자 하는 바를 단 한 번도 막지 않으시고 지원해주시고 믿어주신, 존경하는 아버지와 어머니께 고마움을 전합니다. 내 인생의 첫 스승이었던 큰오빠야 이정록 목사님과 멋진 상남자 이정욱 작은오빠야, 십 년지기 벗이자 선배이며 연인인 김훈성 신랑에게 감사드리고 사랑의 마음 전합니다. 부족한 저와 기꺼이 가족이 되신 이기자 어머니, 김연실 형님과 박기주 아주버님, 남현숙 큰올케언니, 김명진 작은올케언니도 계셔서 너무 감사하네요. 아무쪼록 오래 함께 행복하게 살아요~

열정적인 학자의 모습으로 처음 저를 이끄시고 현재의 저를 있게 하신 우희철 교수님께 감사드립니다. 양손에 채찍과 당근으로 가르쳐주시고 지켜봐 주신 지난 십 년이 저에겐 피와 살이 되었습니다. 진심어린 마음으로 격려해주시는 이용걸 교수님, 믿음의 선배 김남식 선생님, 둘도 없이 친근하고 카리스마 넘치는 송민경 박사님, 선한 마음 베푸시는 허광선 교수님, 자상한 인사말을 먼저 건네시던 남석우 박사님, 유중환 박사님, 임형미 박사님, 산의 마음을 알게 해주신 남승우 선생님, 친근한 스승 문명준 교수님, 세심하신 이민규 교수님, 정말 고맙습니다. 학위논문 심사를 맡으시고 면밀한 조언으로 도움주신 이석희 교수님, 임준혁 교수님, 유준 교수님, 동아대 이정규 교수님께 깊은 감사의 말씀 전합니다. 주신 은혜는 제 손길이 필요한 사람들을 기꺼이 돕는 것으로나마 보답하겠습니다.

내 안에 또 다른 나 같은 친구 김경남 박사, 도련님 같은 박래성 선배, 나보다 나를 더 잘 아는 미희언니, 오랜 친구 미선이, 혜영이, 미나, 내 유일한 목자 선교사 김미 언니, 격 없이 편한 윤숙이, 솔직 단아 서영희, 가느다란 대쪽 효영이, 언니 같은 동생 애란이, 지도교수님이 알아본 알곡들 단국대 보석 경숙이, 찬현이, 성열이, 진우, 그리고 재간동이 우택이까지 모두 너무 멋진 사람들인데, 내 곁에 있어줘서 항상 고마워요. 감사표현에 인색한 제가 이제 철이 드나봅니다.

2002년부터 현재에 이르기까지 연구실에서 동고동락했던 선배님들과 후배들, 도움주신 공동실험실습관 선생님들께도 감사드립니다. 박사과정 중에 다사다난했던 연구실에서 희노애락을 함께했던 행정선생님들, 부지런하고 예의바른 유학생 Phuoc과 Duc, 궂은 일 도맡은 우형이, 용범이, 성찬이, 지윤씨, 재형이, 은영이 모두에게 감사의 뜻을 전하고, 김우형과 이성찬의 학위취득과 Duc의 결혼도 축하하며, 모든 것이 함께여서 가능했다고 생각합니다. 학교나 연구소에서 연을 맺어 오며가며 힘이 되어준 정두선배, 정원영, 박이슬 박사, 이형석, 윤동신, 김정택, 유수용, 김명환 박사님과 흥섭오빠, 혜진이, 현하, 광열이, 규민이, 옥희에게도 고마운 마음 보냅니다.

어릴 적 꿈처럼, 오랜 시간 학업을 이어오면서 깨닫는 것은, 자신의 부족함과 배움 자체가 기쁨이자 보상이었다는 사실입니다. 자주 마주하는 현실은 이 사실을 부인하게 했지만, 결국은 이것이었습니니다. 앞으로도 끊임없이, 겸손하게 배움을 연속하는 인생을 살겠노라 다짐해봅니다. 계속 지켜봐주시고 응원해주십시오!

청춘은 남기고 떠날 용당캠퍼스에서

2014년 1월

이 소 연 배상